ROLES OF DELAYED REPOLARIZATION AND ALTERED CALCIUM HANDLING IN DETERMINING REGIONAL ARRHYTHMIA PROPENSITY UNDER CONDITIONS OF REDUCED INWARD-RECTIFIER POTASSIUM CURRENT

by

Przemysław Radwański

A dissertation submitted to the faculty of
The University of Utah
in partial fulfillment of the requirements for the degree of

Doctor of Philosophy

Department of Pharmacology and Toxicology

The University of Utah

December 2010

The University of Utah Graduate School

STATEMENT OF DISSERTATION APPROVAL

The dissertation of **Przemysław Radwański**

has been approved by the following supervisory committee members:

Steven L. Bealer	, Chair	**10/08/2010** Date Approved
Steven Poelzing	, Co-chair	**10/08/2010** Date Approved
Annette E. Fleckenstein	, Member	**10/08/2010** Date Approved
Donald K. Blumenthal	, Member	**10/08/2010** Date Approved
Mark A. Munger	, Member	**10/08/2010** Date Approved

and by **William R. Crowley**, Chair of the Department of **Pharmacology and Toxicology**

and by Charles A. Wight, Dean of The Graduate School.

ABSTRACT

Andersen-Tawil syndrome Type 1 (ATS1) is a disorder linked to a loss of function of the inward rectifier current I_{K1}. Such a reduction in repolarization reserve has an established link with heterogeneous action potential duration (APD) prolongation. This in turn can serve as a substrate for reentrant arrhythmias. While APD prolongation and increased dispersion have been reported in pharmacological models of ATS1 they have not been linked with arrhythmogenesis.

APD prolongation secondary to reduced I_{K1} can increase Ca^{2+} entry into myocytes. The resultant accumulation of cytosolic Ca^{2+} has been linked with ventricular ectopies which can trigger arrhythmias. Indeed this mechanism of arrhythmogeneis has been proposed in ATS1 based on previous *in silico* and *ex vivo* studies. However, ATS1-associated cytosolic Ca^{2+} overload and increased arrhythmia propensity has not been demonstrated in tissue preparations.

The overall goal of this research was to characterize the factors that underlie arrhythmia propensity in a pharmacological model of ATS1. To this end we performed two studies. The first study analyzed APD gradients to determine whether they were sufficient for induction of reentrant arrhythmias. The results indicated they were not. However, this study revealed increased arrhythmia propensity which correlated with cytosolic Ca^{2+} overload. Therefore, the second study focused on Ca^{2+} handling and showed that ectopic activity originated from regions of higher Na^{+}/Ca^{2+} exchanger

(NCX) functional expression relative to sarcoplasmic reticulum Ca^{2+} ATPase (SERCA2a), which we term "NCX dominant" regions of the heart. In support of the idea that NCX is an important determinant of ectopy, we were able to modulate both the timing as well as the frequency of ectopy by pharmacologically modulating NCX dominance.

The data presented in this dissertation provide an insight into the factors by which Ca^{2+} handling contributes to ectopy under conditions of partial loss of I_{K1} function. This concept may aid in the identification of novel targets for antiarrhythmic therapy when I_{K1} is reduced in ATS1, as well as more prevalent disorders such as heart failure.

A.M.D.G.

TABLE OF CONTENTS

LIST OF FIGURES

ACKNOWLEDGEMENTS

I would like to express my gratitude to the following people for their contributions to my personal and scientific development and who made this dissertation possible.

First, I am deeply indebted to my advisor, Dr. Steven Poelzing, for his continued support and encouragement during tough times. Particularly, I am grateful for the freedom to explore the boldest of hypotheses, while keeping me from exerting too much effort on fruitless pursuits. Dr. Poelzing encouraged the development of my scientific communication skills and taught me the art of effective communication of research ideas and results. I am very grateful for both his support and advice.

I am deeply grateful to my dissertation committee members for their support and guidance. Dr. Mark Munger introduced me to the fascinating world of cardiology. I am obliged to him for engaging me in clinical research and for supporting my pursuits in basic science research.

I am also thankful to Dr. Steven Bealer, who introduced to me to scientific method as my research mentor during my first year rotation. His guidance was not only crucial during my time in his laboratory but also during the development of this thesis.

I owe a great deal of thanks to Dr. Annette Fleckenstein whose dedication to detail has encouraged me to think critically, conscientiously, and deliberately. Further, I am grateful to her for encouraging me whenever I felt lost and discouraged.

A special thank you belongs to Dr. Donald Blumenthal, whose good spirit, enthusiasm and love for science imbued in me an equal appreciation for scientific research. Dr. Blumenthal also taught me how to teach, and showed me the rewards associated with being an effective teacher.

I was privileged and extremely lucky to work in the wonderful environment provided by all the members of the Cardiovascular Research and Training Institute (CVRTI). Dr. Kenneth Spitzer, Director of CVRTI, was always available for discussion and encouraged and supported me throughout my time at CVRTI as a research assistant, while Dr. John Bridge fuelled my interest in the arena of excitation-contraction coupling research. Lastly, I would like to thank Dr. Phil Ershler, Nancy Allen, Alicja Booth, Jerry Jenkins, Dennis King, Wilson Lobaina and Bruce Steadman whose technical expertise and assistance was invaluable to the completion of the work presented in this thesis.

Next, I would like to thank my wife for her love and support, but most of all for putting up with my shortcomings.

Last, but certainly not least, the strong and enduring friendships and scientific/technical expertise of my colleagues at the CVRTI are greatly cherished. Sai, Anders Peter and Ryan have all aided significantly in the successful completion of this dissertation, and more importantly, in making my every day at work a little lighter and certainly more rewarding.

CHAPTER 1

INTRODUCTION

Sudden arrhythmic death is the most common consequence of cardiac disease, accounting for around 450,000 deaths annually in the US alone.[1] It is estimated that in about 80% these cases, sudden death results from ventricular arrhythmias.[2] Such arrhythmias, which can be precipitated by reentry as well as by ventricular ectopy (i.e., abnormal impulse formation), occur both in patients with structural heart disease,[3,4] most notably heart failure, as well as in seemingly healthy individuals.

Classically, two conditions are thought to be necessary for arrhythmias to occur: firstly, there must be present heterogeneous electrophysiology between cells of neighboring regions[5,6], and secondly, an abnormally timed beat, a trigger.[7,8] Electrophysiologic heterogeneities contribute to diverse pathophysiological conditions ranging from heart failure[9] to inherited channelopathies.[10] For instance, in heart failure, remodeling of ion channels exacerbates existing electrophysiologic heterogeneities, resulting in heterogeneously delayed repolarization. However, it is difficult to resolve the precise contribution of electrophysiologic heterogeneities to arrhythmogenesis in a complex milieu such as heart failure.[11-14] Similarly, it is difficult to pinpoint the mechanisms behind arrhythmia triggers (such as ventricular ectopy) in conditions like heart failure. However, inherited channelopathies such as Andersen-Tawil syndrome Type 1 (ATS1), which result from altered function of just one ionic current, offer a convenient experimental test bed for such inquiries.

The purpose of this dissertation is to elucidate the mechanism by which a single channelopathy leads to increased arrhythmia propensity. To this end we have used a drug-induced model of ATS1 to investigate the contributions of two arrhythmogenic mechanisms: heterogeneously delayed repolarization[5,6] and ventricular ectopy.[7,8]

Whereas the former is primarily associated with reentrant arrhythmias,[15-17] the latter has been linked to Ca^{2+} accumulation in the cytosol and consequent ectopy.[8,18-20] We have demonstrated that gradients of action potential duration (APD; an index of delayed repolarization) were insufficient for reentrant arrhythmia occurrence in an intact ventricular experimental model of ATS1. Importantly, we have demonstrated in this model that cytosolic Ca^{2+}accumulation can underlie the observed arrhythmias. Based on this finding, we have investigated the contribution of the heterogeneous Ca^{2+} handling protein distribution to the regional arrhythmia susceptibility.

Overview of Cardiac Function

In order to facilitate understanding of pathological mechanisms discussed in subsequent sections, some basic elements of cardiac physiology are briefly described below.

The Cardiac Action Potential

The heart is a pump, where its mechanical function resulting from cellular contraction synchronized by electrical signals. In a normal heart, these electrical signals originate in the pacemaking cells of the sino-atrial node, from whence it spreads across the atria and into the atrio-ventricular node. From there, after a delay, it travels rapidly through the highly specialized His-Purkinje network which branches into the two ventricles. The His-Purkinje network enables simultaneous activation of both ventricles resulting in synchronous contraction.

All cardiac myocytes are coupled electrically so that excitation of one cell soon leads to the excitation of its neighbors. The result is a propagating wave of excitation that spreads through the heart until every cell is excited. Such excitation takes the form of transient changes in transmembrane electrical potential called action potentials. Briefly, a cell at rest is electrically negative with respect to the extracellular space and its membrane is said to be polarized. The inward rectifier potassium current (I_{K1}) is the major determinant for keeping myocytes at rest. The introduction of positive charge into a resting cell, i.e., excitatory current, raises the transmembrane potential, triggering rapid entry of sodium (Na^+) ions into the cell through voltage-gated Na^+ channels. The membrane is now said to be depolarized and this process corresponds to the AP upstroke (phase 0, Figure 1.1). Immediately following the upstroke, the membrane potentially drops by a few millivolts due to a small amount of K^+ ions leaving the cell through K^+ channels (phase 1, Figure 1.1). At this point, Ca^{2+} ions enter the cell through L-type Ca^{2+} channels which maintains the membrane at a depolarized state, inscribing the AP plateau (phase 2, Figure 1.1). Eventually, the L-type Ca^{2+} channels close and a multitude of K^+ channels open up, causing significant amounts of K^+ to leave the cell and the membrane to return to its polarized state. This process is termed repolarization (phases 3; Figure 1.1). Throughout the action potential, Na^+/K^+ ATPase exchanges Na^+ for K^+ (Na^+-out – K^+-in) thereby restoring the Na^+ and K^+ gradients between the inside and the outside of the cell that are altered by ion movement during the action potential. Finally, returning full circle, I_{K1} is also responsible for the late phase of depolarization and as well as maintaining the resting membrane potential between action potentials as mentioned previously (phases 4; Figure 1.1). Importantly, it is a mutation in I_{K1} which underlies

ATS1, and the first purpose of this dissertation is to understand how loss of I_{K1} function leads to heterogeneous repolarization and increased arrhythmia susceptibility.For a more complete description of the action potential during normal as well as pathological conditions, please refer to comprehensive reviews by Luo and Rudy[21] as well as Kleber and Rudy.[22]

Excitation-Contraction Coupling

Changes in transmembrane potential are coupled to mechanical contraction and relaxation of the cell by changes in intracellular Ca^{2+}, a mechanism called excitation-contraction coupling.[23] Briefly, Ca^{2+} influx through L-type Ca^{2+} channels during Phase 2 (Figure 1.1 anf 1.2) of the action potential triggers the release of intracellular Ca^{2+} stores from the sarcoplasmic reticulum (SR) into the cytosol through ryanodine receptor channels (RyR) – a process dubbed Ca^{2+}-induced-Ca^{2+}-release. The quantity of Ca^{2+} thus released from the SR exceeds the amount that enters through the L-type Ca^{2+} channels by more than an order of magnitude. Consequently cytosolic Ca^{2+} concentration is raised a thousand fold from around 100nM to over 10μM. The resulting high cytosolic Ca^{2+} concentration actuates the contractile machinery of the cell composed primarily of actin and myosin, causing cellular contraction. As the L-type Ca^{2+} channels inactivate and the cell begins to repolarize at the start of phase 3 (Figure 1.1 and 1.2), Ca^{2+} is shuttled from the cytosol back into the SR by the SR Ca^{2+} ATPase (SERCA2a) and out of the cell by the Na^{+}/Ca^{2+}exchanger (NCX). The consequent reduction in cytosolic Ca^{2+} results in Ca^{2+} unbinding from contractile proteins and mechanical relaxation of the cell, thereby restoring its resting state.

Given the aforementioned components of action potential generation and the excitation-contraction coupling, one can appreciate that perturbation in of just one of the components can result in arrhythmias. The second purpose of this dissertation is to highlight the mechanisms by which a loss of I_{K1} function results in abnormal calcium handling and increased arrhythmia susceptibility.

Andersen-Tawil Syndrome – Type 1

Genetic Basis

Andersen-Tawil Syndrome – Type 1 (ATS1) is attributed to loss-of-function mutations in *KCNJ2*, the gene that encodes for the Kir2.1 channel, which in turn carries the inward rectifier current (I_{K1}).[24,25] Despite being first reported in 1963[26], the characterization of ATS1 is still ongoing,[27] with significant insights into the genetic basis and molecular aspects of ATS1 being gained as recently as the last decade. Plaster et al.,[25] through a linkage analysis in a large kindred, identified a locus corresponding to a genetic region of over 40 centiMorgans (cM) on chromosome 17q23. Study of the eight *KCNJ2* mutations initially identified in ATS1 patients revealed dominant-negative effects on Kir 2.1 channel function. These findings suggest that mutations in *KCNJ2* impair Kir2.1 channel function, thereby reducing I_{K1}. Despite dysmorphic features being one of the most common systemic phenotypic manifestations of the aforementioned mutation of Kir 2.1,[24] the destabilization of the resting membrane potential in skeletal muscle and the resultant periodic paralysis, particularly during hypokalemia,[28] is an important systemic electrophysiological manifestation. Of note, such an alteration of the resting membrane potential and the resultant prolongation of APD in the cardiomyocytes is a key factor that predisposes ATS1 patients to ventricular arrhythmias.[25]

In order to recapitulate the ATS1 arrhythmia phenotype in a guinea pig ventricular model, we perfused $BaCl_2$, a relatively specific I_{K1} blocker.[29] A concentration of 10 μM $BaCl_2$ was used, which is similar to that used in a canine model of I_{K1} blockade[30] and a guinea pig model of ventricular fibrillation.[31] Since arrhythmias in ATS1 are often unmasked by extreme reductions in serum K^+ levels,[24] I_{K1} current density was further reduced by decreasing the extracellular K^+ concentration to levels observed in patients exhibiting increased ventricular ectopy (2mM).[32] Henceforth, the aforementioned drug-induced model of ATS1 will be referred to as DI-ATS1.

Regional Arrhythmia Manifestation and Mechanisms

Although the incidence of sudden cardiac death in ATS1 is low, patients experience frequent ectopy and nonsustained runs of ventricular tachycardia (VT).[25] However, such frequent arrhythmias are associated dilated cardiomyopathy,[33] which can contribute to increased morbidity and mortality.[2] Such consequences can be avoided and potentially even reversed by anti-arrhythmic therapy.[33,34] Clues as to what underlies arrhythmias in ATS1 may be gained from examining the other clinical electrophysiologic manifestations of the pathology. For instance, individuals with ATS1 often present with mild QT interval prolongation (hence, its characterization as long QT syndrome 7) [25,28] and/or a prominent U wave.[35] This combination of QT prolongation and the U wave suggests delayed repolarization, which most likely is heterogeneous between regions.[35] Such heterogeneous dispersion of repolarization between or even within the ventricles in turn can constitute a substrate for reentrant arrhythmias.[36,37,30]

Gradients of repolarization and reentrant arrhythmias. Reentrant arrhythmias result from an abnormal, persistent wave of excitation that fails to terminate. For reentry to occur, the wave of excitation requires an obstruction to excitation, either anatomical or functional, around which the wave can propagate in a loop. This phenomenon is associated with unidirectional block (Figure 1.3).[22] In the majority of long QT syndromes, heterogeneous delay of repolarization creates functional obstructions, providing a substrate for reentry.[15-17]

The aforementioned heterogeneity of delayed repolarization is often an unmasking/exacerbation of regional ion channel heterogeneities, intrinsic to the normal heart. The existence of such ion channel heterogeneities, whether across the ventricular wall, between the apex and the base or between the ventricles, is widely recognized.[38,39] For instance, in guinea pig, left ventricle (LV) expresses a larger I_{K1} density relative to right ventricle (RV),[31,40] which may be exacerbated during DI-ATS1 in a pro-arrhythmic manner. In other words, the alterations in refractoriness observed in DI-ATS1 when combined with intrinsic ion channel heterogeneities can transform relatively benign repolarization heterogeneity into a potent substrate for unidirectional block and thereby, arrhythmias.[30]

Indeed, unidirectional block of transmural impulse propagation due to dispersion of repolarization has been reported in a model of failing canine LV wedge.[6] On the other hand, the cardiac anatomy and particularly the heart size of smaller animals such as guinea pig may preclude the occurrence of reentrant arrhythmia. Despite such concerns, successful arrhythmia induction by programmed electrical stimulation previously

reported in a guinea pig model of LQT3 suggests that occurrence of reentry is not precluded by the size of the guinea pig heart.[15]

Without a whole-heart model of ATS1, it was unknown whether gradients of repolarization could in fact underlie arrhythmogenesis in ATS1. Therefore, the role of heterogeneous dispersion of repolarization on arrhythmogenesis was tested in the research outlined in Chapter 2. In short, we report that gradients of repolarization were below the previously reported threshold for reentrant arrhythmia initiation.[6] Furthermore, we were unable to initiate arrhythmias with gradients of repolarization present in DI-ATS1 using accepted reentrant arrhythmia induction protocols.[15]

Ca^{2+} Mediated Ectopy

Based on the frequency of ventricular ectopy and the non-sustained nature of VT in ATS1, it has been suggested that abnormal Ca^{2+} handling secondary to APD prolongation may be the underlying electrophysiologic change leading ectopy.[35] The putative mechanism for such an abnormality in Ca^{2+} handling, manifest as cytosolic Ca^{2+} overload during loss of I_{K1} function is linked to intracellular K^+ accumulation. The rise in cytosolic K^+ levels during partial I_{K1} blockade in turn leads to Na^+/K^+ ATPase dysfunction and consequent intracellular Na^+ overload (Figure 1.2). Given NCX's exquisite sensitivity to intracellular Na^+ levels, cytosolic Na^+ overload increases the rate and duration of Na^+ extrusion (i.e. Ca^{2+} entry) through NCX. This in turn increases the cytosolic Ca^{2+} concentration.

Support for the aforementioned assertion of abnormal Ca^{2+} handling and cytosolic Ca^{2+} overload underlying ectopic activity in models of long QT syndromes has come in

the form of experimental observations demonstrating that ectopy originates from areas of elevated cytosolic Ca^{2+} levels during APD prolongation. Importantly such ectopy caused by membrane depolarization via forward mode NCX (Na^{+}-in – Ca^{2+}-out) in response to Ca^{2+} release from the SR is called "triggered activity" and/or "Ca^{2+}mediated ectopy," because abnormal Ca^{2+} handling, rather than electrical stimulation causes the ectopy.[41-43] Spontaneous SR Ca^{2+} release was proposed as the cellular mechanism of such ectopy. Such an event can result either from elevated cytosolic Ca^{2+} (which may be due to increased Ca^{2+} leak from the SR) or increased Ca^{2+} sensitivity of ryanodine receptors (the specialized SR release channels, RyR).[44] Alternatively, the combination of elevated cytosolic Ca^{2+} and enhanced Ca^{2+} uptake via the SERCA2a may overload the SR with Ca^{2+}, increasing the probability for a spontaneous Ca^{2+} release from the SR.[41,45-49] Indeed, results from previous models of ATS1, both *in silico*[50,51] and *in vivo*,[36,37] support the hypothesis that cytosolic Ca^{2+} overload underlies increased triggered arrhythmias during partial I_{K1} blockade.[50,51] However, to date, direct experimental evidence for cytosolic Ca^{2+} overload in a whole heart model of ATS1 has been lacking. In Chapter 2 we demonstrate that DI-ATS1 is associated with a rise in cytosolic Ca^{2+}, as previously postulated. Further, the observed cytosolic Ca^{2+} accumulation was associated with an increased arrhythmia burden in accord with the clinical arrhythmia phenotype of ATS1. However, the precise cellular mechanism by which rises in cytosolic Ca^{2+} translate into ectopy remains a subject of intense debate.[52] The factors that could influence such a phenomenon in DI-ATS1 are discussed below.

Elevated cytosolic Ca^{2+} and SR Ca^{2+} release. It has been proposed the increases in cytosolic Ca^{2+}, whether in ATS1, or heart failure[53] or during cardiac glycoside

administration,[54] can result in Ca^{2+} mediated ectopy. Under conditions of cytosolic Ca^{2+} overload, cytosolic Ca^{2+} concentrations can be further increased by rapid pacing and/or increasing Ca^{2+}entry through the L-type Ca^{2+} channel. The consequence of increased cytosolic Ca^{2+} can potentially increase SR Ca^{2+} loading with consequent increased ectopy.[46] This is a point of intense debate, however.

The controversy regarding the relationship of ectopy and cytosolic Ca^{2+} arises from three principal experimental observations:

1. In intact myocardium, regions with the lowest SERCA2a expression have preferentially increased cytosolic Ca^{2+} and higher arrhythmia propensity.[8] This means that the regions with the weakest ability to load the SR with Ca^{2+} demonstrate a higher propensity for ectopy.
2. Pharmacologically blocking SERCA2a in isolated cardiomyocytes increases cytosolic Ca^{2+} [55] but lowers such propensity for spontaneous depolarization.[56]
3. Inhibiting NCX lowers ectopy without significantly altering cytosolic Ca^{2+}.[57]

These three observations suggest that cytosolic Ca^{2+} overload by itself poorly correlates with an increased propensity for ectopy. It is possible, therefore, that there may be other mechanisms, apart from cytosolic Ca^{2+} overload, associated with ectopy. These mechanisms are discussed below (Figure 1.2).

SERCA2a. The first proposed arrhythmogenic mechanism involves SERCA2a, which is responsible for active Ca^{2+} uptake into the SR. Previous research suggested that Ca_D accumulation as a result of low SERCA2a expression could paradoxically increase the efficiency of SERCA2a via Ca^{2+}/calmodulin-dependent protein kinase activation.[58] This could result in paradoxically greater SR Ca^{2+} loading in regions with reduced

SERCA2a expression. However, this theory is inconsistent with studies that demonstrated that lowering SERCA2a function via pharmacological block not only decreases the propensity of ectopy, but elevates diastolic Ca^{2+}.[55,56] Further, the regions with lowest SERCA2a protein expression evidence the highest incidence of ectopy.[8] These data, therefore, put into question the involvement of SR Ca^{2+} overload as one of the arrhythmogenic mechanisms in DI-ATS1.

Leaky SR. The second proposed mechanism for increased incidence of SR Ca^{2+} release is that elevated cytosolic Ca^{2+} increases the probability that the RyR will open in response to an influx of Ca^{2+}. The inconsistency in this theory is that blocking SERCA2a should elevate cytosolic Ca^{2+} and further increase the probability that the RyR channels will spontaneously release Ca^{2+} from the SR. Again, experimental data shows that blocking SERCA2a raises cytosolic Ca^{2+} but decreases propensity for ectopy.[55,56] One possible explanation for this paradoxical phenomenon is that if the SR cannot sufficiently overload itself with Ca^{2+} during SERCA2a blockade, then the SR has a decreased propensity for spontaneous overload and release. However, this assertion is also inconsistent with the observation that sites with greatest propensity for ectopy have the lowest SERCA2a functional expression.[8]

NCX. The third proposed mechanism for increased incidence of SR Ca^{2+} release is related to NCX and its role in elevating cytosolic Ca^{2+}. It has been previously demonstrated that Ca^{2+} influx through NCX can trigger SR Ca^{2+} release and thereby, ectopy.[59-62] Recently a mathematical model of ATS1 suggested an upward shift in the NCX current towards more positive potentials during the repolarization phase of the action potential, allowing NCX to operate predominantly in the reverse mode (Ca^{2+}-in –

Na^+-out) during repolarization.[63] Further, reports of enhanced late Na^+ current associated with increased cytosolic Ca^{2+} concentrations can further promote reverse mode NCX function (Figure 1.2).[64] These studies along with recent reports NCX modulation of SR Ca^{2+} release[65-67] form a foundation for a plausible hypothesis of enhanced ectopic frequency during partial I_{K1} blockade, as evidenced in DI-ATS1 being linked to reverse mode NCX.

Altered membrane excitability. Alternatively, reduced I_{K1} density has been shown to destabilize the resting membrane potential.[68] This mechanism allows for spontaneous pacemaking activity (automaticity) that is independent of the SR. Specifically, during conditions of elevated cytosolic Ca^{2+}, forward mode NCX ($3Na^+$-in – $1Ca^{2+}$-out) could raise membrane potential particularly in late phases of the action potential and diastole by slowly depolarizing myoctes. Without I_{K1} maintaining a stable resting membrane potential (Figure 1.1), NCX could depolarize the cell to the activation thresholds of either voltage-gated Na^+ or Ca^{2+} channels. However, previous work by our group[40] and others[31] have demonstrated a significantly higher Kir2.1 protein density and consequent I_{K1} in the LV, the region with highest ectopic activity incidence, which suggests that these regions would be most resistant to pacemaker-like activity secondary to a greater resting membrane potential stability in such regions.

In Chapter 3 we discuss the effect of experimentally modulating the afore-mentioned factors involved in Ca^{2+} handling on regional arrhythmia propensity in DI-ATS1.

Research Objectives

The aim of this work is to characterize cytosolic Ca^{2+} accumulation and triggered arrhythmia during partial I_{K1} current inhibition in a whole ventricular preparation, and further, to investigate the potential implications of regional distribution of Ca^{2+} cycling proteins (SERCA2a and NCX), as the underlying modulators of arrhythmias in DI-ATS1. Chapter 2 will focus on regional arrhythmia vulnerability during DI-ATS1. Although previous studies in DI-ATS1 have revealed APD prolongation and dispersion,[36,30] whether this dispersion is sufficient for reentry to occur remains unknown. To investigate the roles of APD prolongation and dispersion on increased arrhythmogenicity during DI-ATS1, incidence of VT and ventricular ectopy were quantified. Subsequently, spatio-temporal characteristics of ventricular ectopy were determined. Lastly, using a ratiometric Ca^{2+} optical mapping system, which was designed and validated for this study, the correlation between ventricular ectopy and elevated cytosolic Ca^{2+} levels was established.

Chapter 3 discusses the role of regional distribution of Ca^{2+} cycling proteins (SERCA2a and NCX) in arrhythmia incidence. To test the hypothesis that increased incidence of ventricular ectopy correlates particularly with regions of higher NCX functional expression relative to SERCA2a (which we term "NCX dominance") and greater cytosolic Ca^{2+} accumulation relative to other regions, the effects of pharmacological modulation of NCX dominance were determined: during decreased NCX dominance, secondary to NCX inhibition and enhanced NCX dominance during SERCA2a inhibition. Finally, Chapter 4 highlights the major findings of these studies,

relates them to arrhythmia research in general, and concludes with future directions for this project.

References

1. Zheng Z, Croft JB, Giles WH, Mensah GA. Sudden cardiac death in the United States, 1989 to 1998. *Circulation*. 2001;104(18):2158-2163.

2. Mehra R. Global public health problem of sudden cardiac death. *J Electrocardiol*. 40(6, Supplement 1):S118-S122.

3. Pogwizd SM. Nonreentrant mechanisms underlying spontaneous ventricular arrhythmias in a model of nonischemic heart failure in rabbits. *Circulation*. 1995;92(4):1034-48.

4. Pogwizd SM. Focal mechanisms underlying ventricular tachycardia during prolonged ischemic cardiomyopathy. *Circulation*. 1994;90(3):1441-58.

5. Laurita KR, Girouard SD, Akar FG, Rosenbaum DS. Modulated dispersion explains changes in arrhythmia vulnerability during premature stimulation of the heart. *Circulation*. 1998;98(24):2774-2780.

6. Akar FG, Rosenbaum DS. Transmural electrophysiological heterogeneities underlying arrhythmogenesis in heart failure. *Circ Res*. 2003;93(7):638-45.

7. Laurita KR, Katra RP. Delayed after depolarization-mediated triggered activity associated with slow calcium sequestration near the endocardium. *J Cardiovasc Electrophysiol*. 2005;16(4):418-24.

8. Katra RP, Laurita KR. Cellular mechanism of calcium-mediated triggered activity in the heart. *Circ Res*. 2005;96(5):535-42.

9. Pogwizd SM, Schlotthauer K, Li L, Yuan W, Bers DM. Arrhythmogenesis and contractile dysfunction in heart failure: Roles of sodium-calcium exchange, inward rectifier potassium current, and residual beta-adrenergic responsiveness. *Circ Res*. 2001;88(11):1159-67.

10. Morita H, Wu J, Zipes DP. The QT syndromes: long and short. *Lancet*. 2008;372(9640):750-63.

11. Viswanathan PC, Shaw RM, Rudy Y. Effects of IKr and IKs heterogeneity on action potential duration and its rate dependence : A simulation study. *Circulation*. 1999;99(18):2466-2474.

12. Anyukhovsky EP, Sosunov EA, Rosen MR. Regional differences in electrophysiological properties of epicardium, midmyocardium, and endocardium: In vitro and in vivo correlations. *Circulation*. 1996;94(8):1981-1988.

13. Akar FG, Yan G, Antzelevitch C, Rosenbaum DS. Unique topographical distribution

of M cells underlies reentrant mechanism of Torsade de Pointes in the long-QT syndrome. *Circulation*. 2002;105(10):1247-1253.

14. Lesh MD, Pring M, Spear JF. Cellular uncoupling can unmask dispersion of action potential duration in ventricular myocardium. A computer modeling study. *Circ Res*. 1989;65(5):1426-1440.

15. Restivo M, Caref EB, Kozhevnikov DO, El-Sherif N. Spatial dispersion of repolarization is a key factor in the arrhythmogenicity of long QT syndrome. *J Cardiovasc Electrophysiol*. 2004;15(3):323-31.

16. Shimizu W, Antzelevitch C. Effects of a K+ channel opener to reduce transmural dispersion of repolarization and prevent Torsade de Pointes in LQT1, LQT2, and LQT3 models of the long-QT syndrome. *Circulation*. 2000;102(6):706-712.

17. Lankipalli RS, Zhu T, Guo D, Yan G. Mechanisms underlying arrhythmogenesis in long QT syndrome. *J Electrocardiol*. 2005;38(4, Supplement 1):69-73.

18. Laurita KR, Rosenbaum DS. Mechanisms and potential therapeutic targets for ventricular arrhythmias associated with impaired cardiac calcium cycling. *J Mol Cell Cardiol*. 2008;44(1):31-43.

19. Pruvot EJ, Katra RP, Rosenbaum DS, Laurita KR. Role of calcium cycling versus restitution in the mechanism of repolarization alternans. *Circ Res*. 2004;94(8):1083-90.

20. ter Keurs HEDJ, Boyden PA. Calcium and arrhythmogenesis. *Physiol Rev.* 2007;87(2):457-506.

21. Luo CH, Rudy Y. A model of the ventricular cardiac action potential. Depolarization, repolarization, and their interaction. *Circ Res*. 1991;68(6):1501-1526.

22. Kleber AG, Rudy Y. Basic mechanisms of cardiac impulse propagation and Associated Arrhythmias. *Physiol Rev.* 2004;84(2):431-488.

23. Bers DM. Cardiac excitation-contraction coupling. *Nature*. 2002;415(6868):198-205.

24. Tristani-Firouzi M, Jensen JL, Donaldson MR, et al. Functional and clinical characterization of KCNJ2 mutations associated with LQT7 (Andersen syndrome). *J Clin Invest*. 2002;110(3):381-8.

25. Plaster NM, Tawil R, Tristani-Firouzi M, et al. Mutations in Kir2.1 cause the developmental and episodic electrical phenotypes of Andersen's syndrome. *Cell*. 2001;105(4):511-9.

26. Klein R, Ganelin R, Marks JF, Usher P, Richards C. J Periodic paralysis with cardiac arrhythmia. *J Pediatr*. 1963;62:371-385.

27. Donaldson MR, Yoon G, Fu Y, Ptacek LJ. Andersen-Tawil syndrome: a model of clinical variability, pleiotropy, and genetic heterogeneity. *Ann Med*. 2004;36 Suppl 1:92-97.

28. Tawil R, Ptacek LJ, Pavlakis SG, et al. Andersen's syndrome: potassium-sensitive periodic paralysis, ventricular ectopy, and dysmorphic features. *Ann Neurol*. 1994;35(3):326-30.

29. Shi H, Wang H, Wang Z. Extracellular Ba2+ blocks the cardiac transient outward K+ current. *Am J Physiol Heart Circ Physiol*. 2000;278(1):H295-299.

30. Tsuboi M, Antzelevitch C. Cellular basis for electrocardiographic and arrhythmic manifestations of Andersen-Tawil syndrome (LQT7). *Heart Rhythm*. 2006;3(3):328-35.

31. Warren M, Guha PK, Berenfeld O, et al. Blockade of the inward rectifying potassium current terminates ventricular fibrillation in the guinea pig heart. *J Cardiovasc Electrophysiol*. 2003;14(6):621-631.

32. Tawil R, Ptacek LJ, Pavlakis SG, et al. Andersen's syndrome: potassium-sensitive periodic paralysis, ventricular ectopy, and dysmorphic features. *Ann Neurol*, 1994;35(3):326-330.

33. Schoonderwoerd B, Wiesfeld A, Wilde A, et al. A family with Andersen-Tawil syndrome and dilated cardiomyopathy. *Heart Rhythm*. 2006;3(11):1346-1350.

34. Pellizzón OA, Kalaizich L, Ptácek LJ, Tristani-Firouzi M, Gonzalez MD. Flecainide suppresses bidirectional ventricular tachycardia and reverses tachycardia-induced cardiomyopathy in Andersen-Tawil syndrome. *J Cardiovasc Electrophysiol*. 2008;19(1):95-97.

35. Zhang L, Benson DW, Tristani-Firouzi M, et al. Electrocardiographic features in Andersen-Tawil syndrome patients with KCNJ2 mutations: characteristic T-U-wave patterns predict the KCNJ2 genotype. *Circulation*. 2005;111(21):2720-6.

36. Poelzing S, Veeraraghavan R. Heterogeneous ventricular chamber response to hypokalemia and inward rectifier potassium channel blockade underlies bifurcated T wave in guinea pig. *Am J Physiol Heart Circ Physiol*. 2007;292(6):H3043-51.

37. Morita H, Zipes DP, Morita ST, Wu J. Mechanism of U wave and polymorphic ventricular tachycardia in a canine tissue model of Andersen-Tawil syndrome. *Cardiovasc Res*. 2007;75(3):510-8.

38. Shimizu W, Antzelevitch C. Sodium channel block with mexiletine is effective in reducing dispersion of repolarization and preventing Torsade de Pointes in LQT2 and LQT3 models of the long-QT syndrome. *Circulation*. 1997;96(6):2038-2047.

39. Di Diego JM, Sun ZQ, Antzelevitch C. I(to) and action potential notch are smaller in left vs. right canine ventricular epicardium. *Am J Physiol*. 1996;271(2 Pt 2):H548-561.

40. Veeraraghavan R, Poelzing S. Mechanisms underlying increased right ventricular conduction sensitivity to flecainide challenge. *Cardiovasc Res*. 2008;77(4):749-56.

41. Marban E, Robinson SW, Wier WG. Mechanisms of arrhythmogenic delayed and early afterdepolarizations in ferret ventricular muscle. *J Clin Invest*. 1986;78(5):1185-92.

42. Boyden PA, Pu J, Pinto J, Keurs HEDJT. Ca2+ transients and Ca2+ waves in purkinje cells : Role in action potential initiation. *Circ Res*. 2000;86(4):448-455.

43. Priori SG, Corr PB. Mechanisms underlying early and delayed afterdepolarizations induced by catecholamines. *Am J Physiol*. 1990;258(6 Pt 2):H1796-1805.

44. Egdell RM, De Souza AI, Macleod KT. Relative importance of SR load and cytoplasmic calcium concentration in the genesis of aftercontractions in cardiac myocytes. *Cardiovasc Res*. 2000;47(4):769-777.

45. Nuss HB, Kaab S, Kass DA, Tomaselli GF, Marban E. Cellular basis of ventricular arrhythmias and abnormal automaticity in heart failure. *Am J Physiol*. 1999;277(1 Pt 2):H80-91.

46. Diaz ME, Trafford AW, O'Neill SC, Eisner DA. Measurement of sarcoplasmic reticulum Ca2+ content and sarcolemmal Ca2+ fluxes in isolated rat ventricular myocytes during spontaneous Ca2+ release. *J Physiol*. 1997;501 (Pt 1):3-16.

47. Lukyanenko V, Subramanian S, Györke I, Wiesner TF, Györke S. The role of luminal Ca2+ in the generation of Ca2+ waves in rat ventricular myocytes. *J Physiol*. 1999;518(1):173-186.

48. Györke I, Györke S. Regulation of the cardiac ryanodine receptor channel by luminal Ca2+ involves luminal Ca2+ sensing sites. *Biophys J*. 1998;75(6):2801-2810.

49. Miura M, Boyden PA, Ter Keurs HE. Ca2+ waves during triggered propagated contractions in intact trabeculae. *Am J Physiol Heart Circ Physiol*. 1998;274(1):H266-276.

50. Sung RJ, Wu SN, Wu JS, Chang HD, Luo CH. Electrophysiological mechanisms of ventricular arrhythmias in relation to Andersen-Tawil syndrome under conditions of reduced IK1: a simulation study. *Am J Physiol Heart Circ Physiol*. 2006;291(6):H2597-605.

51. Silva J, Rudy Y. Mechanism of pacemaking in I(K1)-downregulated myocytes. *Circ Res*. 2003;92(3):261-3.

52. Laurita KR, Yong SL. Don't overlook overload of calcium. *Heart Rhythm*. 2010;7(10):1436-1437.

53. Despa S, Brette F, Orchard CH, Bers DM. Na/Ca exchange and Na/K-ATPase function are equally concentrated in transverse tubules of rat ventricular myocytes. *Biophys J*. 2003;85(5):3388-3396.

54. Ruch SR, Nishio M, Wasserstrom JA. Effect of Cardiac Glycosides on Action Potential Characteristics and Contractility in Cat Ventricular Myocytes: Role of Calcium Overload. *J Pharmacol Exp Ther*. 2003;307(1):419 -428.

55. Lewartowski BPB. Effects of thapsigargin on stimulation frequency--dependent changes in mitochondrial calcium in rat cardiac myocytes. *J Physiol Pharmacol*. 2002;53(4 Pt 2):751-759.

56. Janiak R, Lewartowski B. Early after-depolarisations induced by noradrenaline may be initiated by calcium released from sarcoplasmic reticulum. *Mol Cell Biochem*. 1996;163-164:125-130.

57. Nagy ZA, Virág L, Tóth A, et al. Selective inhibition of sodium–calcium exchanger by SEA-0400 decreases early and delayed afterdepolarization in canine heart. *Br J Pharmacol*. 2004;143(7):827-831.

58. Toyofuku T, Curotto Kurzydlowski K, Narayanan N, MacLennan DH. Identification of Ser38 as the site in cardiac sarcoplasmic reticulum Ca(2+)-ATPase that is phosphorylated by Ca2+/calmodulin-dependent protein kinase. *J Biol Chem*. 1994;269(42):26492-26496.

59. Leblanc N, Hume JR. Sodium current-induced release of calcium from cardiac sarcoplasmic reticulum. *Science*. 1990;248(4953):372-376.

60. Lipp P, Niggli E. Sodium current-induced calcium signals in isolated guinea-pig ventricular myocytes. *J. Physiol*. 1994;474(3):439-446.

61. Levi AJ, Spitzer KW, Kohmoto O, Bridge JH. Depolarization-induced Ca entry via Na-Ca exchange triggers SR release in guinea pig cardiac myocytes. *Am J Physiol*. 1994;266(4 Pt 2):H1422-1433.

62. Litwin SE, Li J, Bridge JH. Na-Ca exchange and the trigger for sarcoplasmic reticulum Ca release: studies in adult rabbit ventricular myocytes. *Biophys J*. 1998;75(1):359-371.

63. Seemann G, Sachse FB, Weiss DL, Ptacek LJ, Tristani-Firouzi M. Modeling of IK1 mutations in human left ventricular myocytes and tissue. *Am J Physiol Heart Circ Physiol*. 2007;292(1):H549-59.

64. Maltsev VA, Reznikov V, Undrovinas NA, Sabbah HN, Undrovinas A. Modulation of late sodium current by Ca2+, calmodulin, and CaMKII in normal and failing dog cardiomyocytes: similarities and differences. *Am J Physiol Heart Circ Physiol*. 2008;294(4):H1597-1608.

65. Larbig R, Torres N, Bridge JHB, Goldhaber JI, Philipson KD. Activation of reverse Na+-Ca2+ exchange by the Na+ current augments the cardiac Ca2+ transient: evidence from NCX knockout mice. *J Physiol*. 2010;588(17):3267-3276.

66. Lines GT, Sande JB, Louch WE, et al. Contribution of the Na+/Ca2+ exchanger to rapid Ca2+ release in cardiomyocytes. *Biophys J*. 2006;91(3):779-792.

67. Torres NS, Larbig R, Rock AN, Goldhaber JI, Bridge JH. Na+ currents are required for efficient excitation-contraction coupling in rabbit ventricular myocytes: a possible contribution of neuronal Na+ channel to triggering Ca2+ release from the Sarcoplasmic Reticulum. *J Physiol*. 2010. doi: 10.1113/jphysiol.2010.194688.

68. Miake J, Marbán E, Nuss HB. Functional role of inward rectifier current in heart probed by Kir2.1 overexpression and dominant-negative suppression. *J Clin Invest.* 2003;111(10):1529-1536.

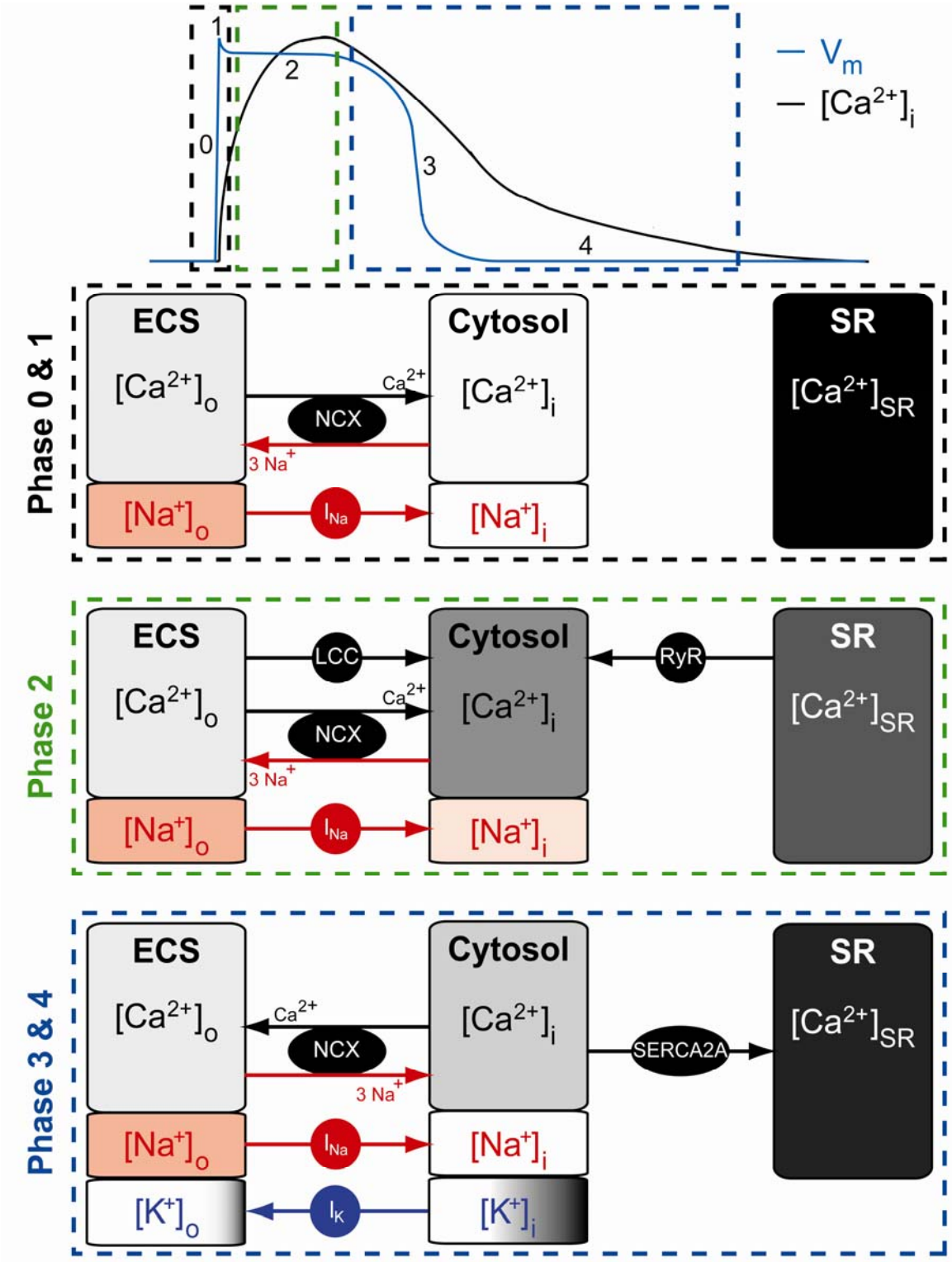

Figure 1.1. The Cardiac Action Potential and Ca^{2+} Handling. The cardiac action potential can be divided into five phases (0-4), while $Ca2^+$ flux occurs predominantly during phase 2-3 as indicated.

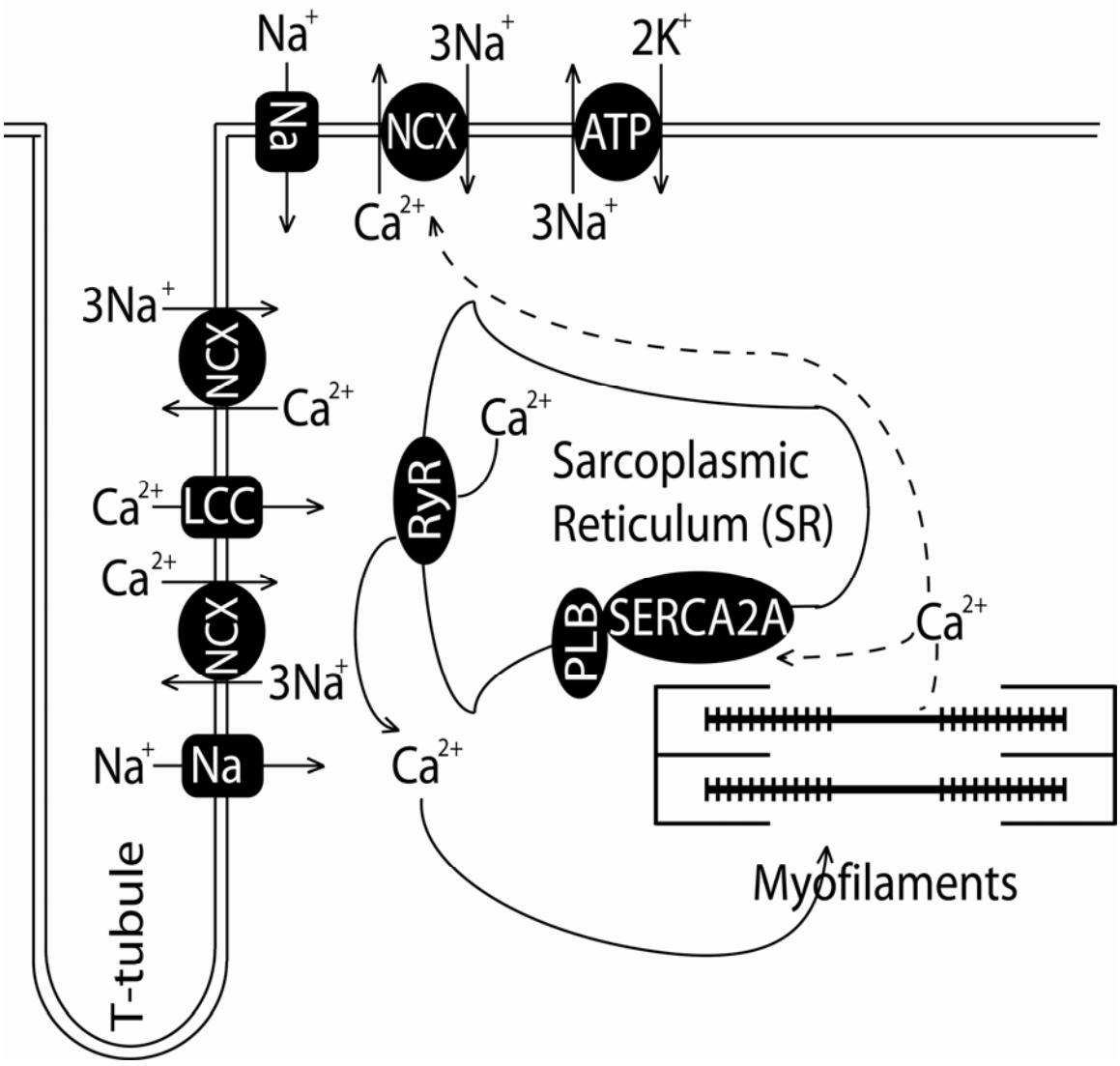

Figure 1.2. Excitation Contraction Coupling. Schematic diagram of Ca^{2+} cycling with the major proteins labeled. Upon membrane depolarization by intracellular Na^+ entry, Ca^{2+} enters via the L-type Ca^{2+} channels (LCC) leading to Ca^{2+} release channels (RyR) activation and consequent Ca^{2+} release (solid arrows) from the sarcoplasmic reticulum (SR). The released Ca^{2+} is then re-sequestered (dashed arrows) into the SR by the SR Ca^{2+} ATP-ase (SERCA), which is regulated by phospholamban (PLB), and extruded by Na^+/Ca^{2+} exchanger (NCX). Lastly, the cytosolic Na^+ that accumulated during depolarization is extruded from the cytosol at that time NCX and by Na^+/K^+ ATPase through the action potential.

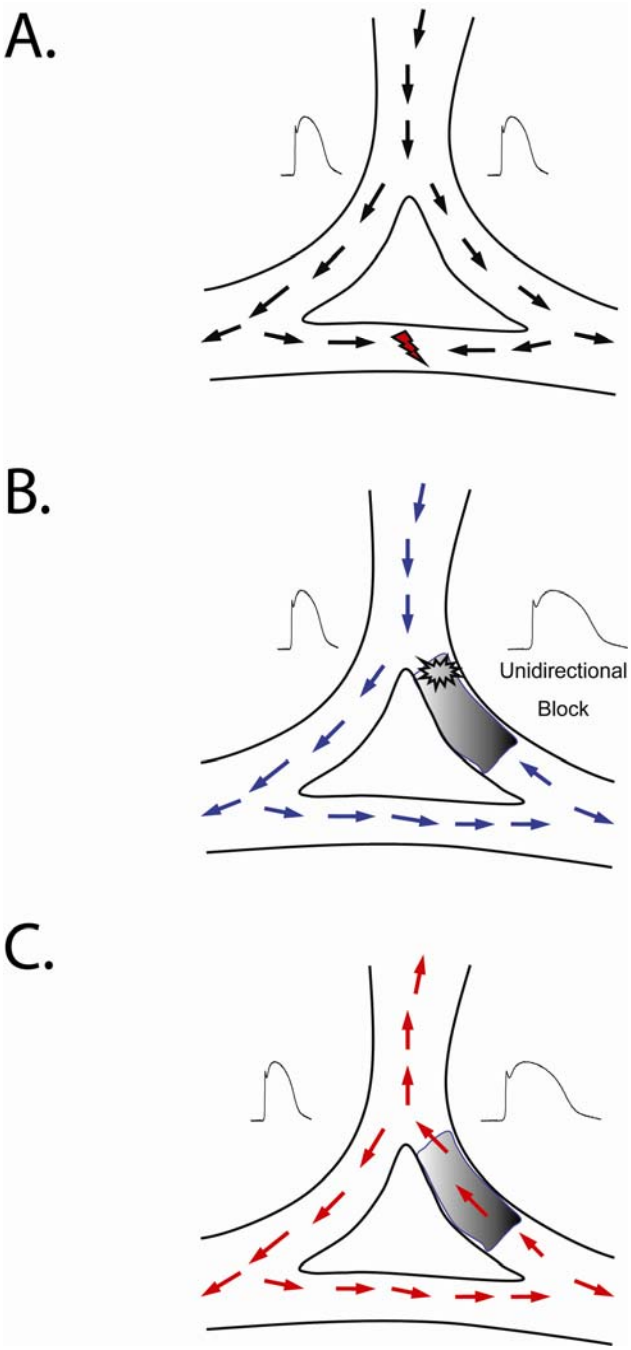

Figure 1.3. Mechanism of Reentry. **A)** Heterogeneities in APD in normal heart are insufficient for areas of refractoriness to form; therefore, impulse propagation will conduct through the two heterogeneous areas at virtually same rate. When those two wave-fronts encounter each other they terminate. **B)** On the other hand, during states of heterogeneous APD prolongation, areas with greatest refractoriness forme an area of block. **C)** The impulse travels through the unblocked area to reactivate previously refractory area in a retrograde fashion leading to excitation of that area and formation of reentry.

CHAPTER 2

CYTOSOLIC CALCIUM ACCUMULATION AND DELAYED REPOLARIZATION ASSOCIATED WITH VENTRICULAR ARRHYTHMIAS IN A GUINEA PIG MODEL OF ANDERSEN-TAWIL SYNDROME

Reprinted with permission from Radwański et al., *Heart Rhythm* 2010;7(10):1428-1435.

Introduction

Anderson-Tawil Syndrome (ATS1) is an inherited channelopathy that results from loss of function of the inward-rectifier K^+ current (I_{K1}) secondary to mutations in *KCNJ2*, the gene that encodes the Kir2.1 channel.[1,2] ATS1 is characterized electrocardiographically by a prolonged QT interval (hence its classification as Long-QT 7 syndrome) and nonsustained ventricular tachycardias (VTs) that are often foreshadowed by frequent triggered activity and occur more frequently during hypokalemia.[2,3] Therefore, it has been proposed that arrhythmias in ATS1 may be caused by electrical substrate remodeling[4,5] giving rise to the prolonged QT interval and increased triggered activity frequency. While heterogeneous action potential duration (APD) prolongation and increased dispersion, both transmural and interventricular, have been reported in experimental models of ATS1,[5-7] it remains unknown whether these gradients of repolarization are sufficient for reentry to occur.

Additionally, the high frequency and focal nature of bidirectional VTs in ATS1 suggest that triggered activity underlies, at least in part, the observed arrhythmias in ATS1.[6] In general, focal arrhythmias have been previously linked to cytosolic Ca^{2+} ($[Ca^{2+}]_i$) accumulation.[8-10] Indeed, *in silico* models of ATS1 support the hypothesis that $[Ca^{2+}]_i$ accumulation underlies increased triggered activity during partial I_{K1} blockade.[11,12] Based on *ex vivo* studies in drug induced ATS1 (DI-ATS1) models, Morita et al. and Poelzing et al. proposed, that arrhythmia propensity in ATS1 derives from $[Ca^{2+}]_i$ accumulation leading to increased triggered activity.[6,7] However, $[Ca^{2+}]_i$ accumulation has yet to be demonstrated in an experimental model of ATS1 in part due to limitations in whole-heart $[Ca^{2+}]_i$ measurement techniques.

While the development of ratiometric (i.e. dual wavelength) fluorescent Ca^{2+} probes has helped minimize artifacts due to inhomogeneities in fluorescence and motion, whole-heart Ca^{2+} optical mapping has lacked a calibration procedure that would satisfactorily account for multiple excitation light exposures.[13,14] We, therefore, designed and validated a ratiometric Ca^{2+} optical mapping system capable of simultaneous, quantitative, multisite measurements and use it here to test the hypothesis that elevated $[Ca^{2+}]_i$ concomitant with APD prolongation rather than APD dispersion underlies arrhythmia propensity during DI-ATS1.

We demonstrate in guinea pig Langendorff perfused ventricles that gradients of epicardial APD dispersion in DI-ATS1 were insufficient for arrhythmia induction by premature stimuli. However, APD prolongation was associated with increased incidence and severity of spontaneous and rapid pacing induced arrhythmias. Importantly, we demonstrate that this increased arrhythmia incidence is associated with significant diastolic $[Ca^{2+}]_i$ accumulation. Further, APD abbreviation with ATP-sensitive potassium channel opener, pinacidil, alleviated both diastolic $[Ca^{2+}]_i$ accumulation and the consequent increased arrhythmia burden.

Methods

This investigation conforms with the *Guide for the Care and Use of Laboratory Animals* published by the US National Institutes of Health (NIH Publication No. 85-23, revised 1996) and has been approved by the Institutional Animal Care and Use Committee of the University of Utah (protocol no. 05-07002).

Guinea Pig Langendorff Preparation

Guinea pig ventricles were perfused as Langendorff preparations as previously described.[7] Briefly, adult male guinea pig breeders (800 to 1000 g) were anesthetized with sodium pentobarbital (30 mg/kg IP), and their hearts rapidly excised, atria removed and perfused as Langendorff preparations (perfusion pressure, 55 mm Hg) with oxygenated (100% O2) Tyrode's solution at 36.5 °C containing (mMol/l) $CaCl_2$ 2, NaCl 140, KCl 4.5, dextrose 10, $MgCl_2$ 1, HEPES 10 (pH 7.41).

Optical Voltage and Ca^{2+} Mapping

We performed ratiometric voltage optical mapping as previously described.[7] See Supplemental Methods for more detail.

We developed an optical calcium mapping similar to that developed by Katra et al.[15] Ratiometric Ca^{2+} transients were determined by dividing the background-subtracted fluorescence Ca^{2+} transients at 405 nm by the background-subtracted fluorescence calcium transients at 485 nm.

$$\text{Ratio} = \frac{F_{405}}{F_{485}} = \frac{\Delta F_{405} - F_{405\text{-Background}}}{\Delta F_{485} - F_{485\text{-Background}}}$$

ΔF is the actual change in fluorescent amplitudes in the cameras after 405 or 485 bandpass filtering, and the subscript “Background” corresponds to light intensity without Indo-1 dye loading. The shorthand F_{405}/F_{485} is an abbreviation to represent the calculated ratiometric Ca^{2+} signal.

Optical Action Potential and $[Ca^{2+}]_i$ Measurements

Motion was reduced by 7.5 mM 2,3-diacetylmonoxime. Ventricles were stimulated at 1.5 times the stimulation threshold with a unipolar silver wire placed on the basal epicardial right ventricle. Activation time was defined as the time of the maximum first derivative of the AP as described previously.[16] Repolarization was defined as the time to 95% repolarization from peak voltage amplitude. APD was the time difference between activation and repolarization, while APD_{50} was the time difference between activation and 50% of repolarization. APD dispersion was defined as the difference between epicardial regions with the longest and shortest APD (using 25 spatially contiguous optically mapped sites per region). Relative diastolic Ca^{2+} level and Ca^{2+} transient amplitude were defined as the minimum ratiometric signal before the Ca^{2+} transient upstroke and the difference between systolic and diastolic $[Ca^{2+}]_i$ values, respectively. Ca^{2+} transient duration was calculated from the time of 90% amplitude during systole to the time of 10% amplitude during diastole.

DI-ATS1

ATS1 was modeled as described previously by perfusion of hypokalemic (2 mM KCl) Tyrode's solution containing 10uM $BaCl_2$.[7] Henceforth, this drug induced model of ATS1 will be referred to as DI-ATS1. Pinacidil was always perfused at 15 μM (Sigma Chemical). For most experiments Ca^{2+} transient recordings made during control, DI-ATS1, and DI-ATS1 with pinacidil were made sequentially. In order to rule out the involvement of the time-dependent component with respect to changes in Ca^{2+} transient

recordings, the order of recordings in a subset of preparations was altered where the perfusion of pinacidil during DI-ATS1 directly followed the control recordings.

Arrhythmia Induction

After a 20-beat drive train delivered to the anterior epicardial surface of the right ventricular base at the BCL of 400 ms (previously demonstrated as the region with the longest APD),[7] an epicardial premature stimulus (S2) at the left ventricular apex (the region with shortest APD)[7] was delivered through the same drive train. The S1-S2 interval was sequentially shortened by 10-ms until refractoriness was reached or an arrhythmia was induced. Rapid pacing induced arrhythmias were quantified at the shortest cycle length allowing for 1:1 capture. Volume-conducted electrocardiograms (ECG) were continuously recorded in a subset of experiments in order to assess arrhythmia burden. QT intervals were corrected for changes in basic cycle length (BCL) using the formula ($[QT_c = QT + (1/BCL - 1)]$).[7] Ventricular Tachycardia (VT) was defined as a run of three or more ventricular beats with a cycle length less than 250ms. A premature ventricular complex (PVC) was defined as any QRS complex with different morphology that occurred less than 1.5 standard deviations of the intrinsic cycle length. Arrhythmia was defined as any type of VT or PVC. PVC frequency was defined as the number of PVCs per minute. In order to account for inter-animal variability, PVC frequency for each animal was normalized to the PVC frequency during the DI-ATS1 recording.

Statistical Analysis

Statistical analysis was performed with a two-tailed Student's *t*-test for paired and unpaired data. Multiple regression analyses were used to characterize fluorescence Ca^{2+} signal drift both *in vitro* and in *ex vivo* preparations. A Fisher's Exact test was used to test differences in nominal data. A $p < 0.05$ was considered statistically significant. All values are reported as means ± standard error unless otherwise noted.

Results

Drug Induced-ATS1

A representative volume-conducted ECG in Figure 2.1A demonstrates QT-interval prolongation by approximately 60 ms during DI-ATS1 relative to control. Additionally, the T-wave, which was monophasic under control conditions, was biphasic during DI-ATS1. Over all experiments, QT_c during DI-ATS1 (286.7 ± 15.2ms) was significantly longer relative to control (210.7 ± 5.2ms, Figure 2.1B). Underlying the observed QT_c prolongation during DI-ATS1 was APD prolongation illustrated by representative optical action potentials in Figure 2.2A. For all experiments, global APD and APD_{50} was prolonged during DI-ATS1 relative to control (222.5 ± 3.5 ms vs.151.3 ± 1.3 ms, Figure 2.2B; and 130.1 ± 5.5 ms vs. 99.8 ± 6.1 ms, Figure 2.2D, respectively). Additionally, APD dispersion was greater during DI-ATS1 relative to control (16.9 ± 1.0 ms vs. 13.8 ± 1.3 ms, Figure 2.2C).

No arrhythmias (defined as one or more premature beats) were induced by premature programmed stimulation under any condition. Furthermore, VTs were neither spontaneous nor inducible under control conditions. However, during DI-ATS1, 38% of

preparations experienced spontaneous VTs, 19% experienced rapid pacing induced VTs. Some preparations experienced one or more VT type. In total, 0% of control and 8 of 21 DI-ATS1 preparations experienced some type of VT. During DI-ATS1, all preparations experienced PVCs. PVC frequency for all experiments was normalized to the PVC frequency during DI-ATS1 (Table). PVC frequency during control conditions was significantly lower (by 99.5± 0.3%) than during DI-ATS1 alone (100%, Table). In total, only 2 of 8 preparations during control experienced any type of arrhythmia, all due to PVCs, relative to 17 of 17 preparations with at least one type of arrhythmia (VT and/or PVC) during DI-ATS1 (Table).

APD Shortening During DI-ATS1 Reduces Frequency and Duration of Arrhythmias

Perfusion of pinacidil during DI-ATS1 (DI-ATS1+Pinacidil) shortened the QT_c to near control values as demonstrated by a representative trace in Figure 2.1A (right). Over all experiments, pinacidil shortened QT_c relative to DI-ATS1 (Figure 2.1B); however, QT_c was still prolonged (240.8 ± 5.8ms, Figure 2.1B) relative to control. QT-shortening during DI-ATS1+Pinacidil was associated with an abbreviation of APD relative to DI-ATS1 alone (Figure 2.2A). Specifically, DI-ATS1+Pinacidil significantly shortened APD to 190.6 ± 3.7ms (Figure 2.2B), which was significantly greater relative to control. Additionally, DI-ATS1+Pinacidil significantly shortened APD_{50} to 99.5 ± 6.1ms (Figure 2.2D), which was not significantly different from control. Lastly, DI-ATS1+Pinacidil reduced APD dispersion to 5.0 ± 0.4 ms (Figure 2.2C), which was significantly lower than during control or DI-ATS1 alone.

DI-ATS1+Pinacidil abolished spontaneous VTs, while the incidence of rapid pacing induced VTs was not significantly reduced (6%, Table). Importantly, DI-ATS1+Pinacidil significantly reduced PVC frequency by 79.5±0.1% relative to DI-ATS1 alone (Table), which was significantly greater relative to control (0.5±0.3%). Lastly, the ECG was continuously monitored in a subset of DI-ATS1+Pinacidil preparations (n=5). In this group, all preparations exhibited some form of arrhythmia (VT and/or PVC), which was not significantly different from DI-ATS1 but was significantly greater than control.

Validation of Ratiometric $[Ca^{2+}]_i$ Mapping

In order to quantify relative changes in $[Ca^{2+}]_i$ during ATS1, it was important to validate Ca^{2+} independent drift. The F_{405}/F_{485} drift was measured *in vitro* (see Supplemental Results) and *ex vivo* in Langendorff-perfused guinea pig ventricles (n=3), where recordings were made every 5 minutes for 1 hour. Ca^{2+} transients recorded from the same epicardial site at different exposure times demonstrate an upward shift in the signal consistent with the *in vitro* observations (Figure 2.3A, Exp 1 – black, first exposure, Exp 13 – gray, last exposure). Both diastolic $[Ca^{2+}]_i$ and Ca^{2+} transient amplitude were significantly higher during Exp 13 relative to Exp 1 (Figure 2.3E). Multiple regression analysis revealed a significant correlation of observed drift with cumulative exposure (parameterized as number of exposures). Specifically, diastolic $[Ca^{2+}]_i$ increased at a rate of 3.77% ([95% CI, 3.37-4.17], R^2=0.79) per exposure (Figure 2.3B). Importantly, Ca^{2+} transient duration (Figure 2.4A), QRS duration, and QT interval (Supplemental Figure 2.2) were unaffected by the number of exposures.

Mathematically correcting measured transients by subtracting 3.77% per exposure from the ratiometric fluorescence Ca^{2+} signal resulted in a high degree of morphological correspondence between Ca^{2+} transients recorded several exposures apart (Figure 2.3C). Over all experiments, the mathematical drift correction returned Ca^{2+} transient amplitude and diastolic $[Ca^{2+}]_i$ after 13 exposures to Exp 1 levels (Figure 2.3D & E).

Validation of Ca^{2+} Drift Correction

Under control conditions, rapid pacing (BCL=200 ms, Exp 2, Figure 2.4) significantly increased drift-corrected diastolic $[Ca^{2+}]_i$ by 7.6 ± 1.4% (n = 3) relative to baseline pacing (BCL=400 ms, Exp 1) as demonstrated by representative data in Figure 2.4A. Cessation of rapid pacing (BCL=400, Exp 3) returned drift corrected diastolic $[Ca^{2+}]_i$ to values similar to baseline (BCL=400, Exp 1, 6.7 ± 0.9% decrease). To further validate our ability to measure changes in diastolic $[Ca^{2+}]_i$ we inhibited SERCA2a with 5μM cyclopiazonic acid (CPA), which significantly increased drift-corrected diastolic $[Ca^{2+}]_i$ by 15.2 ± 1.5% (n = 3) relative to control as demonstrated by representative data in Figure 2.4B. All subsequent $[Ca^{2+}]_i$ measurements were therefore corrected for drift. In order to compare relative changes between different experiments, the offset of diastolic $[Ca^{2+}]_i$ was normalized to the offset of diastolic $[Ca^{2+}]_i$ in the first recording of each experiment.

DI-ATS1 Alters $[Ca^{2+}]$ Handling

Representative Ca^{2+} transients in Figure 2.5A, demonstrate that DI-ATS1 shifts the ratiometric Ca^{2+} transients upward. Diastolic $[Ca^{2+}]_i$ during DI-ATS1 was

significantly greater relative to control (by 17.9 ± 1.8%, n = 10, Figure 2.5B). Additionally, DI-ATS1 significantly elevated Ca^{2+} transient amplitude by 18.1 ± 1.3% relative to control (Figure 2.5A and B). Perfusion of pinacidil (15μM) during DI-ATS1 attenuated the upward shift in diastolic $[Ca^{2+}]_i$ (Figure 2.5A). This effect was observed irrespective of the experimental order. For all experiments, DI-ATS1+Pinacidil reduced diastolic $[Ca^{2+}]_i$ by 12.7 ± 1.7% (Figure 2.5C) relative to DI-ATS1 alone; however, diastolic $[Ca^{2+}]_i$ remained significantly greater relative to control (6.5 ± 2.2%). Further, pinacidil did not reverse the rise in Ca^{2+} transient amplitude (Figure 2.5B & C). Specifically, Ca^{2+} transient amplitude during DI-ATS1 was not significantly different after pinacidil perfusion, and therefore, Ca^{2+} transient amplitude during DI-ATS1+Pinacidil remained significantly greater relative to control (19.4 ± 2.3%).

Discussion

Several studies hypothesized that $[Ca^{2+}]_i$ accumulation concomitant with APD prolongation underlies arrhythmias in ATS1[11,17] and DI-ATS1.[6,7] However, $[Ca^{2+}]_i$ accumulation had not been demonstrated in whole heart preparations in part because of methodological difficulties in quantitative $[Ca^{2+}]_i$ measurement using ratiometric Ca^{2+} optical mapping. In this study, we demonstrate that DI-ATS1 was associated with $[Ca^{2+}]_i$ accumulation concomitant with APD prolongation. Attenuating $[Ca^{2+}]_i$ accumulation during DI-ATS1 and reducing APD significantly reduced spontaneous VTs and PVC frequency. Further, programmed electrical stimulation failed to induce arrhythmias despite increased APD dispersion during DI-ATS1. However These data suggest that

APD prolongation in DI-ATS1 is associated with $[Ca^{2+}]_i$ accumulation, which subsequently is associated with the increased arrhythmogenic burden in ATS1.

APD and Arrhythmias in Drug Induced-ATS1

The electrocardiographic features observed in our DI-ATS1 model were consistent with previous experimental studies[6,7] as well as clinical observations:[2] The QT-interval prolonged on the volume-conducted ECG and a double-repolarization wave was observed during DI-ATS, which was not present during control (Figure 2.1A). QT-interval prolongation was associated with APD prolongation quantified from the anterior epicardial surface of guinea pig myocardium (Figure 2.2A), which is consistent with previous experimental and *in silico* studies of ATS1.[5-7,11,17]

Additionally, APD prolonged heterogeneously in DI-ATS1 resulting in increased interventricular APD gradients relative to control. Despite the larger APD gradients, programmed electrical stimulation failed to induce an arrhythmia in any of the hearts tested in this study. This suggests that APD dispersion may have been of insufficient magnitude to precipitate reentrant arrhythmias.[18,19] Successful arrhythmia induction by programmed electrical stimulation previously reported in a guinea pig model of LQT3[20] suggests that occurrence of reentry is not precluded by the size of the guinea pig heart. Further, that study reported a significantly larger APD dispersion than observed in our model, lending credence to the hypothesis that there was insufficient dispersion of repolarization in our model for reentry to occur. Therefore, our data argue against involvement of dispersion of repolarization on arrhythmogenesis in our model, but do not completely rule out its involvement. Further, it is important to note that the

methodologies used in the present study also preclude the assessment of transmural dispersion of repolarization. However, Tsuboi et al. concluded that transmural dispersion of repolarization gradients were insufficient for arrhythmia induction by programmed electrical stimulation in a canine LV wedge model of DI-ATS1.[5] Taken together, these data still suggest that the degree of dispersion observed in DI-ATS1 was likely insufficient for re-entrant arrhythmia induction.

In order to test the effects of APD abbreviation on the DI-ATS1 phenotype, we perfused pinacidil, an ATP-sensitive potassium channel opener. Pinacidil decreased APD gradients in DI-ATS1 below those observed in DI-ATS1 alone or control and reduced the incidence of arrhythmias but did not abolish them. Specifically, PVC frequency, a marker of arrhythmia vulnerability,[21,22] during pinacidil perfusion was lower relative to DI-ATS1 but still higher relative to control. Therefore, these data suggest that gradients of repolarization in DI-ATS1 are unlikely to be a significant substrate for arrhythmias in this condition.

On the other hand, pinacidil attenuated the rise in APD_{50} due to DI-ATS1 such that APD_{50} during control and DI-ATS1+Pinacidil were not significantly different. Therefore, the observation that arrhythmias were reduced but still present during DI-ATS1+Pinacidil further suggests that these arrhythmias are not correlated to APD_{50} or action potential plateau prolongation.

Both conditions, DI-ATS1 and DI-ATS1+Pinacidil, exhibited final repolarization (APD) prolongation and $[Ca^{2+}]_i$ accumulation relative to control. These findings suggest two mechanisms, which may not necessarily be independent. Specifically, prolongation of final repolarization, as estimated by APD could also be a substrate for increased

triggered activity in DI-ATS1. The hypothesis that APD prolongation leads to recovery from inactivation of L-type calcium channels is not well supported by changes in APD_{50}, but could be supported by total APD prolongation. However, it is well established that APD prolongation can increase $[Ca^{2+}]_i$ accumulation.[10] Therefore, triggered activity observed in our DI-ATS1 model, still suggests a prominent, but not necessarily exclusive role for $[Ca^{2+}]_i$ accumulation as an arrhythmia mechanism in DI-ATS1

Proposed Arrhythmia Mechanism in ATS1

Arrhythmias in ATS1 patients are often preceded by a high PVC incidence, presumably due to triggered activity, and PVC burden in ATS1 is exacerbated by hypokalemia.[3,24] Importantly, it has been demonstrated that hypokalemia alone leads to $[Ca^{2+}]_i$ accumulation and the increased incidence of arrhythmias.[25] Based on these findings, the following mechanism of increased incidence of arrhythmias has been proposed. $[Ca^{2+}]_i$ accumulation is associated with increased sarcoplasmic reticular Ca^{2+} loading and an increased propensity for triggered activity, presumably due to spontaneous Ca^{2+} release from the sarcoplasmic reticulum.[23] The resultant spontaneous Ca^{2+} release may lead to depolarization via transient inward currents carried by the forward mode Na^+/Ca^{2+} exchanger, facilitating triggered activity.[8-10] This lead to the hypothesis that $[Ca^{2+}]_i$ accumulation, secondary to hypokalemia underlies triggered activity in ATS1 or DI-ATS1.[6,7]

Sung et al. tested this hypothesis in an *in silico* study and suggested a role for abnormal $[Ca^{2+}]_i$ cycling in ATS1-associated arrhythmias.[11] This was indirectly affirmed by Morita et al., who reported that Ca^{2+} channel blockade by verapamil abolished all

arrhythmic activity in a canine LV wedge model of DI-ATS1.[6] However, $[Ca^{2+}]_i$ accumulation during DI-ATS1 has not been previously demonstrated in an *ex-vivo* intact ventricular model.

Validation of Ratiometric Calcium Mapping

In order to assess the effects of DI-ATS1 on $[Ca^{2+}]_i$ handling, it is important to characterize any Ca^{2+} independent changes in Indo-1 fluorescence. Despite previous calibration attempts,[26] many reports indicated that incomplete de-esterification of Indo-1/AM, along with excitation-intensity dependent photo-bleaching of Indo-1 affect ratiometric fluorescent Ca^{2+} measurement.[27-30] Specifically, the fluorescent signals corresponding to bound and unbound Indo-1 (F_{405} and F_{485} respectively) drift toward zero at two different rates, resulting in an apparent decrease in the ratiometric Ca^{2+} signal.[28] In our experimental setup, individual fluorescent Ca^{2+} signals (F_{405} and F_{485}) also decreased, yet the ratiometric Ca^{2+} increased (Supplemental Figure 2.1A). These seemingly contradictory findings could be attributed to the following experimental differences: the choices of dye of Indo-1 versus the ester form of Indo-1 (Indo-1/AM), emission filters, and/or photo-detector spectral response. The relative drift rates of the F_{405} and F_{485} signals will dictate whether the ratiometric signal drifts upward or downward.

Importantly, future studies that measure $[Ca^{2+}]_i$ over time should validate $[Ca^{2+}]_i$ response as a function of exposure.[28,30] The absence of concomitant changes in ECG parameters or Ca^{2+} transient duration (Supplemental Figure 2.2), suggest that these changes in fluorescent Ca^{2+} signals may be dye-related rather than physiological in origin. Importantly, mathematical correction of ratiometric fluorescent Ca^{2+} transients by

subtracting the observed drift from the signal resulted in a high degree of morphological correspondence between ratiometric transients recorded several exposures apart (Figure 2.3C). Lastly, the optically measured, drift-corrected diastolic $[Ca^{2+}]_i$ increased during rapid pacing and returned to baseline upon cessation of rapid pacing (Figure 2.4A), which is consistent with previous studies.[31,22] Likewise, SERCA2a inhibition by 5μM CPA perfusion lead to $[Ca^{2+}]_i$ accumulation as was previously demonstrated.[32] Therefore, this mathematical drift correction was applied to all subsequent recordings.

DI-ATS1 Alters $[Ca^{2+}]_i$ Handling

DI-ATS1 was associated with a significant rise in $[Ca^{2+}]_i$ as reflected in both diastolic $[Ca^{2+}]_i$ and Ca^{2+} transient amplitude, and an increased incidence of ventricular arrhythmias. These data are the first direct evidence in an intact ventricular preparation for $[Ca^{2+}]_i$ accumulation during DI-ATS1. Furthermore, these data are consistent with the theoretical mechanisms proposed for arrhythmias in ATS1.[6,7,11] More generally, the finding that $[Ca^{2+}]_i$ accumulation concomitant with APD prolongation is related to increased arrhythmia propensity is also consistent with previous studies utilizing alternative methods of $[Ca^{2+}]_i$ loading to increase the incidence of triggered activity.[8-10,21,22] Future studies, however, are necessary to elucidate the relationship between the extent of $[Ca^{2+}]_i$ accumulation, APD prolongation, and the origin of triggered activity during DI-ATS1.

Conclusion

This study suggests that arrhythmias during DI-ATS1 may be a result of triggered activity secondary to prolonged APD and altered $[Ca^{2+}]_i$ cycling and less likely dependent on large gradients of repolarization acting as a substrate for reentrant arrhythmias. Therefore, ameliorating myocyte $[Ca^{2+}]_i$ load may prove a more effective therapeutic goal in ATS1 compared to decreasing APD gradients.

Limitations

While APD gradients in guinea pig (present study) or canine[5] were not associated with increased arrhythmia propensity, it is known that APD distribution and heterogeneity varies between animal models.[33,34] The nature of electrophysiological remodeling induced by chronic functional I_{K1} down-regulation, as occurs in patients with ATS1, remains unclear.[5-7,11,17] Furthermore, it is well appreciated that pharmacological models of cardiac disease should be interpreted cautiously due to the acute nature of the study as well as the specificity of the intervention.[35]

References

1. Plaster NM, Tawil R, Tristani-Firouzi M, et al: Mutations in Kir2.1 cause the developmental and episodic electrical phenotypes of Andersen's syndrome. *Cell* 2001;105:511-9.

2. Tristani-Firouzi M, Jensen JL, Donaldson MR, et al: Functional and clinical characterization of KCNJ2 mutations associated with LQT7 (Andersen syndrome). *J Clin Invest* 2002;110:381-8.

3. Tawil R, Ptacek LJ, Pavlakis SG, et al: Andersen's syndrome: potassium-sensitive periodic paralysis, ventricular ectopy, and dysmorphic features. *Ann Neurol* 1994;35:326-30.

4. Zhang L, Benson DW, Tristani-Firouzi M, et al: Electrocardiographic features in Andersen-Tawil syndrome patients with KCNJ2 mutations: characteristic T-U-wave patterns predict the KCNJ2 genotype. *Circulation* 2005;111:2720-6.

5. Tsuboi M, Antzelevitch C: Cellular basis for electrocardiographic and arrhythmic manifestations of Andersen-Tawil syndrome (LQT7). *Heart Rhythm* 2006;3:328-35.

6. Morita H, Zipes DP, Morita ST, Wu J: Mechanism of U wave and polymorphic ventricular tachycardia in a canine tissue model of Andersen-Tawil syndrome. *Cardiovasc Res* 2007;75:510-8.

7. Poelzing S, Veeraraghavan R: Heterogeneous ventricular chamber response to hypokalemia and inward rectifier potassium channel blockade underlies bifurcated T wave in guinea pig. *Am J Physiol Heart Circ Physiol* 2007;292:H3043-51.

8. Marban E, Robinson SW, Wier WG: Mechanisms of arrhythmogenic delayed and early afterdepolarizations in ferret ventricular muscle. *J Clin Invest* 1986;78:1185-92.

9. Nuss HB, Kaab S, Kass DA, Tomaselli GF, Marban E: Cellular basis of ventricular arrhythmias and abnormal automaticity in heart failure. *Am J Physiol* 1999;277:H80-91.

10. Volders PG, Vos MA, Szabo B, et al: Progress in the understanding of cardiac early afterdepolarizations and torsades de pointes: time to revise current concepts. *Cardiovasc Res* 2000;46:376-92.

11. Sung RJ, Wu SN, Wu JS, Chang HD, Luo CH: Electrophysiological mechanisms of ventricular arrhythmias in relation to Andersen-Tawil syndrome under conditions of reduced IK1: a simulation study. *Am J Physiol Heart Circ Physiol* 2006;291:H2597-605.

12. Silva J, Rudy Y: Mechanism of pacemaking in I(K1)-downregulated myocytes. *Circ Res* 2003;92:261-3.

13. Brandes R, Figueredo VM, Camacho SA, Massie BM, Weiner MW: Suppression of

motion artifacts in fluorescence spectroscopy of perfused hearts. *Am J Physiol* 1992;263:H972-80.

14. Kong W, Walcott GP, Smith WM, Johnson PL, Knisley SB: Emission ratiometry for simultaneous calcium and action potential measurements with coloaded dyes in rabbit hearts: reduction of motion and drift. *J Cardiovasc Electrophysiol* 2003;14:76-82.

15. Katra RP, Pruvot E, Laurita KR: Intracellular calcium handling heterogeneities in intact guinea pig hearts. *Am J Physiol Heart Circ Physiol* 2004;286:H648-56.

16. Girouard SD, Pastore JM, Laurita KR, Gregory KW, Rosenbaum DS: Optical mapping in a new guinea pig model of ventricular tachycardia reveals mechanisms for multiple wavelengths in a single reentrant circuit. *Circulation* 1996;93:603-13.

17. Seemann G, Sachse FB, Weiss DL, Ptacek LJ, Tristani-Firouzi M: Modeling of IK1 mutations in human left ventricular myocytes and tissue. *Am J Physiol Heart Circ Physiol* 2007;292:H549-59.

18. Akar FG, Rosenbaum DS: Transmural electrophysiological heterogeneities underlying arrhythmogenesis in heart failure. *Circ Res* 2003;93:638-45.

19. Coronel R, Wilms-Schopman FJ, Opthof T, Janse MJ: Dispersion of repolarization and arrhythmogenesis. *Heart Rhythm* 2009;6:537-43.

20. Restivo M, Caref EB, Kozhevnikov DO, El-Sherif N: Spatial dispersion of repolarization is a key factor in the arrhythmogenicity of long QT syndrome. *J Cardiovasc Electrophysiol* 2004;15:323-31.

21. Laurita KR, Katra RP: Delayed after depolarization-mediated triggered activity associated with slow calcium sequestration near the endocardium. *J Cardiovasc Electrophysiol* 2005;16:418-24.

22. Katra RP, Laurita KR: Cellular mechanism of calcium-mediated triggered activity in the heart. *Circ Res* 2005;96:535-42.

23. Diaz ME, Trafford AW, O'Neill SC, Eisner DA: Measurement of sarcoplasmic reticulum Ca2+ content and sarcolemmal Ca2+ fluxes in isolated rat ventricular myocytes during spontaneous Ca2+ release. *J Physiol* 1997;501 (Pt 1):3-16.

24. Nichols CG, Makhina EN, Pearson WL, Sha Q, Lopatin AN: Inward rectification and implications for cardiac excitability. *Circ Res* 1996;78:1-7.

25. Tribulova N, Manoach M, Varon D, Okruhlicova L, Zinman T, Shainberg A: Dispersion of cell-to-cell uncoupling precedes low K+-induced ventricular fibrillation. *Physiol Res* 2001;50:247-59.

26. Brandes R, Figueredo VM, Camacho SA, Baker AJ, Weiner MW: Quantitation of cytosolic. *Biophys J* 1993;65:1973-82.

27. Wahl M, Lucherini MJ, Gruenstein E: Intracellular Ca2+ measurement with Indo-1 in substrate-attached cells: advantages and special considerations. *Cell Calcium* 1990;11:487-500.

28. Scheenen WJ, Makings LR, Gross LR, Pozzan T, Tsien RY: Photodegradation of indo-1 and its effect on apparent Ca2+ concentrations. *Chem Biol* 1996;3:765-74.

29. Luckhoff A: Measuring cytosolic free calcium concentration in endothelial cells with indo-1: the pitfall of using the ratio of two fluorescence intensities recorded at different wavelengths. *Cell Calcium* 1986;7:233-48.

30. Lee HC, Mohabir R, Smith N, Franz MR, Clusin WT: Effect of ischemia on calcium-dependent fluorescence transients in rabbit hearts containing indo 1. Correlation with monophasic action potentials and contraction. *Circulation* 1988;78:1047-59.

31. Laurita KR, Katra R, Wible B, Wan X, Koo MH: Transmural heterogeneity of calcium handling in canine. *Circ Res* 2003;92:668-75.

32. Abe F, Karaki H, Endoh M: Effects of cyclopiazonic acid and ryanodine on cytosolic calcium and contraction in vascular smooth muscle. *Br J Pharmacol* 1996;118:1711-6.

33. Liu DW, Antzelevitch C: Characteristics of the delayed rectifier current (IKr and IKs) in canine ventricular epicardial, midmyocardial, and endocardial myocytes. A weaker IKs contributes to the longer action potential of the M cell. *Circ Res* 1995;76:351-65.

34. Warren M, Guha PK, Berenfeld O, et al: Blockade of the inward rectifying potassium current terminates ventricular fibrillation in the guinea pig heart. *J Cardiovasc Electrophysiol* 2003;14:621-31.

35. Baker LC, Wolk R, Choi BR, et al: Effects of mechanical uncouplers, diacetyl monoxime, and cytochalasin-D on the electrophysiology of perfused mouse hearts. *Am J Physiol Heart Circ Physiol* 2004;287:H1771-9.

TABLE: Ventricular Preperations Exhibiting Arrhythmias

Arrhythmia type:	Control	DI-ATS1	DI-ATS1 + Pin
Programmed Stimulated VT or PVC	-	0/6	0/6
Spontaneous VT	0/8	8/21*	0/16†
Rapid Pacing VT	0/4	4/21	1/16
Preparations exhibiting VTs	0/8	8/21*	1/16†
PVC frequency (% of ATS1)	0.5±0.3%	100%‡	20.5±0.1%‡§
Arrhythmic Preparations	2/8	17/17*	5/5*

PVC frequency: normalized to the PVC frequency (number of PVCs/min) during DI-ATS1
Arrhythmic Preparation: Preparations exhibiting VT's and/or PVCs.
* Fisher's Exact test for one-tailed probability vs. control $p < 0.05$
† Fisher's Exact test for one-tailed probability vs. DI-ATS1 $p < 0.05$
‡ Two-tailed Student's *t*-test vs. control, $p < 0.05$
§ Two-tailed Student's *t*-test vs. ATS1, $p < 0.05$

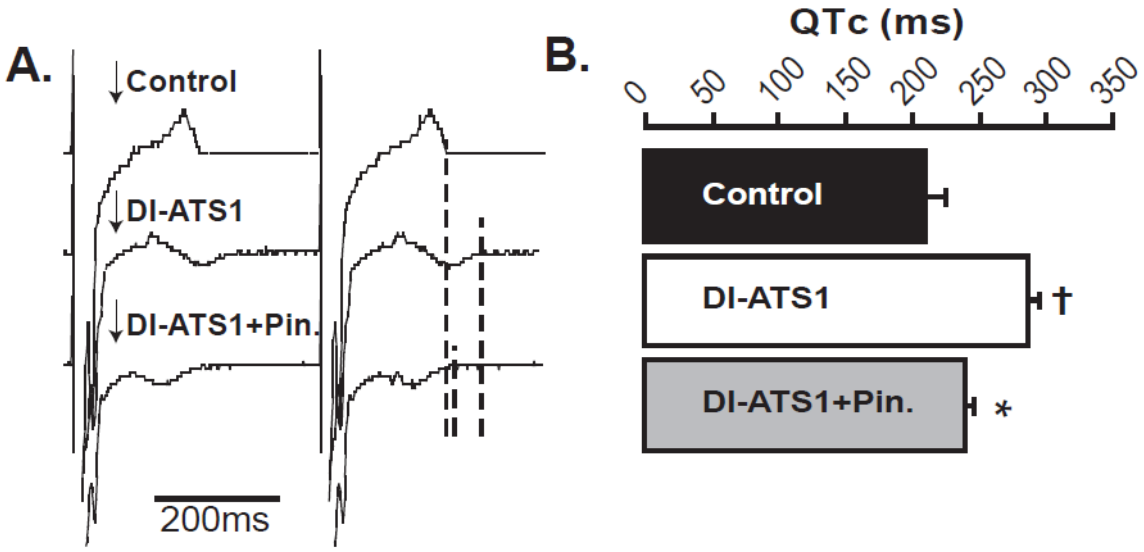

Figure 2.1: Volume-conducted ECG. A) Representative volume-conducted ECGs obtained during control (top), DI-ATS1 (middle), and DI-ATS1 and 15μM pinacidil (bottom). DI-ATS1 is associated with a bifurcated T-wave, while pinacidil perfusion abolished such morphology. **B)** DI-ATS1 increased QTc compared to control (†, $p < 0.05$, n = 6). Pinacidil (15μM) perfusion decreased QTc compared to DI-ATS1 alone; however, it was still longer relative to control (*, $p < 0.05$, relative to control and DI-ATS1).

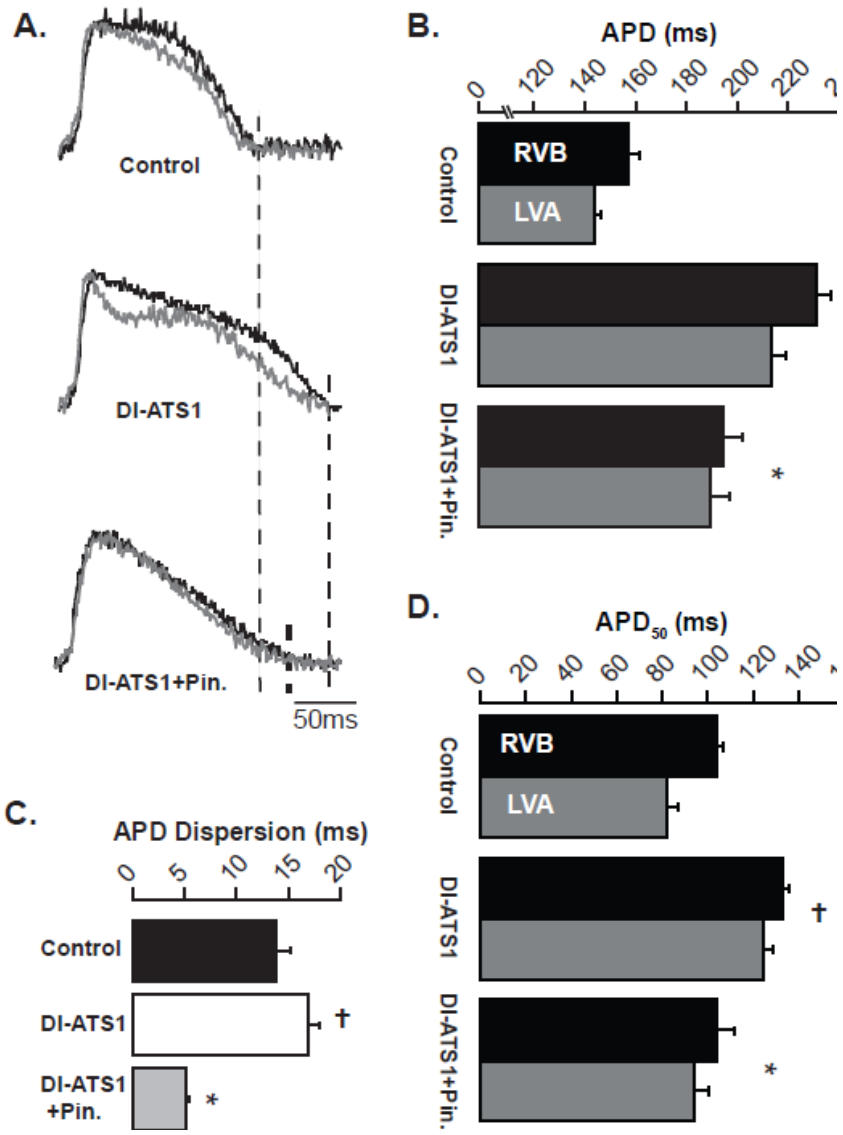

Figure 2.2: DI-ATS1 Increases APD. A) Representative optical action potentials recorded from the same ventricular regions (RVB – black and LVA – gray) during control (top), DI-ATS1 (middle) and DI-ATS1 and 15μM pinacidil (bottom). DI-ATS1 prolonged the APD and enhanced total APD dispersion, defined as the difference in mean APD (calculated over 25 spatially contiguous sites per region) between epicardial regions with the longest (RVB) and shortest APD (LVA). Pinacidil (15μM) perfusion reversed both phenomena. **B)** Mean APDs demonstrate a rise in APD during DI-ATS1 compared to control (†, $p < 0.05$, n = 6) that was mitigated by pinacidil (15μM) perfusion (*, $p < 0.05$ relative to DI-ATS1 alone). However, APD after pinacidil (15μM) perfusion remained prolonged relative to control (*, $p < 0.05$). **C)** Total APD dispersion was greater during DI-ATS1 relative to control (†, $p < 0.05$). Pinacidil (15μM) perfusion decreased dispersion relative to both control and DI-ATS1 (*, $p < 0.05$). **D)** Mean APD_{50} demonstrate a rise in APD_{50} during DI-ATS1 compared to control (†, $p < 0.05$, n = 6) that was mitigated by pinacidil (15μM) perfusion (*, $p < 0.05$ relative to DI-ATS1 alone).

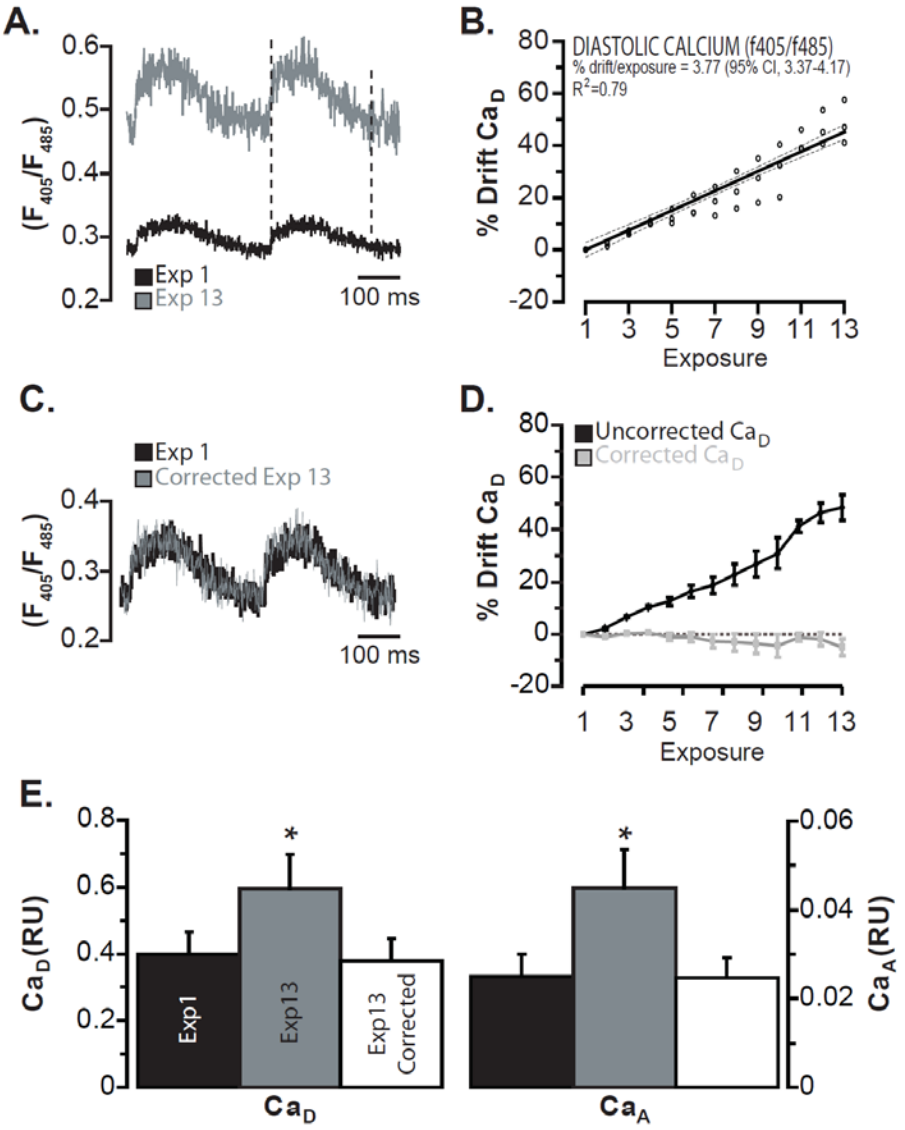

Figure 2.3: *Ex Vivo* Characterization of Ca^{2+} Drift. A) Representative ratiometric Ca^{2+} transients (black – Exp 1, gray – Exp 13) recorded during repeated exposures to excitation light at 5 minute intervals. The 13th exposure (Exp 13) exhibited an upward shift of Ca^{2+} transients relative to the first recording (Exp 1). **B)** Multiple regression analysis of diastolic $[Ca^{2+}]_i$ (Ca_D) drift (n = 3) revealed a significant correlation between the drift and the number of exposures. Drift = 3.77% ([95% CI 3.37-4.17], R^2=0.79) increase in Ca_D per exposure. **C)** Representative Ca^{2+} transients from Exp 1 (black) and drift corrected Ca^{2+} transients from Exp 13 (grey). Subtraction of Ca_D drift leads to high degree of morphological correspondence between Ca^{2+} transients recorded several exposures apart. **D)** Pooled Ca_D data depicting % Ca_D drift per exposure (black). Correction for observed drift leads to no change in Ca_D (grey). Dotted grey line marks zero level. **E)** Summary data for all experiments depicting changes in Ca_D (left) and Ca^{2+} transient amplitude (Ca_A) (right) secondary to exposure. During last recording (Exp 13) both Ca_D and Ca_A rose significantly (*, $p < 0.05$ vs. Exp 1). Drift correction returned both parameters to baseline.

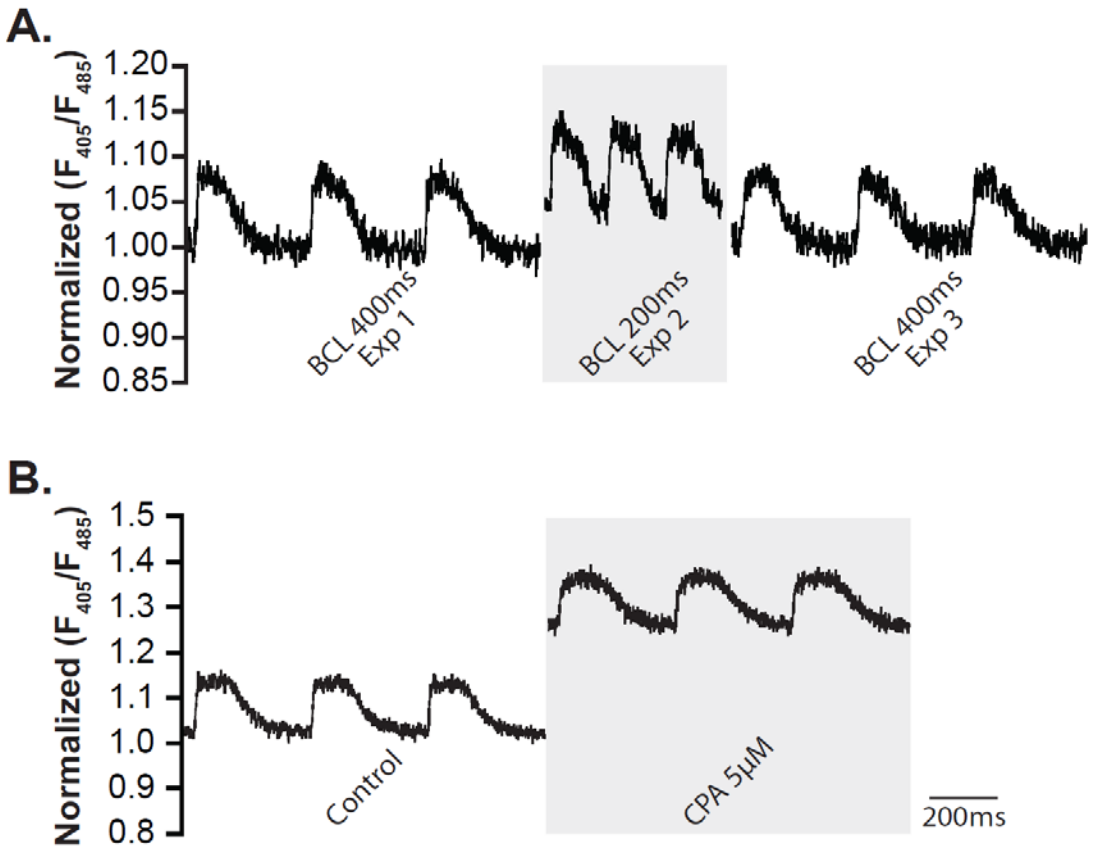

Figure 2.4: *Ex Vivo* Validation of Ca^{2+} Drift Correction. A) Representative drift-corrected, Ca^{2+} transients during baseline pacing at BCL 400ms (left), followed by rapid pacing at BCL 200 and subsequent return to baseline pacing. Diastolic $[Ca^{2+}]_i$ (Ca_D) after mathematical correction were normalized to Ca_D in the first recording. Rapid pacing significantly increased Ca_D, while a return to baseline pacing reversed the rise in Ca_D. **B)** Representative drift-corrected Ca^{2+} transients recorded during control (left), followed by (5μM) cyclopiazonic acid (CPA) perfusion. CPA perfusion significantly increased Ca_D.

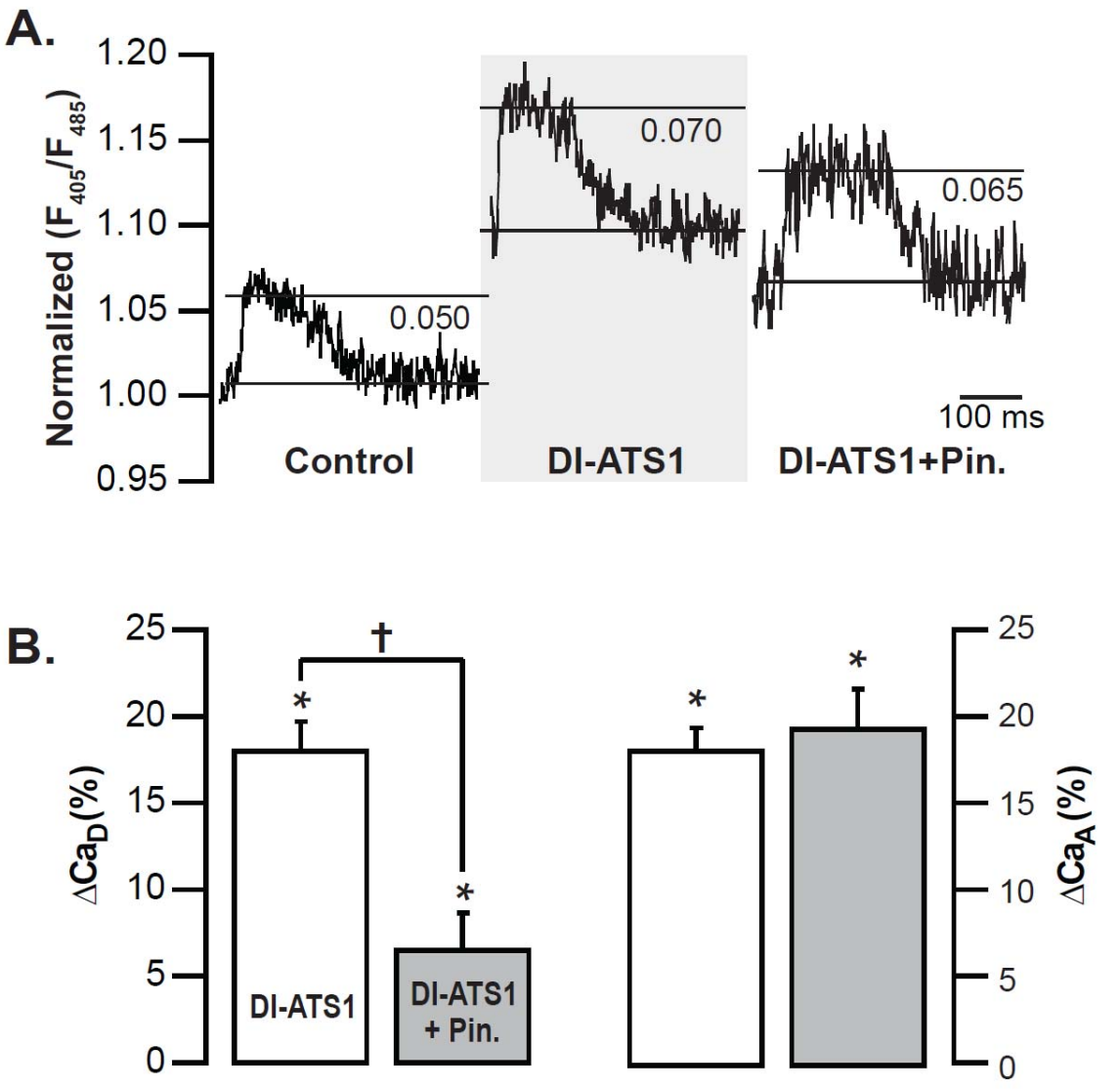

Figure 2.5: DI-ATS1 Alters [Ca^{2+}] Handling. A) Representative drift-corrected Ca^{2+} transients recorded during control, DI-ATS1 and (15μM) pinacidil perfusion. During DI-ATS1, Ca^{2+} transients were shifted upward, while pinacidil partially reversed that shift. Both DI-ATS1 and DI-ATS1 with pinacidil exhibit greater Ca^{2+} transient amplitude (Ca_A) (horizontal lines) relative to control. **B)** Summary of ΔCa_D (left) and ΔCa_A (right) relative to control. DI-ATS1 significantly increased Ca_D and Ca_A relative to control (*, $p < 0.05$, n = 10). Pinacidil perfusion (15μM) decreased Ca_D relative to DI-ATS1 alone (†, $p < 0.05$). Pinacidil did not completely revert Ca_D to control levels (*, $p < 0.05$). Pinacidil had no effect on Ca_A relative to DI-ATS1 alone.

Appendix

Supplemental Materials

Optical voltage mapping. Optical voltage mapping was performed as previously described.[1] Briefly, we used two SciMedia MiCam02 HS CCD cameras (SciMedia) in a tandem lens configuration capable of resolving membrane potential changes as small as 2 mV with 1 ms temporal resolution from 90 x 60 sites simultaneously. The hearts were stained by direct coronary perfusion for 10 minutes with the voltage-sensitive indicator di-4-ANEPPS (Molecular Probes) at a final concentration of 15 μmol/L. The dye in the preparation was excited by three-60 LED light sources (RL5-A9018, Superbrightleds) fitted with 510 ± 5 nm filters (Chroma) and a 50 mm aspheric lens (Edmund Optics). Fluorescent light passed through a 150 mm achromatic (BK7/Flint) lens and was incident on a 565DXR dichroic mirror (Chroma) set at 45º angles to the recording surface. Transmitted light passed through a 50 mm aspheric B270 crown glass lens (Edmund Optics), a 35 mm planoconvex BK7 lens (Edmund Optics), and a 610 nm LP filter (Newport) before it was incident on the CCD array. Reflected light passed through a 50-mm aspheric B270 crown glass (Edmund Optics), a 35-mm planoconvex BK7 lens (Edmund Optics), and a 540 ± 10 nm filter (Chroma) where it was incident on the second CCD array. CCD arrays were optically aligned at fixed and equal optical path lengths. The interpixel resolution was 0.184 mm in the x-direction (90 pixels) and 0.199 mm in the y-direction (60 pixels). The relative change in voltage (V_m) was defined as $V_m = \Delta F_{610}/\Delta F_{540}$, where ΔF represents the change in fluorescence for a particular wavelength.

Optical Ca^{2+} mapping. We developed an optical mapping system capable of recording high-fidelity fluorescent signals at two wavelengths simultaneously with high

spatial and temporal resolution.[2] Once again we used two SciMedia MiCam02 HS CCD cameras (SciMedia) in a tandem lens configuration capable of resolving membrane potential changes with 1-ms temporal resolution from 90 x 60 sites simultaneously. Before dye loading, background fluorescence representing tissue autofluorescence was recorded at both emission wavelengths (485 nm and 405 nm). The heart was then loaded for 45 min with Indo-1/AM (Invitrogen) at a final concentration of 1 μmol/L. The dye-loading period was followed by a 15-min washout period. All recordings made after Indo-1 loading include fluorescence originating from the dye and the tissue (background fluorescence). Excitation light obtained from a 1000-W mercury arc lamp (Thermo-Oriel) was filtered at 350 ± 10 nm (Chroma) and directed through a flexible liquid light guide (Thermo-Oriel) to the preparation. Fluorescent light passed through a 150 mm achromatic (BK7/Flint) lens and was incident on a 445-nm dichroic long-pass mirror (Chroma) set at 45º angle to the recording surface to transmit wavelengths above 445 nm on to one CCD array and reflect wavelengths below 445 nm on to another. Transmitted and reflected fluorescent light passed through 50 mm aspheric B270 crown glass lenses (Edmund Optics), 35 mm planoconvex BK7 lenses (Edmund Optics) and was limited to 485 ± 10 and 405 ± 10 nm (Chroma), respectively, before it was incident on the respective CCD arrays. CCD arrays were optically aligned at fixed and equal optical path lengths. Ratiometric Ca^{2+} transients were determined by dividing the background-subtracted fluorescence Ca^{2+} transients at 405 nm by the background-subtracted fluorescence calcium transients at 485 nm.

$$\text{Ratio} = \frac{F_{405}}{F_{405}} = \frac{\Delta F_{405} - F_{405\text{-Background}}}{\Delta F_{485} - F_{485\text{-Backgroun}}}$$

Where ΔF is the actual change in fluorescent amplitudes in the cameras after 405 or 485 bandpass filtering. The shorthand F_{405}/F_{485} is an abbreviation to represent the calculated ratiometric Ca^{2+} signal.

Validation of ratiometric flourescent $[Ca^{2+}]_i$ mapping. In order to quantify Ca^{2+} handling dysregulation in DI-ATS1, it was important to validate a Ca^{2+} optical mapping system which would allow for temporal estimation of $[Ca^{2+}]_i$. To this end, vials containing varying concentrations of Ca^{2+} (0, 0.04, 0.07, 0.08, 0.1, 0.23, 0.35, 1, 1.35, 3 μM) and 0.1 μM Indo-1 were exposed to excitation light and recorded at different frequencies of illumination. During the first exposure (Exp 1) of a vial containing 0.1μM Ca^{2+} and 0.1 μM Indo-1 with a 385 nm light source, fluorescent intensity in both cameras decreased monotonically as a function of time (Supplemental Figure 2.1A, Exp 1 - 405 nm-gray trace and 485 nm-black trace). Of note, the fluorescence signals in Supplemental Figure 2.1A were normalized to the fluorescent intensity at the first time point in the first recording (Exp 1) in order to visually demonstrate signal drift. Importantly, in this example the 485 nm fluorescent signal (F_{485}) decreased at a significantly faster rate than the 405 nm fluorescent signal (F_{405}) as determined by multiple regression analysis -0.080% [95% CI, -0.085 – -0.075] per second vs -0.024% [95% CI, -0.027 – -0.020] per second. While not visually apparent, this drift translated into a rise in the ratiometric signal (F_{405}/F_{485}) within a single recording (Supplemental Figure 2.1B, Exp 1). Specifically, the slope of the f405/f485 signal was significantly greater than 0 during a single exposure (0.023% [95% CI, 0.006 – 0.039] per 1 second).

Representative data in Supplemental Figure 2.1A demonstrates that the F_{485} signal again decreased significantly more than the F_{405} signal after 7 consecutive exposures

performed over 15 minutes (Supplemental Figure 2.1A Exp 7, last exposure vs. Exp 1, first exposure). Consequently, F_{405}/F_{485} during Exp 7 was elevated relative to Exp 1 (Supplemental Figure 2.1B). Additionally, consecutive ratiometric optical [Ca^{2+}] measurements were made from vials containing either 0.1μM or 1μM [Ca^{2+}] with an exposure frequency of 1 exposure per 5 minutes (n=12). There was no noticeable difference in F signal drift between the two [Ca^{2+}] (7.22% per exposure [95% CI, 5.10 – 9.35], R^2=0.68 vs 5.85% [95% CI, 3.90 – 7.81], R^2=0.62 for 0.1 μM and 1 μM $[Ca^{2+}]_o$, respectively). Therefore, data were pooled from all experiments (n=57). Multiple regression analysis of pooled measurements made at different exposure frequencies (1 exposure per 2.5, 5 and 15 minutes, n = 10, 30 and 17, respectively) revealed a significant correlation of the ratiometric drift with the number of exposures (Supplemental Figure 2.1C), where ratiometric Ca^{2+} fluorescence drifted at a rate of 5.98% ([95% CI 5.52-6.44], R^2=0.63) per exposure.

References

1. Poelzing S, Veeraraghavan R. Heterogeneous ventricular chamber response to hypokalemia and inward rectifier potassium channel blockade underlies bifurcated T wave in guinea pig. Am J Physiol Heart Circ Physiol. 2007 Jun;292(6):H3043-51.

2. Katra RP, Pruvot E, Laurita KR. Intracellular calcium handling heterogeneities in intact guinea pig hearts. Am J Physiol Heart Circ Physiol. 2004 Feb;286(2):H648-56.

Supplemental Figure 2.1: *In Vitro* characterization of Ca^{2+} fluorescence drift. A) Representative fluorescent Ca^{2+} signals (gray – F_{405}, black – F_{485}) of a vial containing 0.1μM [Ca^{2+}] and 0.1 μM Indo-1 during the first (Exp 1) and last exposures (Exp 7). In this example during Exp 1, F_{485} decreased faster relative to F_{405} (-0.080% [95% CI, -0.085 – -0.075] per second vs -0.024% [95% CI, -0.027 – -0.020] per second, respectively). After 7 exposures (Exp 7), both F_{405} and F_{485} decreased relative to the first recording (Exp 1). **B)** Representative ratiometric fluorescent Ca^{2+} signals corresponding to the F_{405} and F_{485} in Figure 2.3A. The drift in F_{405} and F_{485} during Exp 1 translated into a rise in F_{405}/F_{485} within the recording (0.023% [95% CI, 0.006 – 0.039] per 1 second). After 7 exposures (Exp 7) ratiometric fluorescent Ca^{2+} signals was enhanced relative to Exp 1. **C)** Multiple regression analysis of drift measurements pooled from all experiments (n=57) conducted at different exposure frequencies. The drift demonstrated a significant correlation with the number of exposures with rate of 5.98% ([95% CI 5.52-6.44], R^2=0.63) increase in ratiometric Ca^{2+} fluorescence per exposure.

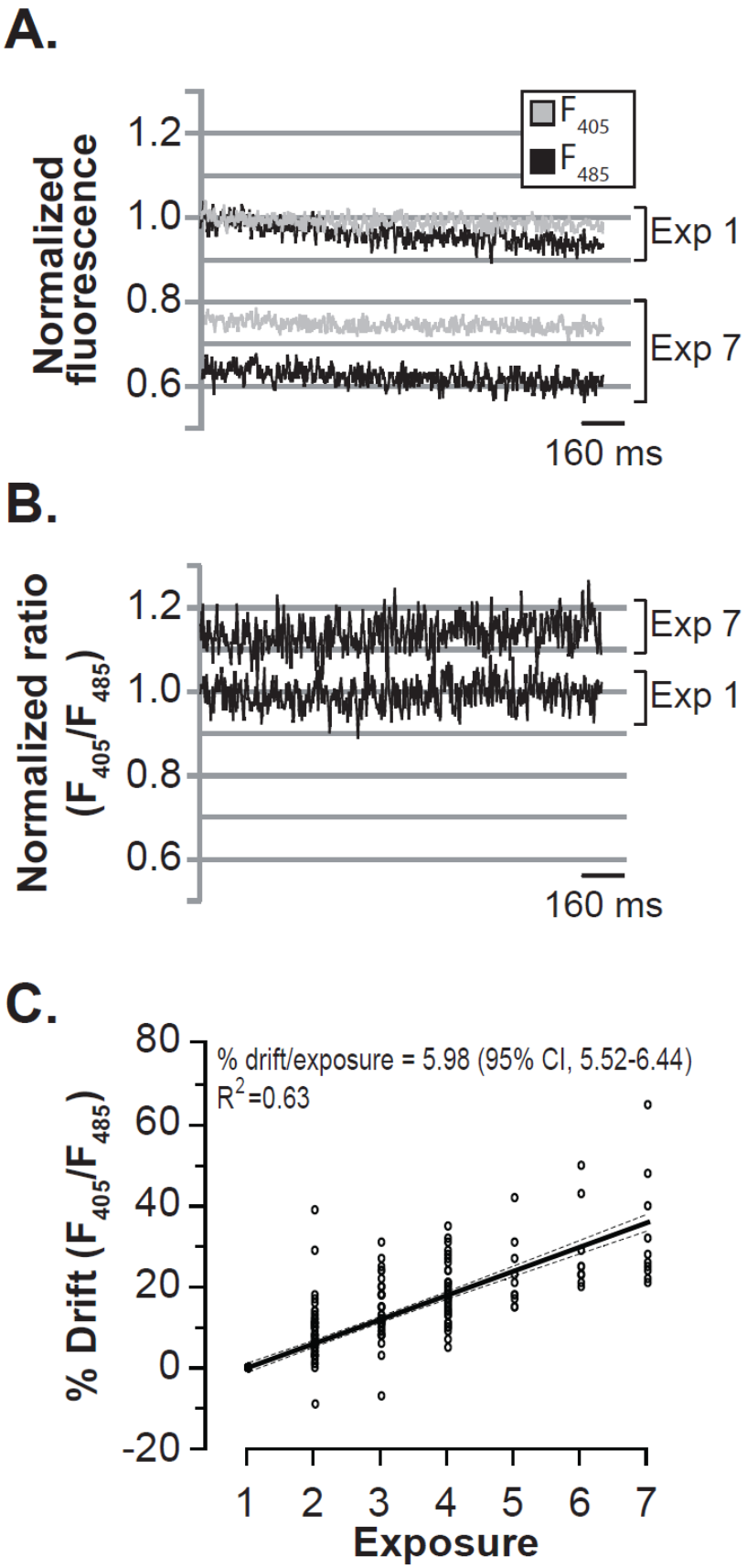
A.
Normalized fluorescence
1.2
1.0
0.8
0.6
F405
F485
Exp 1
Exp 7
160 ms
B.
Normalized ratio (F405/F485)
1.2
1.0
0.8
0.6
Exp 7
Exp 1
160 ms
C.
% Drift (F405/F485)
80
60
40
20
0
-20
% drift/exposure = 5.98 (95% CI, 5.52-6.44)
R2=0.63
1
2
3
4
5
6
7
Exposure

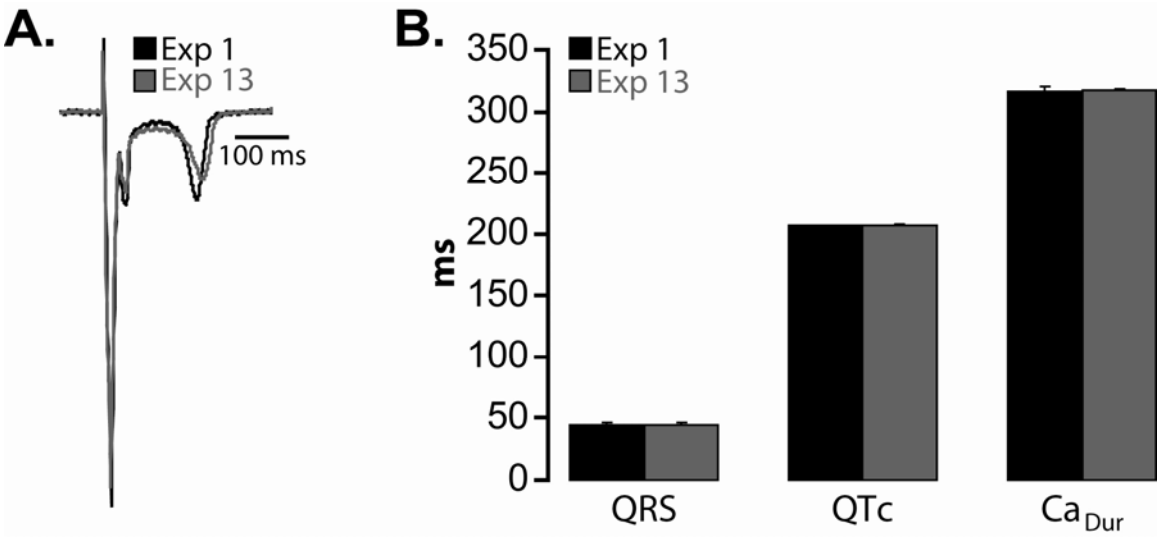

Supplemental Figure 2.2: Effect of time on Ca_{Dur} and ECG parameters. A) Representative volume-conducted ECGs recorded under control conditions to assess Ca^{2+}-independent changes in indo-1 fluorescence. No changes in the ECG morphology were observed between the first (Exp 1 – black) and last recordings (Exp 13 – grey). **B)** Summary data (n = 3) depicting no significant difference in QRS, QT_c, and Ca^{2+} transients duration (Ca_{Dur}) between the first (Exp 1 – black) and last recordings (Exp 13 – grey).

CHAPTER 3

NCX DOMINANCE IS AN IMPORTANT DETERMINANT FOR PREMATURE ACTIVITY PROPENSITY IN A DRUG INDUCED MODEL OF ANDERSEN-TAWIL SYNDROME

Introduction

Anderson-Tawil Syndrome (ATS1) is an autosomal dominant inherited channelopathy linked to a loss of function mutation in *KCNJ2*, the gene that encodes the Kir2.1 channel which is responsible for carrying the inward-rectifier K^+ current.[1] ATS1 is characterized by a mild QT prolongation and ventricular arrhythmias that are initiated by frequent, hypokalemia-exacerbated, premature ventricular activity (PVA).[1] These triggered events have been linked to abnormal Ca^{2+} regulation,[2] particularly elevated diastolic cytosolic Ca^{2+} levels (Ca_D) and presumed sarcoplasmic reticulum (SR) Ca^{2+} overload.[3] However, the relationship between regional perturbation in Ca^{2+} cycling and the origin of PVA from a specific site is not clear.

More specifically, PVA which have been demonstrated to originate from areas of elevated Ca_D and Ca^{2+} overload were caused by membrane depolarization in response to nonelectrically driven Ca^{2+} release from the SR.[4-6] One proposed mechanism is spontaneous SR Ca^{2+} release secondary to elevated Ca_D which may increase Ca^{2+} leak from the SR and increase the sensitivity for the specialized SR release channels, ryanodine receptors, to release Ca^{2+}.[7] Similarly, the combination of elevated Ca_D and enhanced SR Ca^{2+} entry via SR Ca^{2+} ATP-ase (SERCA2a) may overload the SR with Ca^{2+}, further increasing the probability for a spontaneous Ca^{2+} release.[4,8-12]

Regardless of the mechanism leading to spontaneous Ca^{2+} release, the non-electrogenic release of Ca^{2+} from the SR requires the Na^+/Ca^{2+} exchanger (NCX) operating in its forward mode (3 Na^+-in – 2 Ca^{2+}-out) to cause a rise in membrane potential and thereby a propagated beat. We hypothesize that in our drug-induced model of ATS1 (DI-ATS1), regions of higher NCX functional expression relative to SERCA2a

(which we term "NCX dominance") coupled to slower Ca^{2+} uptake and heterogeneities in Ca_D levels may serve as a potential substrate for arrhythmias. To test this hypothesis, we employed ratiometric optical mapping to measure the Ca_D and kinetics of Ca^{2+} cycling from the anterior surface of guinea pig epicardium during pharmacological modulation of global NCX dominance.

Methods

This investigation conforms with the *Guide for the Care and Use of Laboratory Animals* published by the US National Institutes of Health (NIH Publication No. 85-23, revised 1996) and has been approved by the Institutional Animal Care and Use Committee of the University of Utah (protocol no. 05-07002). We have read the detailed *Journal of Physiology* policy and relevant UK regulations regarding animal experimentation as described in Drummond (2009) and our procedures are in compliance with the policies and regulations described in that article.

Experimental Preparation

Retired-breeder guinea pigs (n=28) were anaesthetized [30 mg/kg pentobarbital sodium (Nembutal) IP]. Their hearts were rapidly excised and perfused as Langendorff preparations (perfusion pressure 55 mmHg) with oxygenated (100% O_2) Tyrode's solution at 36.5°C containing (mmol/L) $CaCl_2$ 2, NaCl 140, KCl 4.5, dextrose 10, $MgCl_2$ 1, HEPES 10 (pH 7.41). The right and left atria were excised to avoid competitive stimulation from the atria. Hearts were stained with either the voltage-sensitive dye di-4-ANEPPS (15 μmol/L) or with Indo-1/AM (1 μmol/L) by direct coronary perfusion for 10

or 30 min, respectively. The dye-loading period was followed by a 15 min washout. ATS1 was modeled as described previously by perfusion of hypokalemic (2 mmol/L KCl) Tyrode's solution containing 10 μmol/L $BaCl_2$.[3] Cyclopiazonic acid (CPA) and KB-R7943 (KBR) were always perfused at 5 μmol/L. Motion was reduced using 7.5 mmol/L 2,3-diacetylmonoxime. Ventricles were stimulated at 1.5 times the stimulation threshold with a bipolar stainless steal electrode placed on the septum at a basic cycle length (BCL) of 400 ms unless otherwise specified. Volume-conducted electrocardiograms (ECGs) were continuously recorded with a Mortara H12 Holter (Mortara Instrument, Inc.) in order to assess arrhythmia burden. In order to gain higher spatial resolution from volume-conducted ECGs we employed a three lead recording system as described in Supplement Figure 3.1. Lastly, in a subset of ventricles (n=3) we inserted an intramural multielectrode needle into the basal left ventricular (LVB). This needle carried 3 Ag-AgCl electrodes with an interelectrode spacing of 1 mm.

Optical Voltage Mapping

Optical voltage mapping was used as previously described using ratiometric fluorescence method.[3] Specifically, we used two SciMedia MiCam02 HS CCD cameras (SciMedia) in a tandem lens configuration capable of resolving membrane potential changes as small as 2 mV with 1 ms temporal resolution from 90 x 60 sites simultaneously. Following staining with the voltage-sensitive dye, the preparation was excited by three 60-LED light sources (RL5-A9018, Superbrightleds) fitted with 510 ± 5 nm filters (Chroma) and a 50 mm aspheric lens (Edmund Optics). Fluorescent light was incident on a 565DXR dichroic mirror (Chroma) set at 45º angles to the recording

surface. Transmitted light passed through a 50 mm aspheric B270 crown glass lens (Edmund Optics), a 35 mm planoconvex BK7 lens (Edmund Optics), and a 610 nm LP filter (Newport) before it was incident on the CCD array. Reflected light passed through a 50-mm aspheric B270 crown glass (Edmund Optics), a 35-mm planoconvex BK7 lens (Edmund Optics), and a 540 ± 10 nm filter (Chroma) where it was incident on the second CCD array. CCD arrays were optically aligned at fixed and equal optical path lengths. The relative change in voltage was determined by dividing the fluorescence at 610 nm by the fluorescence at 540 nm.

Optical Ca^{2+} Mapping

Once again we used two SciMedia MiCam02 HS CCD cameras (SciMedia) in a tandem lens configuration.[3] Before Ca^{2+}-sensitive dye loading, background fluorescence representing tissue autofluorescence was recorded at both emission wavelengths (485 nm and 405 nm). Excitation light was obtained from a 1000-W mercury arc lamp (Thermo-Oriel) and filtered at 350 ± 10 nm (Chroma). A dichroic mirror placed between the tandem lens passed light of longer wavelengths (>445 nm) to an emission filter (485 ± 10 nm) and CCD array and reflected light of shorter wavelengths to a second emission filter (405 ± 10 nm) and CCD array. Ratiometric measurements of Ca^{2+} transients were determined by dividing the background-subtracted fluorescence Ca^{2+} transients at 405 nm by the background-subtracted fluorescence Ca^{2+} transients at 485 nm.

Western Blotting

Immediately following heart isolation, the anterior ventricular free walls were divided into four parts (base and apex from the LV and RV). The samples were then snap-frozen and homogenized into a whole-cell homogenate. Western blotting was performed following a previously described procedure.[13] Briefly, the protein concentration in the whole-cell homogenates was assessed using a BCA assay, and equal amounts of protein resolved by SDS polyacrylamide electrophoresis on 4–12% Bis–Tris gels (BioRad, Hercules, CA, USA). The proteins were then transferred onto a nitrocellulose membrane. After treatment with a 5% casein solution to block non-specific binding of antibodies, the membrane was treated with primary antibody [mouse monoclonal anti-SERCA2a / anti-NCX1 monoclonal antibody / anti-actin antibody (Affinity BioReagents, Golden, CO USA)] followed by goat anti-mouse HRP-conjugated secondary antibody (JacksonImmuno, West Grove, PA, USA). The membrane was then treated with enzymatic chemiluminescence reagents, and the bands were visualized on autoradiography film. Protein expression in the samples was quantified on the basis of the size and density of the bands. SERCA2a and NCX expression levels were normalized to the regional actin expression for inter-animal comparison.

Data Analysis

Activation time was defined as the time of the maximum first derivative of the action potential as described previously.[14] Repolarization was defined as the time to 95% repolarization from peak voltage amplitude. Action potential duration (APD) was the time difference between activation and full repolarization. APD dispersion was defined as

the difference between epicardial regions with the longest and shortest APD (using 25 spatially contiguous optically mapped sites per region). The premature ventricular activity (PVA) coupling interval was determined by calculating the percent of the interval of the PVA and the preceding beat in relation to the average beat to beat interval of five preceding beats. Excitation times obtained from the intramural multielectrode needle were estimated from the time of maximum negative slope during the QRS interval in the unipolar electrgorams.[15] Relative Ca_D level was defined as the minimum ratiometric signal before the Ca^{2+} transient upstroke. In order to compare relative changes between different experiments, the offset of diastolic Ca_D was corrected for drift in fluorescent Ca^{2+} signal as previously described.[3] Regional Ca_D levels were normalized to the apical RV Ca_D level obtained during the initial recording (i.e., control or DI-ATS1). To quantify the rate of recovery of cytosolic Ca^{2+} to diastolic levels, the decay portion of the Ca^{2+} transient (from 30% to 100% of the decline phase) was determined using the time constant (τ) of a single exponential fit, as previously used for fluorescent signals.[16] Statistical analysis was performed with a two-tailed Student's *t*-test or a single factor ANOVA with post hoc Student's *t*-tests for continuous, normally distributed paired data, with statistical significance assumed for values of $P < 0.05$, with correction for multiple comparisons (Sidak adjusted) where necessary. A Fisher's Exact and a Mantel-Haenszel test were used to test differences in nominal data. Differences in PVA frequency were analyzed using Wilcoxon signed rank test for non-normally distributed continuous data. All statistical comparisons were made on paired data. All values are reported as means ± standard error unless otherwise noted.

Results

Heterogeneous Manifestations of Triggered Activity During DI-ATS1

Figure 3.1A depicts ECGs of intrinsic beats from three leads. The isochrone map of the resulting epicardial activation (Figure 3.1B) reveals two characteristic anterior epicardial breakthrough sites one on each ventricle.[17] In the case of a premature ventricular depolarization, which we term premature ventricular activity (PVA), the QRS complex was discordant relative to the QRS complexes of the preceding intrinsic beats in all three ECG leads (Figure 3.1C), and the earliest epicardial activation occurred in the LV-Base (LVB; Figure 3.1D). Similarly, concordant PVA depicted on the ECGs (Figure 3.1E) evidenced earliest epicardial activation in LV-Apex (LVA, Figure 3.1F). Activation arising from the anterior RV and indeterminate areas as quantified by optical mapping exhibited QRS morphologies different to the prior two cases (data not shown).

Regional PVA frequency was quantified from ECGs collected over the duration of the experiment, and QRS orientation (all leads concordant or discordant) in 3-leads was used as an index of the PVA origination site. Over 90% of PVA during DI-ATS1 originated from the LV (either the LVB or LVA). PVA originating from other sites (Figure 3.1G) occurred with lower frequency relative to LV PVA (0.1±0.1 PVA/10min vs. 2.8±0.6 PVA/10min, $P < 0.05$, n=10). Among LV PVA, significantly more originated from the LVB relative to the LVA (2.2±0.8 PVA/10min vs. 0.6±0.3 PVA/10min, $P < 0.05$, Figure 3.1G). Further, optically mapped LVB PVA were more closely coupled to the preceding intrinsic beat than LVA PVA (67.7±4.7% vs. 78.5±3.6%, $P < 0.05$, n=7, Figure 3.1H); however, this difference was not noted when comparing all PVA recorded on volume-conducted ECGs (70.8±1.8% vs. 70.7±1.9%, P = ns, n=10, Figure 3.1I).

Lastly, the QRS duration of intrinsic beats were significantly shorter than all PVA (Figure 3.1J). Additionally, QRS duration of LVB PVA was significantly longer relative to LVA PVA (49.3±1.4ms vs. 44.6±1.4ms, $P < 0.05$, n=10, Figure 3.1J).

Multifocal Origins of Premature Ventricular Activity During DI-ATS1

Examining the transmural activatin of the intrinsic activation during DI-ATS1 represented on the volume-conducted ECGs in Figure 3.2A revealed earliest transmural activation on the endocardium followed by the midmyocardium and subsequently epicardium as evidenced by the intramural multielectrode neelde electrograms in Figure 3.2B. In the case of LVB PVA (Figure 3.2C), the layer of earliest transmural activation corresponded to the epicardium (Figure 3.2D). While in an another instance of LVB PVA (Figure 3.2E), the layer of earliest transmural activation corresponded to the endocardium (Figure 3.2F).

Spatio-temporal Correlation of Heterogeneous Cytosolic Ca^{2+} Levels and Premature Ventricular Activity During DI-ATS1

Representative control Ca^{2+} transients (Figure 3.3A, grey traces) demonstrate higher Ca_D in the LV relative to the RV with Ca_D of control (Figure 3.3B, gray bars) being highest in the LVB and lowest in the RVA. During DI-ATS1, Ca_D increased in all regions (Figure 3.3A, black traces) but retained its LV to RV gradient. The LVB still exhibited the highest Ca_D levels during DI-ATS1 (black bars) relative to other anterior epicardial regions (Figure 3.3B).

Ca^{2+} Transient Decay

Comparing representative normalized Ca^{2+} transients (from 0 to 1) recorded at BCLs 400 ms (Figure 3.4A, left) and 200 ms (Figure 3.4A, right), there were no quantifiable differences in the duration (vertical lines) or the decay kinetics of the Ca^{2+} transients between control (grey traces) and DI-ATS1 (black traces). Hearts were paced at 400 and 200 ms basic cycle lengths (BCL) in order to unmask differences in Ca^{2+} uptake kinetics during bradycardic and tachycardic conditions. Ca^{2+} transients in LVA decayed faster then LVB (Figures 3.4B, C insets) or RV regions. However, Ca^{2+} transient decay time constants (τ) were not different between control and DI-ATS1 in any region, at either BCL (Figures 3.4B, C). Further, LVA evidenced significantly shorter τ relative to LVB (by 10.1±2.1ms at BCL 400ms and by 7.3±1.3ms at BCL 200ms, n=5), as well as RV regions under all conditions ($P < 0.05$, Figures 3.4 B, C).

NCX and SERCA2a Protein Expression

NCX and SERCA2a expression were quantified by Western blotting using homogenized tissue samples from guinea pig (n=5 and 6, respectively). Actin was used to normalize for differences in lane loading. Representative bands in Figure 3.5A corresponding to NCX (outlined in red) and actin (outlined in black) demonstrate greater NCX expression in LVB relative to LVA. Over all experiments, actin-normalized NCX expression was significantly greater in the LVB compared to the LVA by 81.2± 30.9% ($P < 0.05$, Figure 3.5B), but no significant differences in NCX expression were noted within the RV.

Representative bands in Figure 3.5C corresponding to SERCA2a (outlined in blue) and actin (outlined in black) demonstrate greater SERCA2a band density in LVA relative to LVB. Indeed, over all experiments, actin-normalized SERCA2a expression was significantly greater in the LVA compared to the LVB by 76.8± 23.6%% ($P < 0.05$, Figure 3.5D), which is consistent with observed heterogeneities in Ca^{2+} transient decay kinetics (Figure 3.4).

Pharmacologically Induced NCX Dominance During DI-ATS1

Representative Ca^{2+} transients in Figure 3.6A demonstrate that NCX inhibition by KBR led to an upward shift of Ca_D in the LV but not in the RV. Indeed over all experiments, perfusion of KBR during DI-ATS1 significantly increased Ca_D in both LVB and LVA by 14.1±3.0% and 13.5±3.0%, respectively ($P < 0.05$, n=5, Figure 3.6B). All values in Figure 3.6B were normalized to DI-ATS1 in the RVA. We were unable to detect an effect of NCX blockade on Ca^{2+} transient decay kinetics at either pacing rate (Figures 3.6C, E). Overall, NCX inhibition did not significantly affect τ at either BCL (Figures 3.6D, F). However, the LVA still maintained the fastest uptake kinetics (lowest τ) relative to all other regions at both cycle lengths.

Pharmacologically Induced SERCA2a Dominance During DI-ATS1

Conversely, SERCA2a inhibition with CPA during DI-ATS1 resulted in a global Ca_D level elevation (Figure 3.6G). Overall, SERCA2a blockade during DI-ATS1 elevated Ca_D across all regions by 21.1±2.6% (n=6, Figure 3.6H) relative to DI-ATS1 alone. Further, SERCA2a inhibition by CPA slowed Ca^{2+} transient decay only in the LV at BCL

400 ms (Figure 3.6I) and in both ventricles at BCL 200 ms (Figure 3.6K). In summary, CPA increased τ in LVB and LVA (by 17.0±5.2ms and 10.9±2.7ms, respectively, Figure 3.6J) at BCL of 400ms and in all regions at BCL 200ms (by 9.8±2.6ms, 11.0±2.7ms, 12.5±2.5ms and 6.2±1.1ms in LVB, LVA, RVB and RVA, respectively, Figure 3.6L).

Pharmacologic Manipulation of DI-ATS1 and Arrhythmia Incidence

NCX inhibition with KBR during DI-ATS1 (DI-ATS1 + KBR) reduced incidence of spontaneous VTs to zero (0 of 8 hearts) from 25% (2 of 8) during DI-ATS1 (Figure 3.7A, $P = 0.11$). DI-ATS1+KBR also lowered the frequency of LVB PVA (Figure 3.7B, 2.8±1.0 PVA/10min vs. 0.6±0.3 PVA/10min, $P < 0.05$), but not LVA PVA (Figure 3.7C, 1.4±0.5 PVA/10min vs. 0.9±0.4 PVA/10min, P = ns). Further, NCX inhibition during DI-ATS1 did not alter the coupling interval of PVA quantified from continuous ECG recordings relative to DI-ATS1 alone (Figure 3.7C, LVB: 76.3±2.9% vs. 74.4±9.8%, P = ns; LVA: 70.4±4.2% vs. 68.8±4.2%, P = ns).

Conversely, enhancing global NCX dominance during DI-ATS1 via SERCA2a inhibition (DI-ATS1 + CPA) increased the incidence of spontaneous VTs three-fold relative to DI-ATS1 (Figure 3.7D, 58.3% vs. 16.7% of preparations respectively, $P < 0.05$, n=10), as well as the frequency of PVA from both LVB (Figure 3.7E, 6.2±2.7 PVA/10min vs. 2.2±0.8 PVA/10min) and LVA (Figure 3.7E, 27.3±18.4 PVA/10min vs. 0.6±0.3 PVA/10min).Yet, the difference in PVA frequency between the LVB and LVA was no longer statistically significant during DI-ATS1 + CPA. Lastly, CPA decreased PVA coupling interval relative to DI-ATS1 alone (Figure 3.7F, LVB: 60.3±2.1% vs. 70.8±1.8%, LVA: 57.0±2.8% vs. 70.7±1.9%).

Action Potential Duration Prolongation During Pharmacological Perturbations of DI-ATS1

Representative action potentials in Figure 3.8A during DI-ATS1 (black traces) demonstrate existing APD heterogeneities between RVB and LVA (previously demonstrated to have the longest and shortest APDs, respectively).[3,18] NCX blockade during DI-ATS1 (blue traces) prolonged APD and enhanced APD dispersion. Over all experiments, APD was prolonged by 31.9±0.9% in RVB and 32.3±1.7% in LVA during DI-ATS1 + KBR relative to DI-ATS1 alone (n=3, Figure 3.8B) resulting in a persistent APD dispersion (Figure 3.8C, 14.4±0.9ms vs 17.6±3.0ms, P = ns). Conversely, SERCA2a inhibition (Figure 3.8D, red traces) prolonged APD in both RVB and LVA relative to DI-ATS1 alone (Figure 3.8D, black traces); however, to a lesser extent when compared to NCX inhibition. Indeed, over all experiments, DI-ATS1 + CPA significantly prolonged APD in RVB and LVA relative to DI-ATS1 alone (by 12.4±1.8% and 17.8±0.4% respectively, n=3, Figure 3.8E), while significantly reducing APD dispersion (1.5±3.1ms vs 14.9±3.3ms, $P < 0.05$, Figure 3.8F).

Discussion

In this study, we investigated the factors underlying the arrhythmogenic burden during cytosolic Ca^{2+} overload as observed in DI-ATS1.[3] We found PVA occurring predominantly in the LV, particularly in regions with relatively higher NCX relative to SERCA2a protein expression which we term "NCX dominance." These regions also exhibited slower Ca^{2+} uptake and elevated Ca_D. Importantly, pharmacologically modulating NCX dominance affected both the timing as well as the frequency of PVA.

Increasing NCX dominance increased the incidence of spontaneous VTs and shortened the time to the first PVA. These data suggest that NCX dominance may represent an important arrhythmogenic substrate of ATS1 contributing to abnormal Ca^{2+} cycling.

Action Potential Duration Prolongation Unlikely to Underlie Arrhythmias During DI-ATS1

It is well accepted that dispersion of repolarization is an important basis for the genesis of ventricular arrhythmias associated with long QT syndromes.[19] Previously, we suggested that when APD prolongation and dispersion were reduced virtually to baseline levels, some arrhythmia vulnerability remained secondary to persistent Ca_D accumulation; however, we were unable then to uncouple APD prolongation from arrhythmias.[3] Here we demonstrate that NCX inhibition during DI-ATS1 prolongs APD heterogeneously, increases dispersion and yet, decreases arrhythmia burden. SERCA2a inhibition during DI-ATS1 also prolonged APD, albeit homogenously, and to a lesser extent than NCX inhibition. However, SERCA2a inhibition decreased APD dispersion, yet significantly increased the arrhythmia burden.

While this study did not measure any transmural parameters and therefore cannot exclude transmural gradients of repolarization playing a role on the electrophysiological substrate of arrhythmia susceptibility, to our knowledge there is no data to suggest that a pharmacological intervention can decrease dispersion of repolarization in one region and increase it in another. Taken together, these data suggest that APD prolongation and dispersion are an unlikely substrate for reentrant arrhythmias during DI-ATS1.

Heterogeneous Manifestations of Triggered Activity During DI-ATS1

We demonstrate that PVA manifests heterogeneously during DI-ATS1; specifically that PVA originates preferentially from the LV, in particular the LVB. This is consistent with the location of PVA origination in a rat heart model of oxidative stress[20] and hypokalemia.[21] Furthermore, Fujiwara *et al.*[21] demonstrated that the PVA originating from LVB were virtually abolished by NCX inhibition, consistent with our results.

We also observed PVA that originated from the LVA, with ECG morphology distinct from LVB PVA. Where the QRS complexes of the former were concordant to the preceding beats in all three leads, those of the latter were discordant. Further, optically mapped PVA originating from LVB were more closely coupled to the preceding intrinsic beats compared to those recorded from the LVA. Since, optical acquisition of irregular, low-frequency events, such as PVA, might have introduced selection bias; volume-conducted ECG were continuously recorded to obtain a similar index of regional arrhythmia burden. Interestingly, the coupling interval between LVA and LVB PVA were statistically different as quantified by optical mapping but not the ECG. One explanation is that PVA misclassification can occur during ECG analysis due to lower regional specificity of the ECG in comparison to optical mapping (see Supplement Figure 3.2).

Lastly, LVB PVA evidenced on average wider QRS complexes relative to LVA PVA. This suggests that LVB PVA may have occurred further from the Purkinje network, while LVA PVA with their narrower QRS might have originated much closer or even within the conduction system. Taken together, the phenomenological differences

between the two main PVA types suggest differences in their coupling fidelity and/or the sites of their origin.

The two-dimensional nature of optical mapping employed in this study does not completely resolve the exact origins of such PVA but only identifies the epicardial breakthrough sites. To this end we recorded transmural electrograms to assess the earliest transmural PVA. These studies revealed that LVB PVA were multifocal in nature. Therfore, this study quantifies all protein expression from the entire ventricular wall in the different regions without distinguishing transmural layers.

In accord with our study, Morita and colleagues[2] demonstrated under similar DI-ATS1 experimental conditions multifocal PVA where the foci migrated across all of the transmural layers of a canine LV wedge preparation. Recent study in rabbit ventricles with diminished inward-rectifier K^+ current, demonstrated a shift in PVA from the endocardium to the epicardium.[22] Further studies are needed to determine though whether the site of earliest activation in ATS1 or DI-ATS1 comes from the epicardium, endocardium, or Purkinje network.

Intraventricular Heterogeneity of Ca^{2+} Handling During DI-ATS1

We have shown previously that PVA during DI-ATS1 is coupled to elevated Ca_D.[3] Here, we compare optically measured Ca_D, Ca^{2+} transient dynamics and arrhythmia burden between regions and across different conditions. During control, we observed greater Ca_D in LV relative to RV, similar to that measured by Katra *et al*.[23] in guinea pig. Further, consistent with our previous report,[3] DI-ATS1 led to a rise in Ca_D across all anterior epicardial regions. Interestingly, Ca_D during DI-ATS1 was highest in the LVB,

the region with the highest TA frequency. However, DI-ATS1 did not alter τ of Ca^{2+} transients with the LVA demonstrating the fastest τ in both control and DI-ATS1. This is consistent with the regional epicardial distribution of τ in guinea pig.[23] The τ values presented in this study are considerably shorter than previously published at BCL = 400ms.[23] This could be in part explained by differences in temperature,[24] which was 36ºC in the present study and 32 ºC in the Katra *et al*. study.

The observed regional heterogeneity in Ca^{2+} dynamics in our model is likely due to regionally heterogeneous expression of Ca^{2+} cycling proteins. We observed reduced SERCA2a expression in the LVB compared with the LVA, which was consistent with observed regional τ differences. Further, lower SERCA2a expression coupled to Ca_D elevation, as evidenced in LVB, has been proposed as the arrhythmia mechanism during enhanced Ca^{2+} entry.[25,26] However, the RV experienced low arrhythmia incidence relative to the LVA despite reduced SERCA2a expression and Ca_D elevation during DI-ATS1; therefore, the aforementioned hypothesis cannot fully explain the high LVB arrhythmia burden. Therefore, we considered the contribution of NCX to regional Ca^{2+} handling heterogeneities and its possible role as a determinant of the observed regional arrhythmia incidence.

Previously, Katra *et al*.[27] demonstrated that under conditions of increased Ca^{2+} leak and enhanced Ca^{2+} entry, the epicardium of canine wedge preparations exhibit the highest incidence of triggered activity, which is the region of highest NCX functional expression.[28,29] We demonstrate, along similar lines in a guinea pig model of enhanced intracellular Ca^{2+} accumulation, that the LVB evidenced higher PVA and NCX expression relative to all other regions. While these data are correlatively similar for PVA

and NCX expression, further studies are warranted to determine the transmural functional distribution of NCX in guinea pig.

Decreased Global NCX Dominance Decreases Triggered Activity

To assess the contribution of NCX dominance to regional heterogeneities in arrhythmias susceptibility during DI-ATS1, we decreased global NCX dominance by inhibiting NCX with KB-R7943 (KBR). While KBR did not alter τ, it did increase Ca_D preferentially in the LV. Despite, the Ca_D elevation, NCX blockade decreased the frequency of LVB PVA strongly suggesting that NCX constitutes an arrhythmogenic substrate in DI-ATS1. Lastly, no spontaneous VTs were observed upon KBR perfusion during DI-ATS1, where as during DI-ATS1 alone 25% of preparations evidenced such arrhythmias. This difference between the two conditions only trended towards, but did not attain significance ($p=0.11$). This is perhaps due to insufficient power ($n=8$) and low frequency of observed events during DI-ATS1 (comparable to previous reports[2,3]) relative to models of other long QT syndromes.[30] Nonetheless, the findings that NCX inhibition decreases PVA and/or arrhythmia burden are consistent with previous reports of the anti-arrhythmic effect of NCX blockade in various models of long QT syndromes as well as during Na^+ overload induced by cardiac glycosides.[30-32]

Importantly, it has been demonstrated that KBR does not increase SR Ca^{2+} load[31] which implies that the mechanism for PVA in this model is not spontaneous Ca^{2+} release due to SR Ca^{2+} overload. This further suggests that KBR may be modulating the coupling fidelity of the spontaneous Ca^{2+} release events and the transient inward current carried by NCX.[21]

Enhanced Global NCX Dominance Increases Triggered Activity

An original finding in this study is that enhancing global NCX dominance via SERCA2a inhibition during DI-ATS1 increased the frequency of both major types of PVA against a backdrop of Ca_D elevation. Importantly, this translated into higher incidence of spontaneous VT compared to DI-ATS1 alone. Taken together, these findings provide evidence that NCX dominance, slower Ca^{2+} uptake, Ca_D elevation is an important determinant of the arrhythmia phenotype. These findings seemingly contradict previous reports which have suggested that SERCA2a inhibition decreased SR Ca^{2+} load[33,34] and thereby, the frequency of spontaneous SR Ca^{2+} events.[8] One possible explanation for this seemingly paradoxical finding may be that the incidence of spontaneous Ca^{2+} releases do not necessarily correlate with triggered activity unless sufficient NCX is present to depolarize the membrane and elicit a propagated response.

Enhanced Global NCX via SERCA2a Inhibition Decreases PVA Coupling Interval

As quantified by optical mapping, regions with lower SERCA2a and higher NCX expression (LVB) during DI-ATS1 exhibit a shorter PVA coupling interval than the region with higher SERCA2a and lower NCX expression (LVA). When NCX is inhibited with KBR during DI-ATS1, there is no change in the PVA coupling interval. From this data, one might come to the conclusion that NCX dominance is not well correlated to the time to PVA; however, KBR also raises Ca_D. Katra and Laurita[25] demonstrated in canine, that the region with highest Ca_D and lowest SERCA2a functional expression experiences the shortest time to PVA. Therefore, the synergistic effect between raising regional Ca_D,

while reducing NCX functional expression may mask the expected increase in PVA coupling interval that would be expected during KBR perfusion. Importantly, raising Ca_D by SERCA2a inhibition decreases the time to PVA globally while increasing the incidence of PVA. This is consistent with the regional PVA timing during DI-ATS1 alone as well as the relationship between Ca_D and time to PVA.

Lastly, Ca_D is also modulated by the myriad Ca^{2+} and Na^+ handling proteins in a myocyte which may also be heterogeneously distributed.[35] Therefore, further studies are required to determine how modulating NCX affects PVA coupling interval. This limitation does not detract from our finding that NCX dominance underlies overall PVA propensity.

Mechanisms of Premature Ventricular Activity in DI-ATS1

The exact mechanism by which cytosolic Ca^{2+} accumulation initiates PVA remains unclear. Previously, it was proposed that increased Ca_D[7] and/or SR Ca^{2+} load[36] can precipitate triggered activity.[9,10] Although we did not measure the SR Ca^{2+} content, Szentesi *et al*.[33] demonstrated in isolated guinea pig cardiomyocytes, using CPA concentrations comparable to those in this study, a 50% reduction in SR Ca^{2+} content. Thus, our data argue against SR Ca^{2+} overload precipitating arrhythmias in DI-ATS1.

The concentration of CPA used in this study prolonged τ in the left ventricle as one would expect of partial SERCA2a inhibition. Functional SERCA2a inhibition is likely the mechanism underlying increased Ca_D because the SR is unable to accumulate as much Ca^{2+} with CPA. Again, these data argue against SR Ca^{2+} overload precipitating arrhythmias in DI-ATS1. This, however, does not preclude Ca_D alone from triggering

spontaneous SR Ca^{2+} releases as has been previously suggested.[7]

Alternatively, reduced inward-rectifier K^+ current has been shown to destabilize the resting membrane potential.[37] This mechanism allows for spontaneous pacemaking activity (automaticity) that is independent of the SR. Specifically, during conditions of elevated Ca_D, forward mode NCX could raise membrane potential particularly in late phases of the action potential and diastole. Without the inward-rectifier K^+ current maintaining a stable resting membrane potential, NCX could depolarize the cell to the activation thresholds of either voltage-gated Na^+ or Ca^{2+} channels. However, previous work by our group[13] and others[38] have demonstrated a significantly higher Kir2.1 protein density in the LV, the region with highest PVA incidence, which would suggest that these regions would be most resistant to pacemaker-like activity.

Lastly, it has been previously demonstrated that Ca^{2+} influx through NCX can trigger SR Ca^{2+} release and thereby PVA.[39-42] Although this hypothesis has been controversial,[43] a mathematical model of ATS1 suggested an upward shift in the NCX current, allowing it to operate primarily in the reverse mode (Ca^{2+}-in – Na^+-out) during the repolarization phase of the action potential.[44] This along with reports of enhanced late Na^+ current during increased cytosolic Ca^{2+} concentrations[45] and recent reports of Na^+ and NCX modulating SR Ca^{2+} release[46-48] form a foundation for a plausible hypothesis of enhanced PVA frequency during DI-ATS1 being linked to reverse mode NCX. Therefore, this hypothesis merits further investigation, particularly in the light of the results presented herein.

References

1. Tristani-Firouzi M, Jensen JL, Donaldson MR, et al. Functional and clinical characterization of KCNJ2 mutations associated with LQT7 (Andersen syndrome). *J Clin Invest*. 2002;110(3):381-8.

2. Morita H, Zipes DP, Morita ST, Wu J. Mechanism of U wave and polymorphic ventricular tachycardia in a canine tissue model of Andersen-Tawil syndrome. *Cardiovasc Res*. 2007;75(3):510-8.

3. Radwański PB, Veeraraghavan R, Poelzing S. Cytosolic Calcium Accumulation and Delayed Repolarization Associated with Ventricular Arrhythmias in Guinea Pig Model of Andersen-Tawil Syndrome. *Heart Rhythm*. 2010;7(10):1428-1435.

4. Marban E, Robinson SW, Wier WG. Mechanisms of arrhythmogenic delayed and early afterdepolarizations in ferret ventricular muscle. *J Clin Invest*. 1986 Nov;78(5):1185-92.

5. Boyden PA, Pu J, Pinto J, Keurs HEDJT. Ca2+ transients and Ca2+ waves in purkinje cells : Role in action potential initiation. *Circ Res*. 2000 Mar 3;86(4):448-455.

6. Priori SG, Corr PB. Mechanisms underlying early and delayed afterdepolarizations induced by catecholamines. *Am J Physiol*. 1990 Jun;258(6 Pt 2):H1796-1805.

7. Egdell RM, De Souza AI, Macleod KT. Relative importance of SR load and cytoplasmic calcium concentration in the genesis of aftercontractions in cardiac myocytes. *Cardiovasc Res*. 2000;47(4):769-777.

8. Diaz ME, Trafford AW, O'Neill SC, Eisner DA. Measurement of sarcoplasmic reticulum Ca2+ content and sarcolemmal Ca2+ fluxes in isolated rat ventricular myocytes during spontaneous Ca2+ release. *J Physiol*. 1997;501 (Pt 1):3-16.

9. Lukyanenko V, Subramanian S, Györke I, Wiesner TF, Györke S. The role of luminal Ca2+ in the generation of Ca2+ waves in rat ventricular myocytes. *J Physiol*. 1999;518(1):173-186.

10. Györke I, Györke S. Regulation of the cardiac ryanodine receptor channel by luminal Ca2+ involves luminal Ca2+ sensing sites. *Biophys J*. 1998;75(6):2801-2810.

11. Nuss HB, Kaab S, Kass DA, Tomaselli GF, Marban E. Cellular basis of ventricular arrhythmias and abnormal automaticity in heart failure. *Am J Physiol*. 1999;277(1 Pt 2):H80-91.

12. Miura M, Boyden PA, Ter Keurs HE. Ca2+ waves during triggered propagated contractions in intact trabeculae. *Am J Physiol Heart Circ Physiol*. 1998 ;274(1):H266-276.

13. Veeraraghavan R, Poelzing S. Mechanisms underlying increased right ventricular conduction sensitivity to flecainide challenge. *Cardiovasc Res*. 2008;77(4):749-56.

14. Girouard SD, Pastore JM, Laurita KR, Gregory KW, Rosenbaum DS. Optical mapping in a new guinea pig model of ventricular tachycardia reveals mechanisms for multiple wavelengths in a single reentrant circuit. *Circulation*. 1996;93(3):603-13.

15. Haws CW, Lux RL. Correlation between in vivo transmembrane action potential durations and activation-recovery intervals from electrograms. Effects of interventions that alter repolarization time. *Circulation*. 1990;81(1):281-288.

16. Bers DM, Berlin JR. Kinetics of [Ca]i decline in cardiac myocytes depend on peak [Ca]i. *Am J Physiol*. 1995;268(1 Pt 1):C271-277.

17. Cerrone M, Noujaim SF, Tolkacheva EG, et al. Arrhythmogenic Mechanisms in a Mouse Model of Catecholaminergic Polymorphic Ventricular Tachycardia. *Circ Res*. 2007;101(10):1039-1048.

18. Poelzing S, Veeraraghavan R. Heterogeneous ventricular chamber response to hypokalemia and inward rectifier potassium channel blockade underlies bifurcated T wave in guinea pig. *Am J Physiol Heart Circ Physiol*. 2007;292(6):H3043-51.

19. Restivo M, Caref EB, Kozhevnikov DO, El-Sherif N. Spatial dispersion of repolarization is a key factor in the arrhythmogenicity of long QT syndrome. *J Cardiovasc Electrophysiol*. 2004;15(3):323-31.

20. Morita N, Sovari AA, Xie Y, et al. Increased susceptibility of aged hearts to ventricular fibrillation during oxidative stress. *Am J Physiol Heart Circ Physiol*. 2009;297(5):H1594-1605.

21. Fujiwara K, Tanaka H, Mani H, Nakagami T, Takamatsu T. Burst emergence of intracellular Ca2+ waves evokes arrhythmogenic oscillatory depolarization via the Na+-Ca2+ exchanger: Simultaneous confocal recording of membrane potential and intracellular Ca2+ in the heart. *Circ Res*. 2008;103(5):509-518.

22. Maruyama M, Joung B, Tang L, et al. Diastolic intracellular calcium-membrane voltage coupling gain and postshock arrhythmias: Role of purkinje fibers and triggered activity. *Circ Res*. 2010;106(2):399-408.

23. Katra RP, Pruvot E, Laurita KR. Intracellular calcium handling heterogeneities in intact guinea pig hearts. *Am J Physiol Heart Circ Physiol*. 2004;286(2):H648-56.

24. Inesi G, Prasad AM, Pilankatta R. The Ca2+ ATPase of cardiac sarcoplasmic reticulum: Physiological role and relevance to diseases. *Biochem and Biophys Res Commun*. 2008;369(1):182-187.

25. Katra RP, Laurita KR. Cellular mechanism of calcium-mediated triggered activity in the heart. *Circ Res*. 2005;96(5):535-42.

26. Laurita KR, Katra R, Wible B, Wan X, Koo MH. Transmural heterogeneity of calcium handling in canine. *Circ Res*. 2003;92(6):668-75.

27. Katra RP, Oya T, Hoeker GS, Laurita KR. Ryanodine receptor dysfunction and triggered activity in the heart. *Am J Physiol Heart Circ Physiol*. 2007;292(5):H2144-2151.

28. Zygmunt AC, Goodrow RJ, Antzelevitch C. INaCa contributes to electrical heterogeneity within the canine ventricle. *Am J Physiol Heart Circ Physiol*. 2000;278(5):H1671-1678.

29. Xiong W, Tian Y, DiSilvestre D, Tomaselli GF. Transmural heterogeneity of Na+-Ca2+ exchange: Evidence for differential expression in normal and failing hearts. *Circ Res*. 2005;97(3):207-209.

30. Milberg P, Pott C, Fink M, Frommeyer G, Matsuda T, Baba A, et al. Inhibition of the Na+/Ca2+ exchanger suppresses torsades de pointes in an intact heart model of long QT syndrome-2 and long QT syndrome-3. *Heart Rhythm*. 2008;5(10):1444-1452.

31. Satoh H, Ginsburg KS, Qing K, Terada H, Hayashi H, Bers DM. KB-R7943 Block of Ca2+ influx Via Na+/Ca2+ exchange does not alter twitches or glycoside inotropy but prevents Ca2+ overload in rat ventricular myocytes. *Circulation*. 2000;101(12):1441-1446.

32. Watano T, Harada Y, Harada K, Nishimura N. Effect of Na+/Ca2+ exchange inhibitor, KB-R7943 on ouabain-induced arrhythmias in guinea-pigs. *Br J Pharmacol*. 1999;127(8):1846-1850.

33. Szentesi P, Pignier C, Egger M, Kranias EG, Niggli E. Sarcoplasmic reticulum Ca2+ refilling controls recovery from Ca2+-induced Ca2+ release refractoriness in heart muscle. *Circ Res*. 2004;95(8):807-813.

34. Lukyanenko V, Viatchenko-Karpinski S, Smirnov A, Wiesner TF, Györke S. Dynamic regulation of sarcoplasmic reticulum Ca(2+) content and release by luminal Ca(2+)-sensitive leak in rat ventricular myocytes. *Biophys J*. 2001;81(2):785-798.

35. Sims C, Reisenweber S, Viswanathan PC, Choi B, Walker WH, Salama G. Sex, age, and regional differences in L-Type calcium current are important determinants of arrhythmia phenotype in rabbit hearts with drug-induced Long QT Type 2. *Circ Res*. 2008;102(9):e86-100.

36. Tweedie D, Harding SE, MacLeod KT. Sarcoplasmic reticulum Ca content,

sarcolemmal Ca influx and the genesis of arrhythmias in isolated guinea-pig cardiomyocytes. *J Mol and Cell Cardiol*. 2000;32(2):261-272.

37. Miake J, Marbán E, Nuss HB. Functional role of inward rectifier current in heart probed by Kir2.1 overexpression and dominant-negative suppression. *J Clin Invest* 2003;111(10):1529-1536.

38. Warren M, Guha PK, Berenfeld O, et al. Blockade of the inward rectifying potassium current terminates ventricular fibrillation in the guinea pig heart. *J Cardiovasc Electrophysiol*. 2003;14(6):621-631.

39. Leblanc N, Hume JR. Sodium current-induced release of calcium from cardiac sarcoplasmic reticulum. *Science*. 1990;248(4953):372-376.

40. Lipp P, Niggli E. Sodium current-induced calcium signals in isolated guinea-pig ventricular myocytes. *J Physiol*. 1994;474(3):439-446.

41. Levi AJ, Spitzer KW, Kohmoto O, Bridge JH. Depolarization-induced Ca entry via Na-Ca exchange triggers SR release in guinea pig cardiac myocytes. *Am J Physiol*. 1994;266(4 Pt 2):H1422-1433.

42. Litwin SE, Li J, Bridge JH. Na-Ca exchange and the trigger for sarcoplasmic reticulum Ca release: studies in adult rabbit ventricular myocytes. *Biophys J*. 1998;75(1):359-371.

43. Sipido KR, Carmeliet E, Pappano A. Na+ current and Ca2+ release from the sarcoplasmic reticulum during action potentials in guinea-pig ventricular myocytes. *J Physiol*. 1995;498(Pt1):1-17.

44. Seemann G, Sachse FB, Weiss DL, Ptacek LJ, Tristani-Firouzi M. Modeling of IK1 mutations in human left ventricular myocytes and tissue. *Am J Physiol Heart Circ Physiol*. 2007;292(1):H549-59.

45. Maltsev VA, Reznikov V, Undrovinas NA, Sabbah HN, Undrovinas A. Modulation of late sodium current by Ca2+, calmodulin, and CaMKII in normal and failing dog cardiomyocytes: similarities and differences. *Am J Physiol Heart Circ Physiol*. 2008;294(4):H1597-1608.

46. Lines GT, Sande JB, Louch WE, Mørk HK, Grøttum P, Sejersted OM. Contribution of the Na+/Ca2+ exchanger to rapid Ca2+ release in cardiomyocytes. *Biophys J*. 2006;91(3):779-792.

47. Larbig R, Torres N, Bridge JHB, Goldhaber JI, Philipson KD. Activation of reverse Na+-Ca2+ exchange by the Na+ current augments the cardiac Ca2+ transient: evidence from NCX knockout mice. *J Physiol*. 2010;588(17):3267-3276.

48. Torres NS, Larbig R, Rock AN, Goldhaber JI, Bridge JH. Na+ currents are required for efficient excitation-contraction coupling in rabbit ventricular myocytes: a possible contribution of neuronal Na+ channel to triggering Ca2+ release from the Sarcoplasmic Reticulum. *J Physiol*. 2010. doi: 10.1113/jphysiol.2010.194688.

Figure 3.1: Premature Ventricular Activity (PVA) Originate Preferentially from LVB During DI-ATS1. A) Representative volume-conducted ECGs of intrinsic beats recorded during DI-ATS1 and **B)** a resulting activation isochrone map. **C)** Discordant premature ventricular activity (PVA) on volume-conducted ECGs (red ECGs) **D)** evidenced the earliest anterior epicardial activation occurred in the **3.**basal LV (LVB). **E)** PVA with concordant QRS morphology (blue ECGs) **F)** originated in the apical LV (LVA). **G)** PVA originating from other sites (right ventricle and indeterminate areas) occurred less frequently relative to the LV PVA (**P* < 0.05, n=10), while those originated from the LVB occurred more frequently relative to the LVA (†*P* < 0.05). **H)** Optically mapped (OM) LVB PVA were more closely coupled to the preceding intrinsic beat than LVA PVA (**P* < 0.05, n=7). **I)** The difference in coupling interval was not noted when comparing all PVA recorded on volume-conducted ECGs (n=10). **J)** The QRS duration of intrinsic beats were shorter than all PVA (**P* < *0.05*) while, QRS duration of LVB PVA was wider relative to LVA PVA (†*P* < *0.05*).

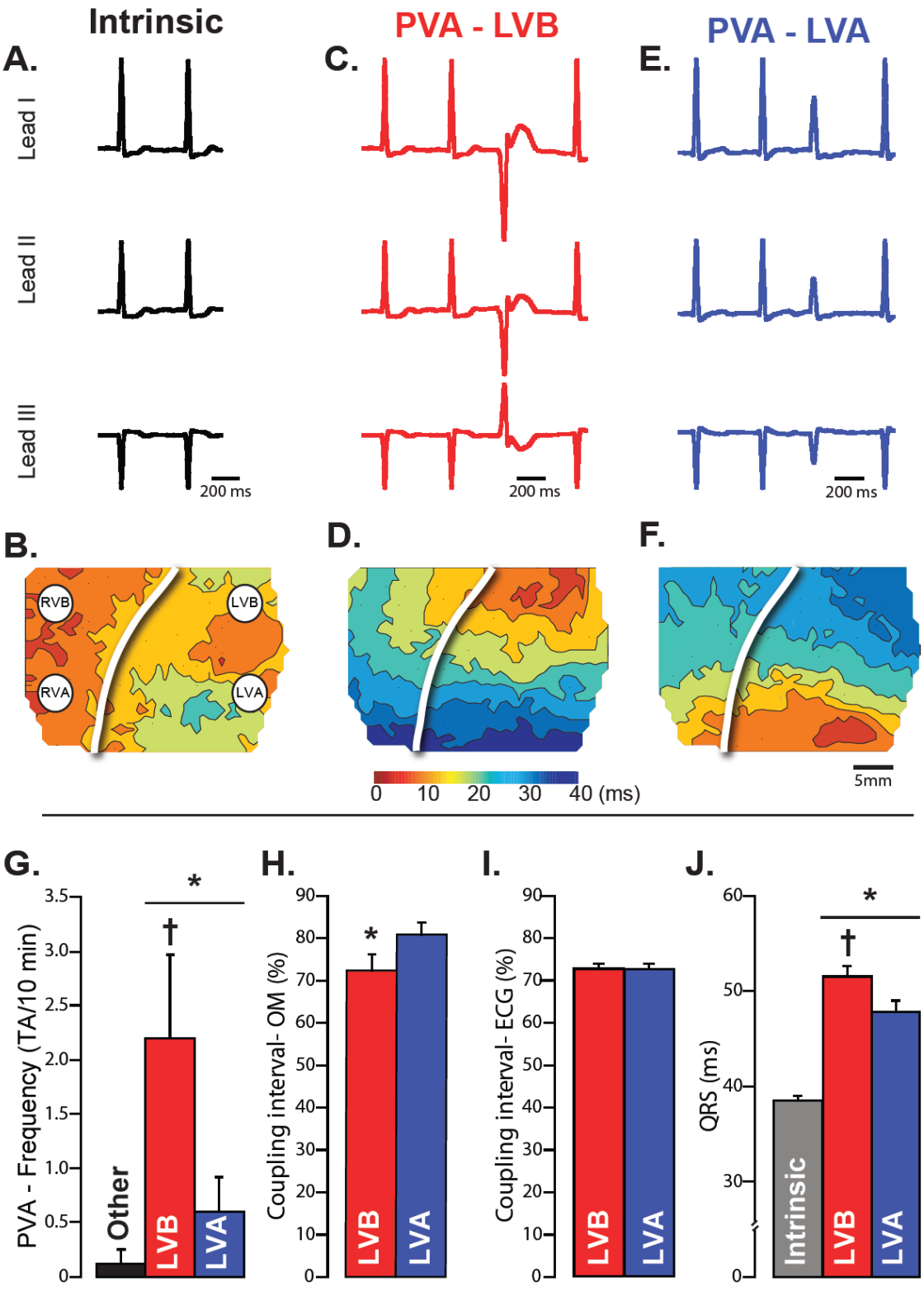
Intrinsic
PVA - LVB
PVA - LVA
A.
C.
E.
Lead I
Lead II
Lead III
200 ms
200 ms
200 ms
B.
D.
F.
RVB
LVB
RVA
LVA
0 10 20 30 40 (ms)
5mm
G.
H.
I.
J.
PVA - Frequency (TA/10 min)
Coupling interval- OM (%)
Coupling interval- ECG (%)
QRS (ms)
Other
LVB
LVA
Intrinsic
*
†

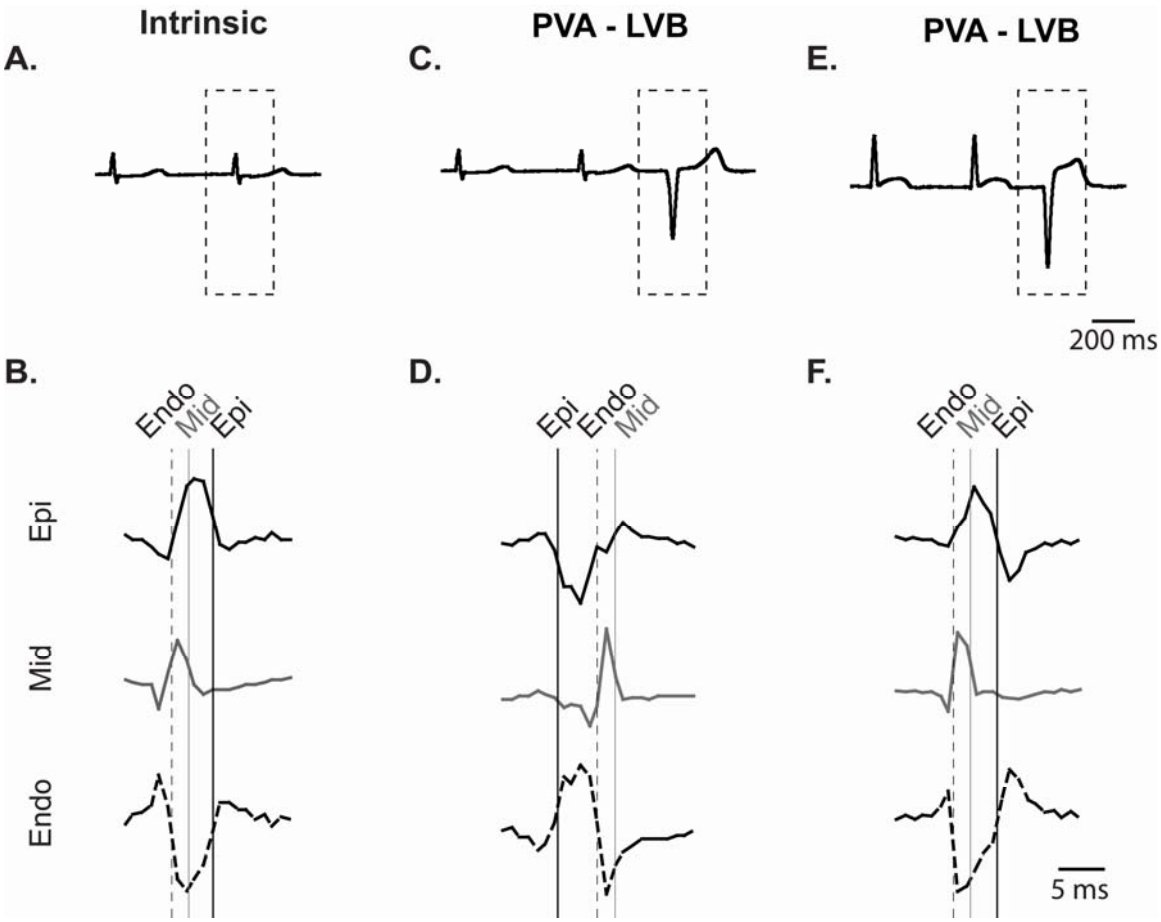

Figure 3.2: Multifocal Origin of PVA During DI-ATS1. A) Representative volume-conducted ECGs of intrinsic beats recorded during DI-ATS1 and **B)** corresponding intramural multielectrode needle electrograms revealing sequential activation of an intrinsic beat starting with endocardium (Endo), proceeding through the midmyocardium (Mid) and lastly activating epicardium (Epi). **C)** PVA consistent with LVB activation reveals **D)** epicardial (Epi) origin of the ectopy, while **E)** another LVB PVA reveals **E)** endocardial (Endo) origin of the ectopy.

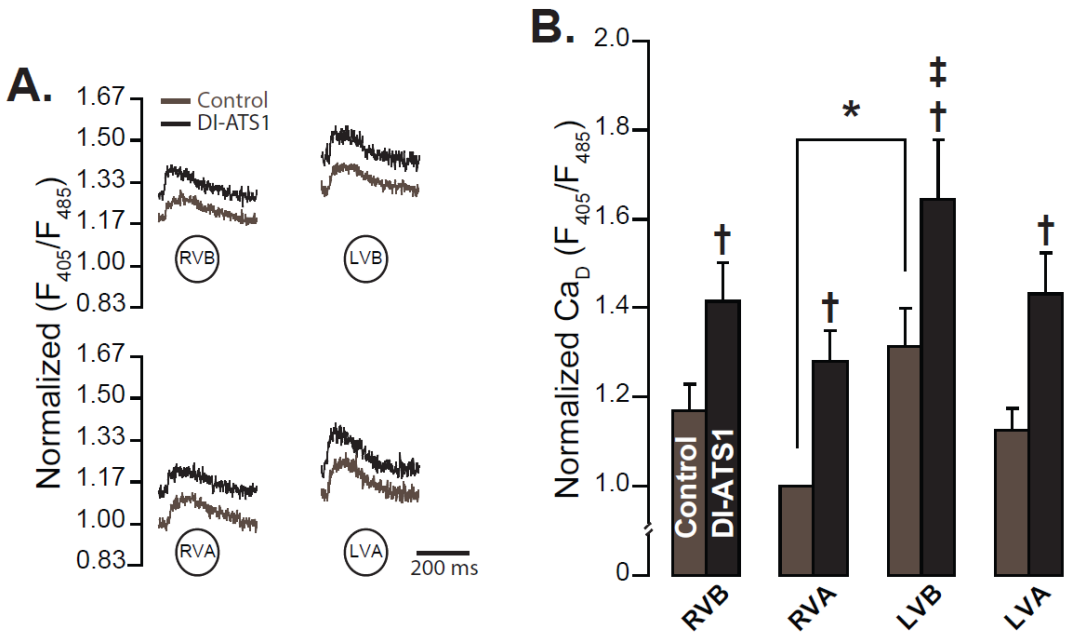

Figure 3.3: Cytosolic Ca^{2+} Levels Correlate with PVA During DI-ATS1. A) Representative Ca^{2+} transients demonstrate higher Ca_D in the LV relative to the RV during control (grey traces) and an upward Ca_D shift in all regions during DI-ATS1 (black traces). **B)** Mean RVA normalized Ca_D during control was greater in LVB relative to RVA (*P < 0.05, n=8). During DI-ATS1, Ca_D increased in all regions (†P < 0.05). The LVB exhibited the highest Ca_D levels relative to other anterior epicardial regions (‡P < 0.05).

Figure 3.4: Ca^{2+} Transient Decay Kinetics Spatially Correlate with SERCA2a Protein Expression. A) Representative normalized Ca^{2+} transients (from 0 to 1) recorded at BCLs 400 ms (left, same ones as in Figure 2) and 200 ms (right), demonstrate high degree of morphological correspondence and no quantifiable difference in Ca^{2+} transient decay constant (τ; marked by vertical lines) within regions between control (grey traces) and DI-ATS1 (black traces). However, LVA Ca^{2+} transients (full line) appeared to decay faster relative to RV (dashed lines) and **B)** LVB (inset) at BCL 400ms. Mean τ was not different between control and DI-ATS1 in any region. LVA evidenced shorter τ relative to LVB a well as RV regions (*$P < 0.05$, n=5). **C)** During pacing at BCL 200ms similar pattern was observed as during BCL 400ms, where LVA evidenced shoert τ relative to other anterior epicardial regions (*$P < 0.05$).

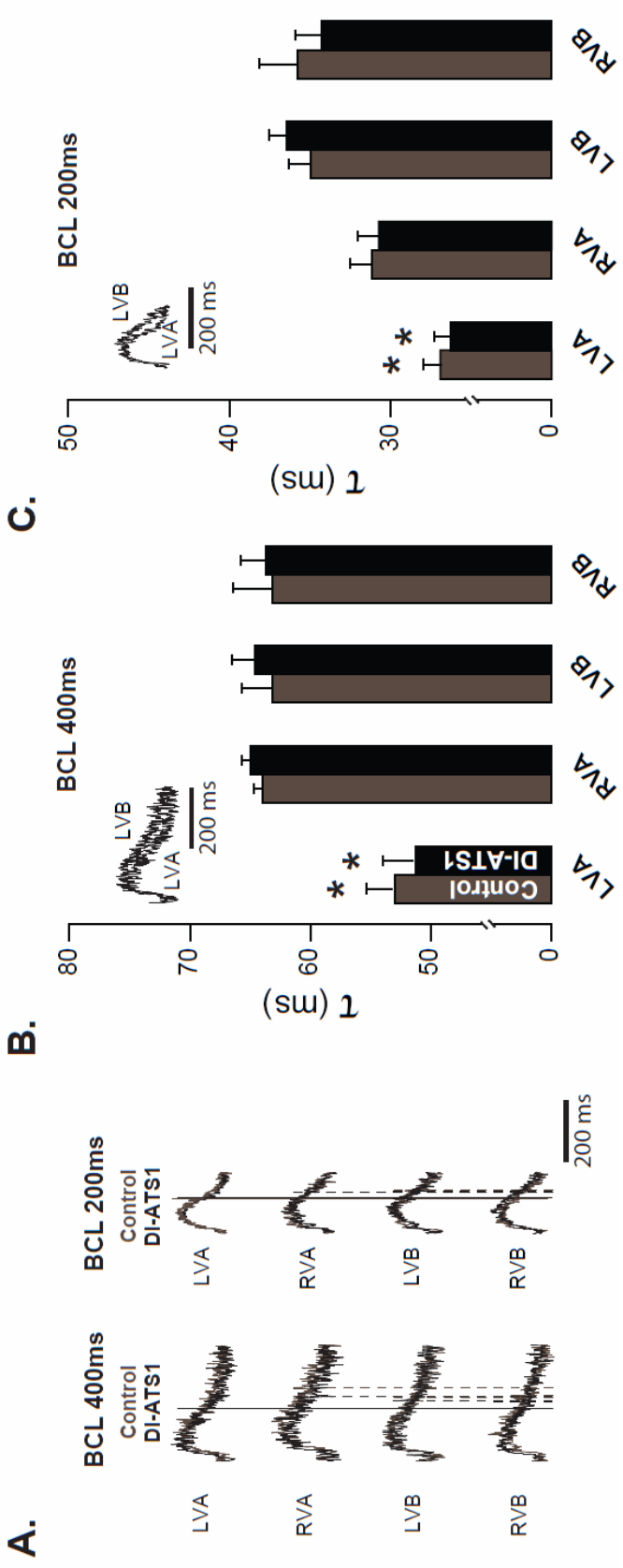
A.
BCL 400ms
Control
DI-ATS1
LVA
RVA
LVB
RVB
BCL 200ms
Control
DI-ATS1
LVA
RVA
LVB
RVB
200 ms
B.
BCL 400ms
LVB
LVA
200 ms
τ (ms)
80
70
60
50
0
Control
DI-ATS1
LVA
RVA
LVB
RVB
C.
BCL 200ms
LVB
LVA
200 ms
τ (ms)
50
40
30
0
LVA
RVA
LVB
RVB

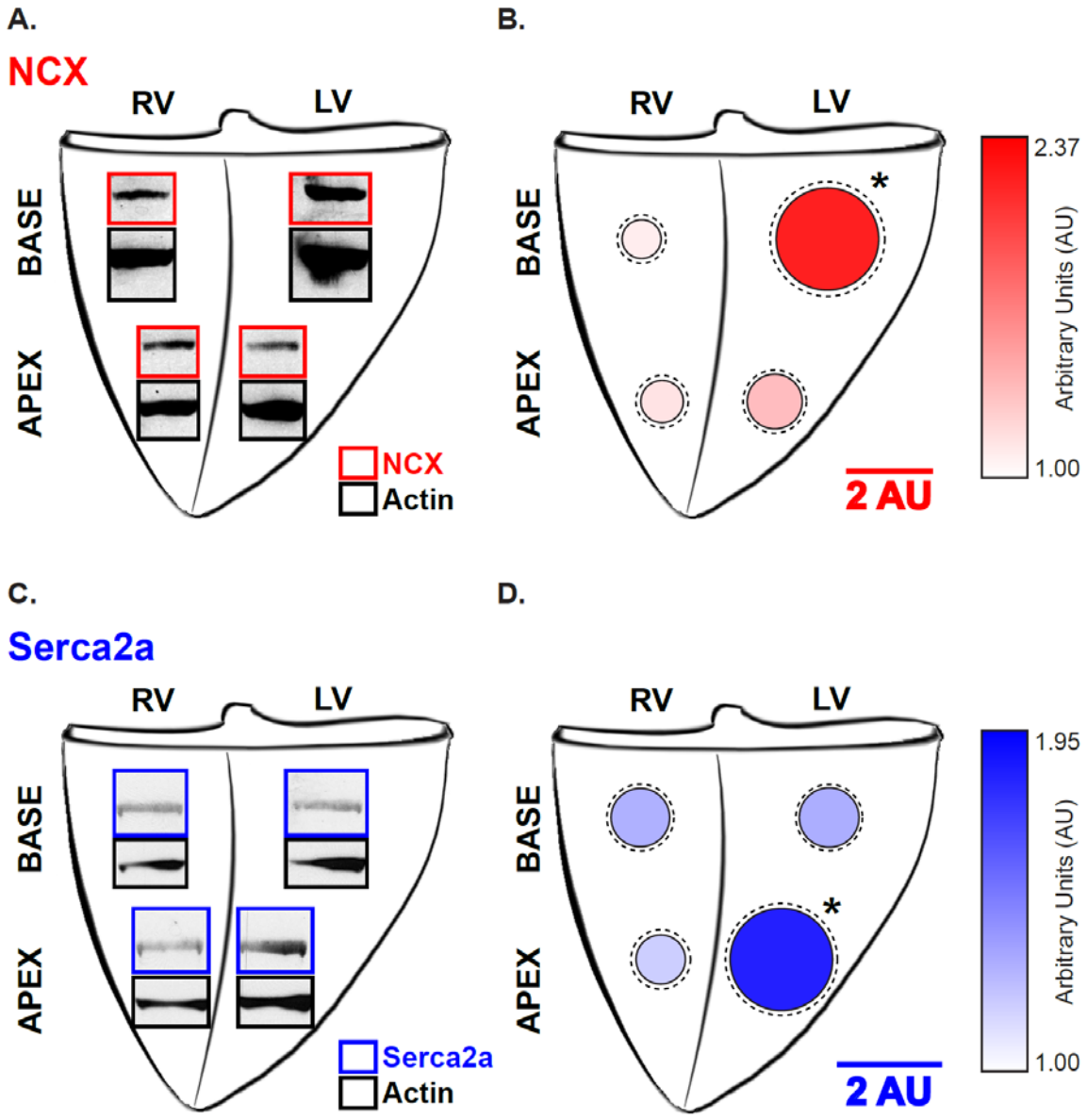

Figure 3.5: NCX Dominance Spatially Correlates with PVA. A) Representative NCX (outlined in red) and actin bands (outlined in black) from different anterior epicardial regions of the heart that were measured. **B)** Actin-normalized NCX protein expression in each region is denoted by the radius and color of the corresponding circle, while dashed circles reflect standard error. Mean actin-normalized NCX protein expression in the LVB was 81.2± 30.9% greater than that in the LVA (*$P < 0.05$, n=5), whereas no significant difference was observed within the RV (P = ns). **C)** Representative SERCA2a (outlined in blue) and actin (outlined in black) demonstrate greater SERCA2a band density in LVA relative to LVB. **D)** Mean, actin-normalized SERCA2a expression was significantly greater in the LVA by 76.8± 23.6% compared to the LVB (*$P < 0.05$, n=6).

Figure 3.6: SERCA2a but Not NCX Inhibition Prolongs Ca^{2+} Transient Decay Kinetics. A) Representative Ca^{2+} transients demonstrate that NCX inhibition by KB-R7943 (KBR) during DI-ATS1 (DI-ATS1+KBR, blue traces) resulted in an upward shift of Ca_D in the LV relative to DI-ATS1 alone (black traces). **B)** Mean Ca_D exhibited highest Ca_D levels during DI-ATS1 in the LVB relative to other anterior epicardial regions (*$P < 0.05$, n=5), while DI-ATS1+KBR resulted in a Ca_D rise only in the LV (†$P < 0.05$). **C)** Representative normalized Ca^{2+} transients recorded at BCLs 400 ms and **E)** 200 ms demonstrate no quantifiable difference in τ between DI-ATS1 and DI-ATS1+KBR. **D & F)** Mean τ was unaltered by DI-ATS1+KBR relative to DI-ATS1 alone during both BCL 400 ms and 200 ms, where LVA evidenced lowest τ relative to other anterior epicardial regions (*$P < 0.05$). **G)** SERCA2a inhibition by cyclopiazonic acid (CPA)during DI-ATS1 (DI-ATS1+CPA, red traces) resulted in an upward shift of representative Ca^{2+} transients compared to DI-ATS1 alone (black traces) resulting in a global Ca_D rise. **H)** Mean Ca_D exhibited highest Ca_D levels during DI-ATS1 in the LVB relative to other anterior epicardial regions (*$P < 0.05$, n=6), while DI-ATS1+CPA resulted in a Ca_D rise across the mapping filed (†$P < 0.05$). **I)** Representative normalized Ca^{2+} transients recorded at BCL 400 ms demonstrate prolongation of τ in the LV during DI-ATS1+CPA relative to DI-ATS1 alone **K)** while DI-ATS1+CPA prolonged τ across the mapping field at BCL 200 ms. **J)** Mean τ was lowest in the LVA during both DI-ATS1 and DI-ATS1+CPA at BCL 400ms (*$P < 0.05$) despite mean τ prolongation in the LV by DI-ATS1+CPA (†$P < 0.05$). **L)** LVA also evidenced shortest mean τ at BCL 200ms during DI-ATS1 (*$P < 0.05$). Mean τ prolonged across the mapping field during perfusion of DI-ATS1+CPA (†$P < 0.05$), resulting in no quantifiable difference in τ between the anterior epicardial regions.

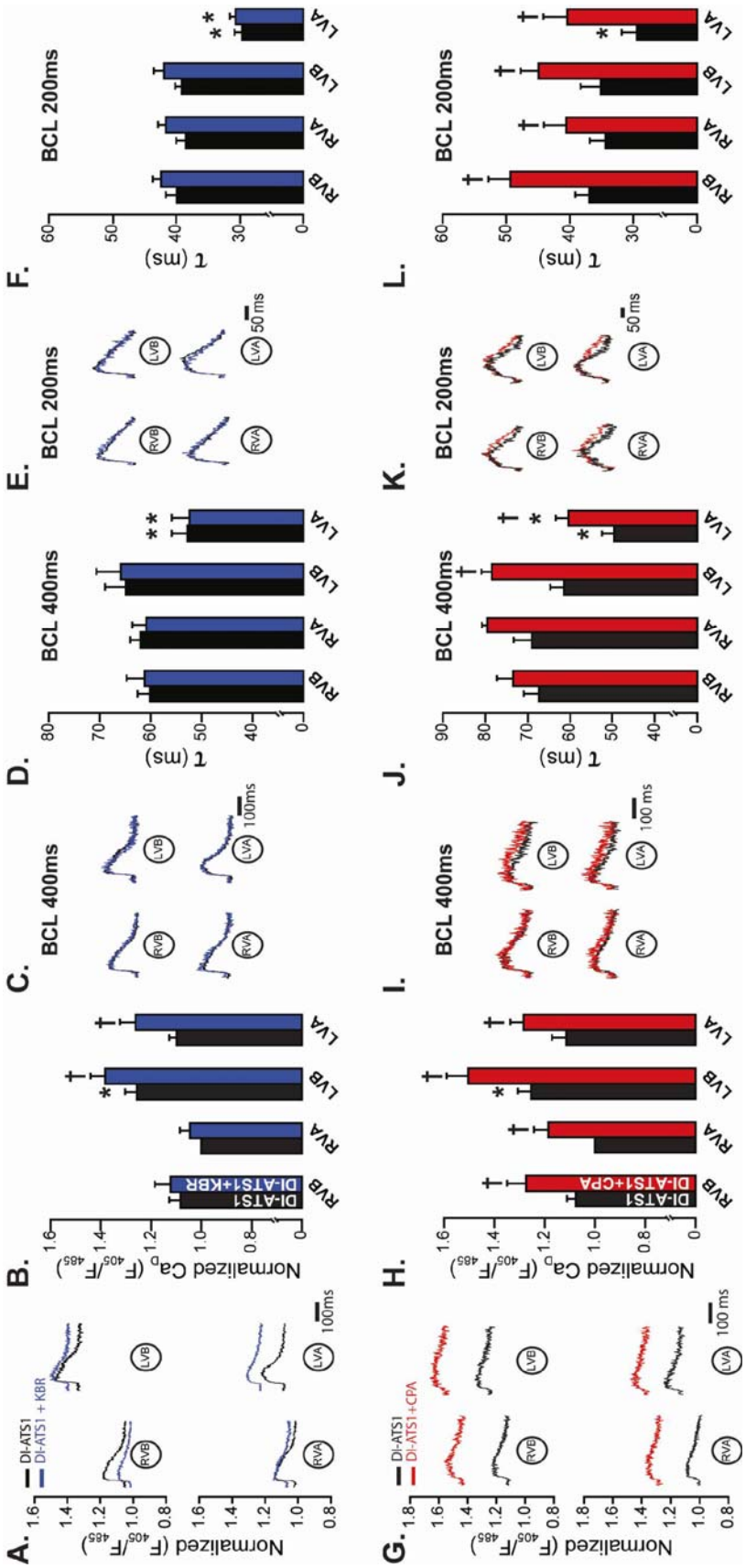
A.
DI-ATS1
DI-ATS1 + KBR
Normalized (F405/F485)
LVB
RVB
LVA
RVA
100ms
B.
Normalized CaD (F405/F485)
DI-ATS1
DI-ATS1+KBR
C.
BCL 400ms
D.
τ (ms)
BCL 400ms
E.
BCL 200ms
50 ms
F.
τ (ms)
BCL 200ms
G.
DI-ATS1
DI-ATS1+CPA
Normalized (F405/F485)
100 ms
H.
Normalized CaD (F405/F485)
DI-ATS1
DI-ATS1+CPA
I.
BCL 400ms
J.
τ (ms)
BCL 400ms
K.
BCL 200ms
50 ms
L.
τ (ms)
BCL 200ms

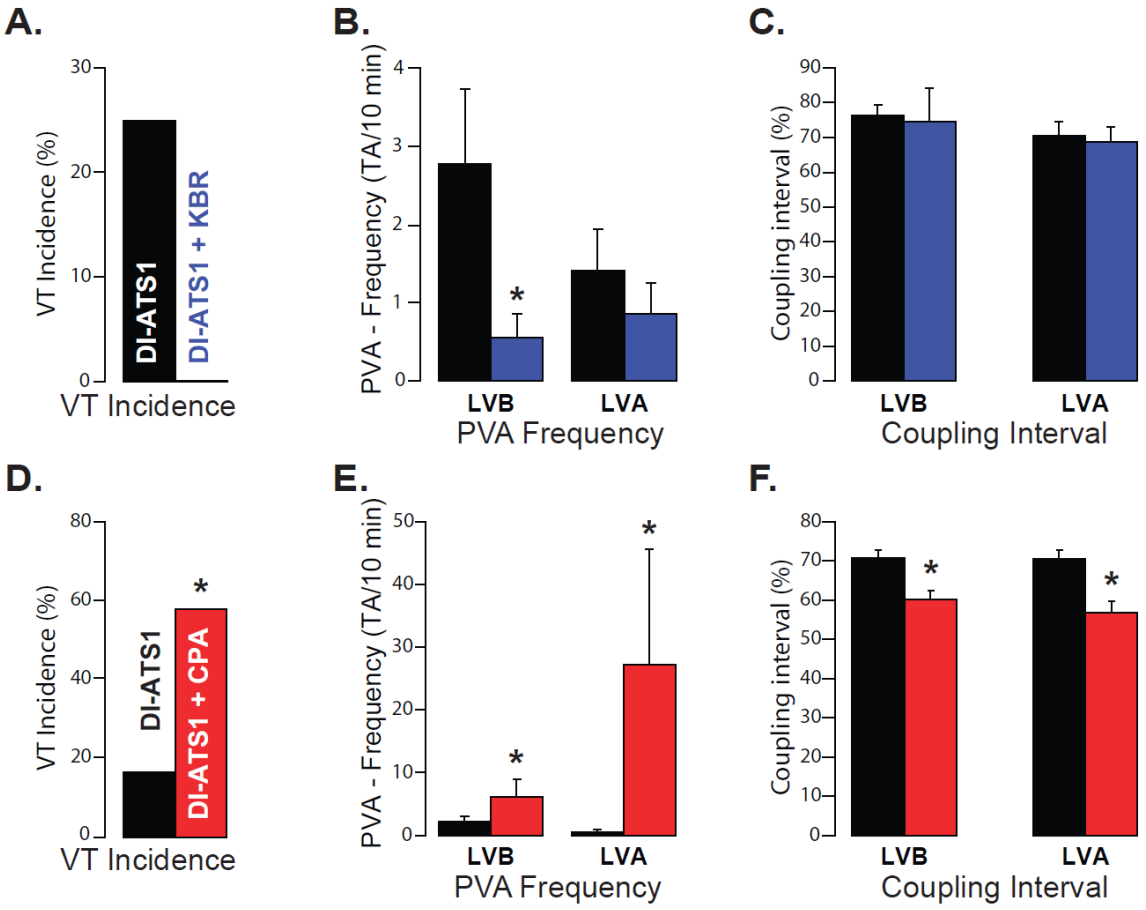

Figure 3.7: NCX Dominance Underlies Arrhythmias During DI-ATS1. A) Out of 8 preparations tested, spontaneous ventricular tachycardia (VT) were observed in 2 (25%) preparations during DI-ATS1 and none during DI-ATS1+KBR ($P = 0.11$). **B)** Over all PVA frequency, defined as number of events per 10 mins, originating from LVB was decreased during DI-ATS1+KBR relative to DI-ATS1 alone ($^*P < 0.05$, n=8). **C)** However, the mean coupling interval of PVA to the preceding intrinsic beat was unaltered in either LV region by DI-ATS1+KBR (P = ns). **D)** DI-ATS1+CPA increased the incidence of spontaneous VT relative to DI-ATS1 alone (7 vs. 2, n=12, respectively, $^*P < 0.05$). **E)** Over all experiments, PVA frequency was increased both in LVB and LVA during DI-ATS1+CPA compared to DI-ATS1 alone ($^*P < 0.05$, n=10). **F)** DI-ATS1+CPA shortened the coupling interval of both LVB and LVA PVA ($^*P < 0.05$). Arrhythmia burden was assessed during a 15 to 30 min. long protocol.

Figure 3.8: Action Potential Duration Prolongation During Pharmacological Perturbations of DI-ATS1. A) Representative optical action potentials recorded from the same ventricular regions during DI-ATS1 (black traces) and DI-ATS1+KBR (blue traces). DI-ATS1+KBR prolonged the action potential duration (APD) and enhanced total APD dispersion, defined as the difference in mean APD (calculated over 25 spatially contiguous sites per region) between epicardial regions with the longest (RVB) and shortest APD (LVA) during DI-ATS1. **B)** Mean APDs demonstrate a rise in APD during DI-ATS1+KBR compared to DI-ATS1 alone (†$P < 0.05$, n=3) where the difference in APD between RVB and LVA was retained (*$P < 0.05$). **C)** Total APD dispersion was unaltered by DI-ATS1+KBR relative to DI-ATS1 alone (P = ns). **D)** Representative optical action potentials recorded during DI-ATS1 (black traces) and DI-ATS1+CPA (red traces). DI-ATS1+CPA prolonged the APD but decreased total APD dispersion. **E)** Mean APDs demonstrate a rise in APD during DI-ATS1+CPA compared to DI-ATS1 alone (†$P < 0.05$, n=3), where the difference in APD between RVB and LVA evidenced during DI-ATS1 alone (*$P < 0.05$) was no longer observed during DI-ATS1+CPA (P = ns). **F)** Total APD dispersion was reduced by DI-ATS1+CPA relative to DI-ATS1 alone (*$P < 0.05$).

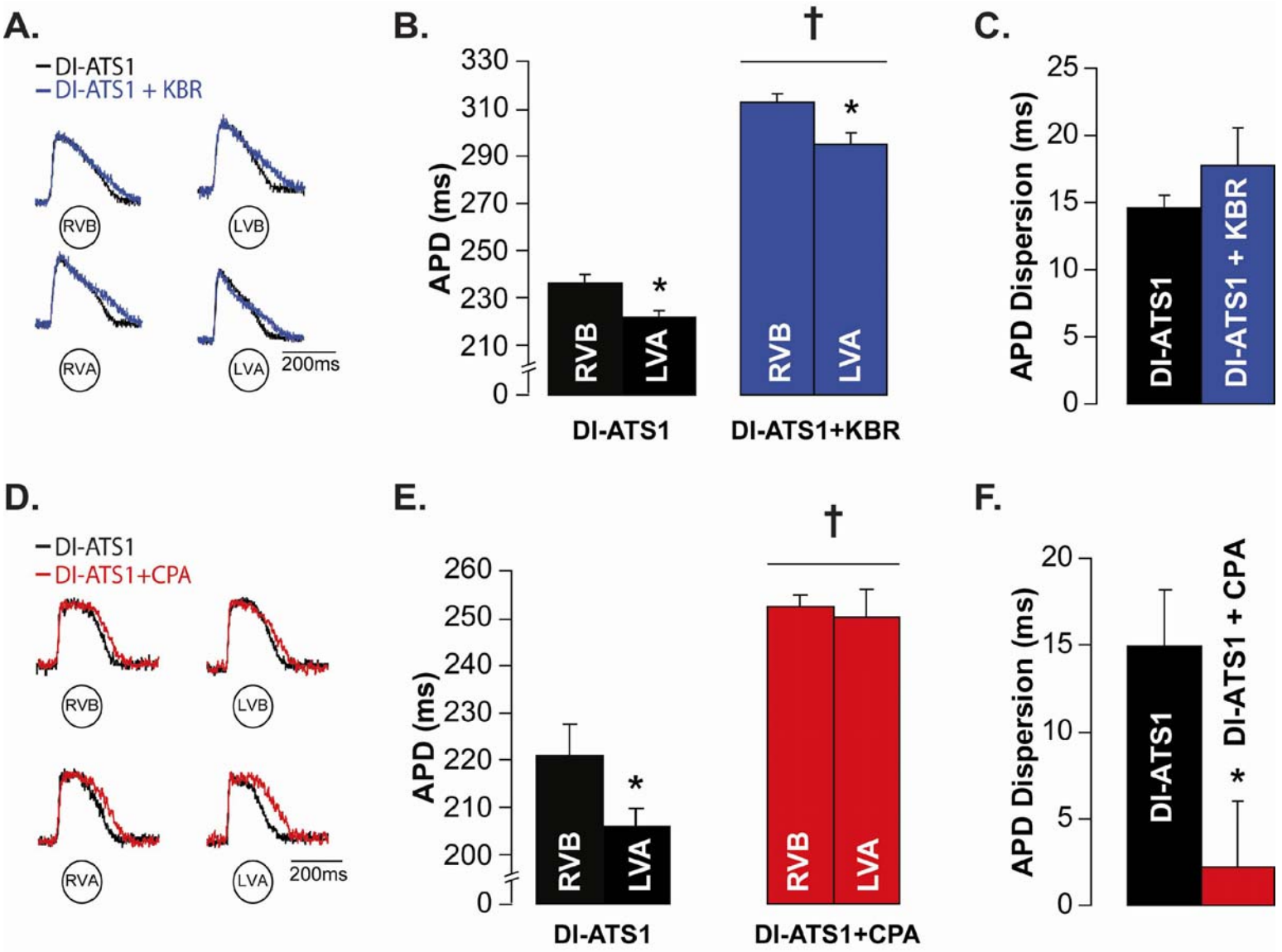
A.
DI-ATS1
DI-ATS1 + KBR
RVB
LVB
RVA
LVA
200ms
B.
†
330
310
290
270
250
230
210
0
APD (ms)
*
RVB
LVA
DI-ATS1
DI-ATS1+KBR
C.
25
20
15
10
5
0
APD Dispersion (ms)
DI-ATS1
DI-ATS1 + KBR
D.
DI-ATS1
DI-ATS1+CPA
RVB
LVB
RVA
LVA
200ms
E.
†
260
250
240
230
220
210
200
0
APD (ms)
*
RVB
LVA
DI-ATS1
DI-ATS1+CPA
F.
20
15
10
5
0
APD Dispersion (ms)
DI-ATS1
* DI-ATS1 + CPA

Appendix

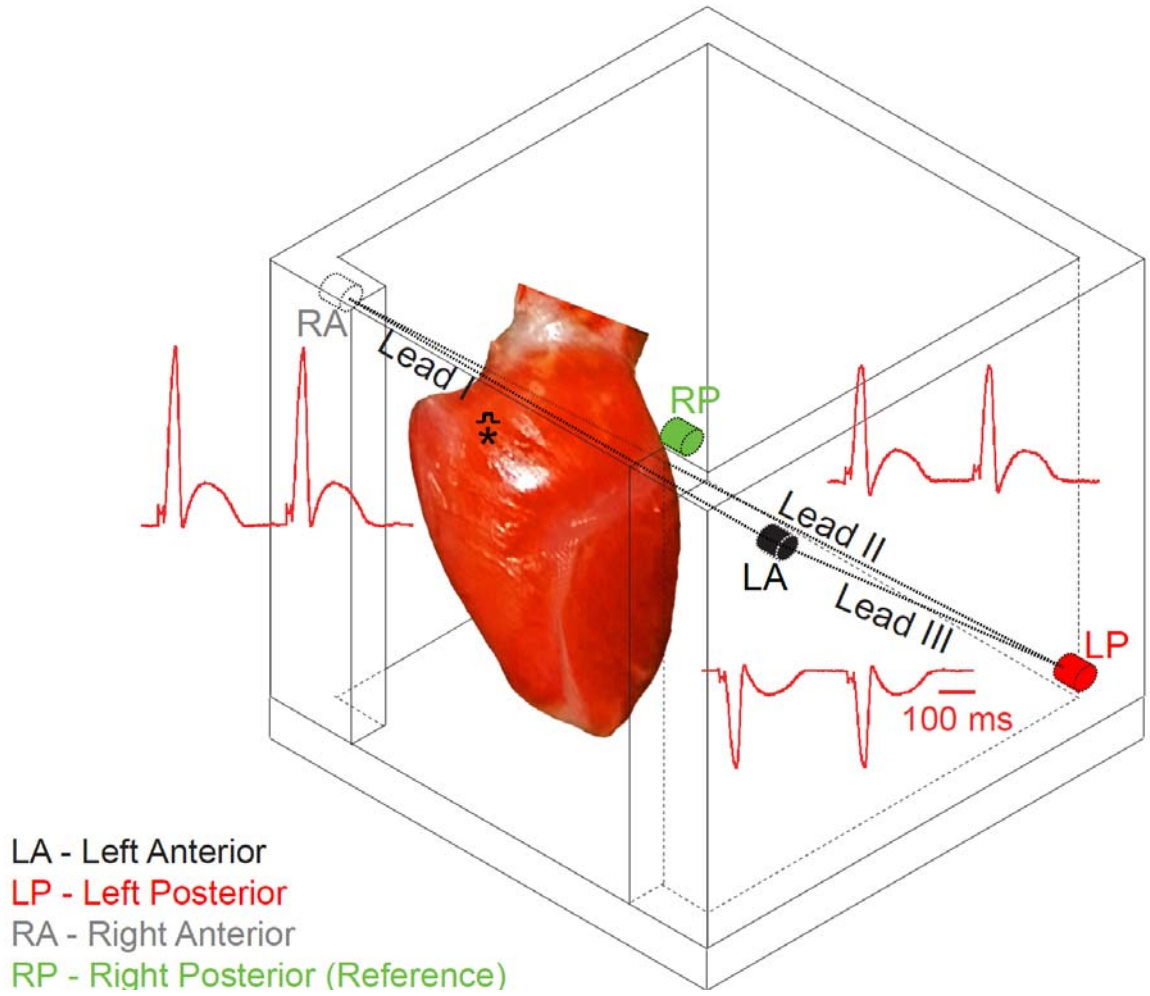

Supplemental Figure 3.1: Three lead volume-conducted ECG acquisition. Schematic representation of the perfusion bath lead placement that allows continuous three lead volume-conducted ECG acquisition. Representative ECG recorded during steady state pacing at basic cycle length 400ms from septum (*, stimulation site on the septum) reveal in Lead I propagation of depolarization from right anterior (RA, grey) to left anterior (LA, black) electrodes, in Lead II from RA to left posterior (LP, red) electrodes and in Lead III from LA to LP electrodes. Right posterior (RP, green) electrode serves as a reference.

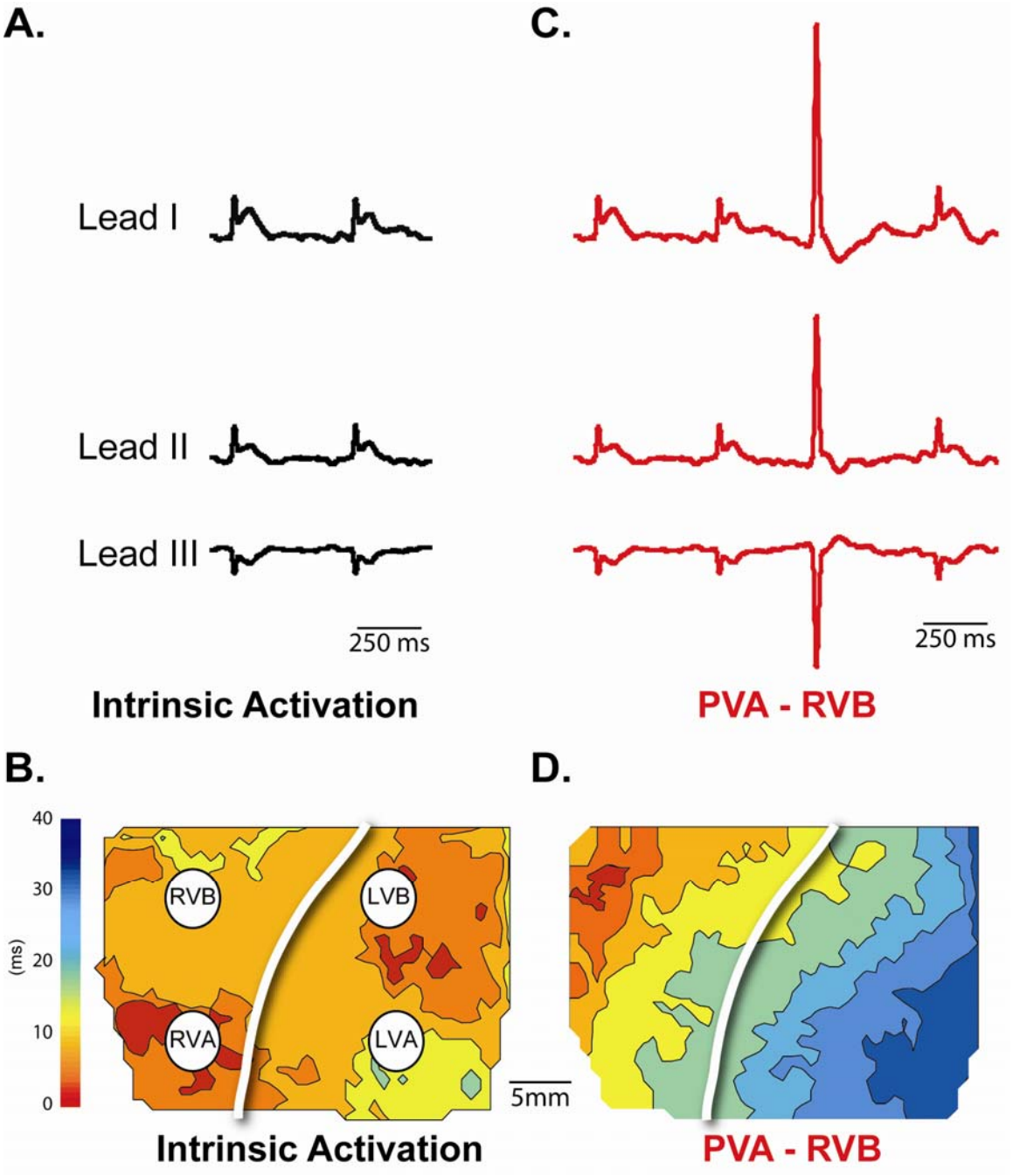

Supplemental Figure 3.2: Premature Ventricular Activity that Originates from RV during DI-ATS1. A) Representative volume-conducted ECG of intrinsic beats recorded during DI-ATS1 and **B)** a resulting activation isochrone map. **C)** In the case of premature ventricular activity (PVA) on volume-conducted ECG (red ECG) **D)** the earliest epicardial activation occurred in the right ventricle (RV).

CHAPTER 4

SUMMARY AND FUTURE DIRECTIONS

The presence of regional heterogeneity within the heart, in both electrophysiology and Ca^{2+} handling, is well established. However, the precise characterization of these heterogeneities is very much a work in progress. While such heterogeneities are crucial for normal cardiac function, they may be unmasked or exacerbated under pathophysiological conditions in a manner that contributes to the disease process. In order to understand and predict the role of regional heterogeneities in disease, it is vital to understand: a) their role in health and under challenging conditions, b) their interrelationships with other determinants of function, and c) how they may be modified by pathophysiological remodeling processes. Regional heterogeneity of the inward rectifier potassium current (I_{K1}) is one such heterogeneity that is prevalent under normal conditions and plays a benign role.[1,2] However, pathophysiological remodeling of I_{K1} as occurs in heart failure and other conditions[1,3] can dramatically alter the functional implications of such regional heterogeneity as well as bring to the fore other, previously dormant heterogeneities. In this work, we have studied the role of various regional heterogeneities in the context of I_{K1} loss-of-function versus normal health.

Anderson-Tawil Syndrome Type 1 (ATS1) is an inherited channelopathy resulting from a loss of I_{K1} function.[4,5] Importantly, it has been proposed that arrhythmias in ATS1 may be caused by electrical substrate remodeling,[6,7] which coupled with the intrinsic electrical and Ca^{2+} handling heterogeneities prolongs the QT interval and increases ectopic activity. Although heterogeneous action potential duration (APD) prolongation and increased dispersion, both transmural and interventricular, have been reported in experimental models of ATS1,[8-10] whether these gradients of repolarization

are sufficient for reentry and Ca^{2+} handling abnormalities to occur has been addressed by research presented in this work.

In Chapter 2, we demonstrate that gradients of epicardial APD dispersion in a drug-induced model of ATS1 (DI-ATS1) were insufficient for reentrant arrhythmia induction. Further, APD prolongation but not dispersion was associated with increased incidence and severity of spontaneous and rapid pacing induced arrhythmias. Further, we demonstrated that even when APD prolongation and dispersion were reduced virtually to baseline levels, some arrhythmia vulnerability remained. Therefore, in Chapter 3 we uncoupled heterogeneous APD prolongation and dispersion from arrhythmias. This was accomplished by pharmacological interventions where we demonstrate that Na^{+}/Ca^{2+} exchanger (NCX) inhibition (↓ NCX dominance) during DI-ATS1 prolonged APD heterogeneously, increased dispersion and yet, decreased arrhythmia burden. On the other hand, sarcoplasmic reticulum (SR) Ca^{2+} ATP-ase (SERCA2a) inhibition (↑ NCX dominance) with cyclopiazonic acid (CPA) during DI-ATS1 also prolonged APD and reduced APD dispersion; however, it significantly increased the arrhythmia burden. These findings strongly suggest that gradients of repolarization are unlikely to constitute the arrhythmogenic substrate in ATS1.

Since, the aforementioned data argued against reentrant mechanisms, we then turned towards ectopic activity as the arrhythmic mechanisms in DI-ATS1. Importantly, we did note a significantly elevated incidence of ectopy during DI-ATS1, which we characterized in detail. We demonstrated that the preponderance of observed ectopy originated from the left ventricle (LV), which will be discussed below. However, there were a few ectopic beats that originated elsewhere. Since the heart is a three dimensional

structure, it is important to know not only the regional origin site of ectopy (i.e., anterior, posterior, left, right, apex, base or septum) but also from which depth of tissue the ectopy arises (i.e. epicardium, midmyocardium or endocardium). To map the site of earliest epicardial activation, one might employ a sock electrogram array. One limitation of the suck array is that the spatial resolution and number of mapping sites is limited by the ability to "pack" the wires around the heart. However, even this reduced resolution overcomes the limitation of optical mapping by allowing one to quantify a larger two-dimensional map of epicardial breakthrough TA sites.

This, however, does not address the precise transmural localization of ectopic events in our model. The two dimensional nature of optical and electrode array mapping does not completely resolve the exact origins of such events but as already stated only identifies the epicardial breakthrough sites. This could potentially be resolved by the use of transmural needle electrodes to pinpoint the transmural site of origin of ectopy. One limitation of this approach is that the needles must penetrate the myocardium.[11] Such an approach can cause tissue injury causing itself ectopic activity to occur.

The aforementioned approach of employment of transmural needle electrodes warrants further consideration particularly if there are discrete number of unique ectopic sites. In a model of catecholaminergic polymorphic ventricular tachycardia (VT), the ectopy origination sites have been suggested to arise from the Purkinje network, which in humans generally terminates in the endocardium.[12] However, pharmacological models of I_{K1} inhibition have revealed ectopy to be multifocal, originating from different depths transmurally.[9,13] Therefore, we expect the origin of ectopy to be likewise multifocal in nature, spanning multiple transmural layers of the guinea pig myocardium.

Whether of Purkinje or myocardial origin, disregulated Ca^{2+} cycling has been suggested as the mechanism underlying ATS1-associated ectopy.[9,10,14,15] However, no direct evidence has been presented in support of such a hypothesis. Importantly, in Chapter 2 we demonstrate that this increased arrhythmia incidence is associated with significant diastolic Ca^{2+} (Ca_D) accumulation, which offers some insights into the arrhythmia mechanism in DI-ATS1. In order to further investigate the effect of APD prolongation on altered Ca^{2+} cycling we shortened APD with the ATP-sensitive potassium channel opener pinacidil, which allows these channels to be opened through the action potential. This pharmacological intervention alleviated the aforementioned APD prolongation but only partially reversed Ca_D accumulation and it did not abolish arrhythmias. These data, therefore, suggest that abnormalities in Ca^{2+} cycling can serve as a substrate for ATS1-associated arrhythmias.

Next we investigated the factors underlying Ca^{2+} mediated arrhythmias in our pharmacological model of ATS1. In Chapter 3, we report ectopic events occurring predominantly in the LV, particularly in regions with relatively higher protein expression of NCX relative to SERCA2a. These regions also exhibited slower Ca^{2+} uptake and elevated Ca_D. Importantly, we were able to modulate both the timing as well as the frequency of such ectopy by pharmacologically modulating NCX dominance. Specifically, increasing NCX dominance increased the incidence of spontaneous VTs and decreased the latency of ectopic events. Conversely, we also demonstrated that decreasing NCX dominance decreased the incidence of spontaneous VTs and ectopy. These data suggest that NCX dominance may represent an important characteristic of the arrhythmogenic substrate in ATS1.

Despite clear correlation between NCX dominance in LV-base (LVB) and the origin of ectopy during DI-ATS1, further questions remain regarding the effects of pharmacological modulation of NCX dominance on regional ectopic propensity. For instance the incidence of ectopic events was significantly elevated both in LVB and LV-apex (LVA) during pharmacologically enhanced NCX dominance (SERCA2a blockade). However, the difference in ectopic frequency between these regions was no longer significant. This coupled with the finding of greatest Ca_D accumulation in the LVB suggests that the coupling fidelity (i.e., coupling of aberrant Ca^{2+} release to the rise of transmembrane potential and consequent ectopy) of the NCX in that particular region is near saturation during DI-ATS1. Therefore, any subsequent perturbation in Ca^{2+} cycling, as occurs during pharmacologically enhanced NCX dominance, had a smaller effect on ectopy in the LVB relative to LVA. Such effect was more pronounced in the LVA, a region more dependent on SERCA2a for Ca^{2+} resequestration into the SR, allowing more room for the NCX to compensate for an induced reduction in Ca^{2+} resequestration. We previously showed that greater expression of $Na_v1.5$ (the protein that carries the cardiac fast Na^+ current) in the anterior LV relative to other myocardial regions.[2] In the LVA, the larger Na^+ current together with NCX may act to bring more Ca^{2+} into the cell via reverse mode exchange during the depolarization phase.[16] This Ca^{2+} influx via NCX could be then sequestered into the SR by SERCA2a, which is also more abundant in the LVA, resulting ultimately in a greater Ca^{2+} transient amplitude observed in this particular region compared to other anterior epicardial regions.[17] Therefore, SERCA2a inhibition during DI-ATS1 resulted in a greater NCX coupling fidelity between aberrant Ca^{2+} release and rise of transmembrane potential (i.e. ectopy) in the LVA compared to LVB,

while the coupling fidelity in the LVB may have become saturated. The relevance of the interplay between Na^+ influx, NCX and propensity for ectopy should be further investigated in isolated cellular preparations.

We have demonstrated here that a key arrhythmogenic mechanism in DI-ATS1 is ectopy secondary to disregulated Ca^{2+} handling, particularly from NCX dominant regions. Such ectopy is believed to be due to triggered activity, which have been demonstrated to originate from areas of elevated Ca_D and Ca^{2+} overload and were caused by membrane depolarization in response to nonelectrically driven Ca^{2+} release from the SR.[18-20] Three hypotheses have been proposed for the cellular mechanism of aberrant Ca^{2+} release which likely underlies the observed ectopy: a) spontaneous SR Ca^{2+} release due to SR overload, b) ryanodine receptor (RyR) sensitization due to Ca_D elevation and c) NCX-triggered SR Ca^{2+} release. The involvement of these mechanisms in ATS1 warrants further investigation. This represents a very important line of inquiry, particularly in the light of the potential therapeutic value of such insight.

In order to gain more insight into the underlying arrhythmic mechanism a future study could employ an isolated cellular model. Such an experimental setup would allow querying the SR Ca^{2+} load by caffeine pulse protocol particularly during highly arrhythmogenic states (DI-ATS1+CPA). Based on previous research,[21,22] we expect that SR Ca^{2+} load will be decreased during DI-ATS1+CPA relative to DI-ATS1 alone secondary to decreased Ca^{2+} resequestration into the SR via SERCA2a. Further, we expect that SR Ca^{2+} load during the aforementioned pharmacological interventions will not correlate with arrhythmia incidence.

An additional benefit of such research would be to investigate the role of cytosolic Ca^{2+} accumulation on SR Ca^{2+} release by application of intracellular Ca^{2+} chelators. Using such an approach will allow to determine the effect of cytosolic Ca^{2+} on spontaneous Ca^{2+} release from SR Ca^{2+}. We expect that lowering cytosolic Ca^{2+} will result in lowered incidence of spontaneous Ca^{2+} release events.

Lastly, research in isolated cells would allow us to investigate the NCX-triggered SR Ca^{2+} release by direct application of NCX selective peptide-inhibitor. Further, in the light of the latest revelations of neuronal Na^{+} channels and NCX involvement in augmenting Ca^{2+} release by the L-type Ca^{2+} channel,[16,23] this study can be augmented by testing the effect of a neuronal Na^{+} channel inhibitor, tetrodotoxin, on NCX-triggered Ca^{2+} release. We expect that modulation of either NCX or neuronal Na^{+} channel in the aforementioned fashion will decrease the incidence as well as alter the kinetics of Ca^{2+} release events.

While our results suggests an important role for NCX in coupling aberrant Ca^{2+} release to rise of transmembrane potential (i.e. ectopy), the roles of other transmembrane currents, in particular the L-type Ca^{2+} current[24] bear investigation. This is particularly relevant in the light of recent findings of L-type Ca^{2+} current density differences between the base and apex of rabbit model of long QT syndrome that was correlated with arrhythmias.[24] Clearly, there may be more than one explanation for heterogeneous arrhythmia manifestation in addition to the regional NCX dominance.

In this work however, we have undertaken a targeted approach for measuring the functional consequences of NCX dominance along with Ca^{2+} handling aberrancy and electrophysiologic alterations present during conditions of partial loss of I_{K1} function.

This research may aid in the identification of novel targets for antiarrhythmic therapy when I_{K1} is reduced as occurs in ATS1 and heart failure.

References

1. Warren M, Guha PK, Berenfeld O, et al. Blockade of the inward rectifying potassium current terminates ventricular fibrillation in the guinea pig heart. *J Cardiovasc Electrophysiol*. 2003;14(6):621-631.

2. Veeraraghavan R, Poelzing S. Mechanisms underlying increased right ventricular conduction sensitivity to flecainide challenge. *Cardiovasc Res*. 2008;77(4):749-56.

3. Pogwizd SM, Schlotthauer K, Li L, Yuan W, Bers DM. Arrhythmogenesis and contractile dysfunction in heart failure: Roles of sodium-calcium exchange, inward rectifier potassium current, and residual beta-adrenergic responsiveness. *Circ Res*. 2001;88(11):1159-67.

4. Tristani-Firouzi M, Jensen JL, Donaldson MR, et al. Functional and clinical characterization of KCNJ2 mutations associated with LQT7 (Andersen syndrome). *J Clin Invest*. 2002;110(3):381-8.

5. Plaster NM, Tawil R, Tristani-Firouzi M, et al. Mutations in Kir2.1 cause the developmental and episodic electrical phenotypes of Andersen's syndrome. *Cell*. 2001;105(4):511-9.

6. Zhang L, Benson DW, Tristani-Firouzi M, et al. Electrocardiographic features in Andersen-Tawil syndrome patients with KCNJ2 mutations: characteristic T-U-wave patterns predict the KCNJ2 genotype. *Circulation*. 2005;111(21):2720-6.

7. Tawil R, Ptacek LJ, Pavlakis SG, et al. Andersen's syndrome: potassium-sensitive periodic paralysis, ventricular ectopy, and dysmorphic features. *Ann Neurol*. 1994;35(3):326-30.

8. Tsuboi M, Antzelevitch C. Cellular basis for electrocardiographic and arrhythmic manifestations of Andersen-Tawil syndrome (LQT7). *Heart Rhythm*. 2006;3(3):328-35.

9. Morita H, Zipes DP, Morita ST, Wu J. Mechanism of U wave and polymorphic ventricular tachycardia in a canine tissue model of Andersen-Tawil syndrome. *Cardiovasc Res*. 2007;75(3):510-8.

10. Poelzing S, Veeraraghavan R. Heterogeneous ventricular chamber response to hypokalemia and inward rectifier potassium channel blockade underlies bifurcated T wave in guinea pig. *Am J Physiol Heart Circ Physiol*. 2007;292(6):H3043-51.

11. Voss F, Opthof T, Marker J, et al. There is no transmural heterogeneity in an index of action potential duration in the canine left ventricle. *Heart Rhythm*. 2009;6(7):1028-34.

12. Cerrone M, Noujaim SF, Tolkacheva EG, et al. Arrhythmogenic mechanisms in a mouse model of catecholaminergic polymorphic ventricular tachycardia. *Circ Res*.

2007;101(10):1039-1048.

13. Maruyama M, Joung B, Tang L, et al. Diastolic intracellular calcium-membrane voltage coupling gain and postshock arrhythmias: Role of purkinje fibers and triggered Activity. *Circ Res*. 2010;106(2):399-408.

14. Sung RJ, Wu SN, Wu JS, Chang HD, Luo CH. Electrophysiological mechanisms of ventricular arrhythmias in relation to Andersen-Tawil syndrome under conditions of reduced IK1: A simulation study. *Am J Physiol Heart Circ Physiol*. 2006;291(6):H2597-605.

15. Silva J, Rudy Y. Mechanism of pacemaking in I(K1)-downregulated myocytes. *Circ Res*. 2003;92(3):261-3.

16. Larbig R, Torres N, Bridge JHB, Goldhaber JI, Philipson KD. Activation of reverse Na+-Ca2+ exchange by the Na+ current augments the cardiac Ca2+ transient: evidence from NCX knockout mice. *J Physiol*. 2010;588(17):3267-3276.

17. Katra RP, Pruvot E, Laurita KR. Intracellular calcium handling heterogeneities in intact guinea pig hearts. *Am J Physiol Heart Circ Physiol*. 2004;286(2):H648-56.

18. Marban E, Robinson SW, Wier WG. Mechanisms of arrhythmogenic delayed and early afterdepolarizations in ferret ventricular muscle. *J Clin Invest*. 1986;78(5):1185-92.

19. Boyden PA, Pu J, Pinto J, Keurs HEDJT. Ca2+ transients and Ca2+ waves in purkinje cells : Role in action potential initiation. *Circ Res*. 2000;86(4):448-455.

20. Priori SG, Corr PB. Mechanisms underlying early and delayed afterdepolarizations induced by catecholamines. *Am J Physiol*. 1990;258(6 Pt 2):H1796-1805.

21. Szentesi P, Pignier C, Egger M, Kranias EG, Niggli E. Sarcoplasmic Reticulum Ca2+ refilling controls recovery from Ca2+-induced Ca2+ release refractoriness in heart muscle. *Circ Res*. 2004;95(8):807-813.

22. Lukyanenko V, Viatchenko-Karpinski S, Smirnov A, Wiesner TF, Györke S. Dynamic regulation of sarcoplasmic reticulum Ca(2+) content and release by luminal Ca(2+)-sensitive leak in rat ventricular myocytes. *Biophys J*. 2001;81(2):785-798.

23. Torres NS, Larbig R, Rock A, et al. Sodium Current-Induced Release of Calcium from the Sarcoplasmic Reticulum in Rabbit Ventricular Myocytes. *Biophysical Journal*. 2010;98(3, Supplement 1):201a.

24. Sims C, Reisenweber S, Viswanathan PC, et al. Sex, Age, and Regional Differences in L-Type Calcium Current Are Important Determinants of Arrhythmia Phenotype in Rabbit Hearts With Drug-Induced Long QT Type 2. *Circ Res*. 2008;102(9):e86-100.